CONTROL OF THE BRANCHING CHANNELS FOR XeCl* FORMATION BY ADDITION OF VIBRATIONAL ENERGY TO CF_2Cl_2, CF_2HCl, and CF_3Cl

by

ANDREW R. SLAGLE

B.S., Southwestern Oklahoma State University

1984

A Master's Thesis

submitted in partial fulfillment of the

requirements for the degree

MASTER OF SCIENCE

Department of Chemistry

Kansas State University
Manhattan, Kansas

1987

Approved:

D.W. Setser

Prof. D.W. Setser

TABLE OF CONTENTS

List of Figures

List of Tables

CHAPTER 1 INTRODUCTION

The advent of the CO_2 laser (1964)[1] provided new methods for the study of molecular dynamics because vibrational excitation could be deposited in a molecule. Prior to that time, virtually all photon induced chemical processes were done with visible, uv, or shorter wavelength radiation. By the early 1970's, high powered CO_2 lasers were commercially available that could provide energies as high as 10 J/pulse and pulse durations on the order of one micro-second in the spectral range of 9.2-10.6 um (1087-943 cm^{-1}).[2,3] For scientists, chemical physicists in particular, the CO_2 laser provided a means of selectively exciting particular vibrational modes which absorbed radiation in this region. In 1970, Karlov et.al.[4] revealed that a high powered infrared laser beam was capable of inducing unimolecular chemical reactions when they observed IR and recombination luminesecence from BCl_3. Since Karlov's initial observation, a great deal of work has been done to understand the absorption of many IR photons by a single molecule in one laser pulse, the energy distributions[5-15] and the processes occuring during[16-20,25] and after[21-24] deposition of the energy. Detailed model calculations have also been described for the multiphoton absorption process.[24-26] The references given here for these types of measurements are only a small

sample of the available literature on infrared multiphoton absorption (IRMPA) and dissociation (IRMPD).

A simple model[27] for the absorption process for infrared photons in a single mode is depicted in figure 1.1. A polyatomic molecule in it´s ground electronic state and initially in it´s ground vibrational state is subjected to an intense monochromatic IR field. If the energy of the photon is resonant with the transition to the first vibrational level, absorption of one photon places the molecule in a v=1 state. Vibrational anharmonicity would be expected to reduce probability of absorption of sucessive photons because the energy match between levels becomes worse as the spacing becomes smaller at higher vibrational levels. However, several factors provide a means for climbing the "vibrational ladder." The most important factor is that even though the lower transitions are not exactly resonant with the IR photons provided, the first few transitions are near resonant and various broadening processes aid the multiphoton absorption. The addition of rotational levels and combination vibrational levels increase the density of states. After clearing the third or fourth vibrational levels, the absorption involves essentially a continuum because of the high state density for polyatomic molecules. A deep understanding of the multiphoton process is not extremely important for our purpose, our goal is to use the CO_2 laser to deposit an internal energy in the polyatomic molecule. A single IR

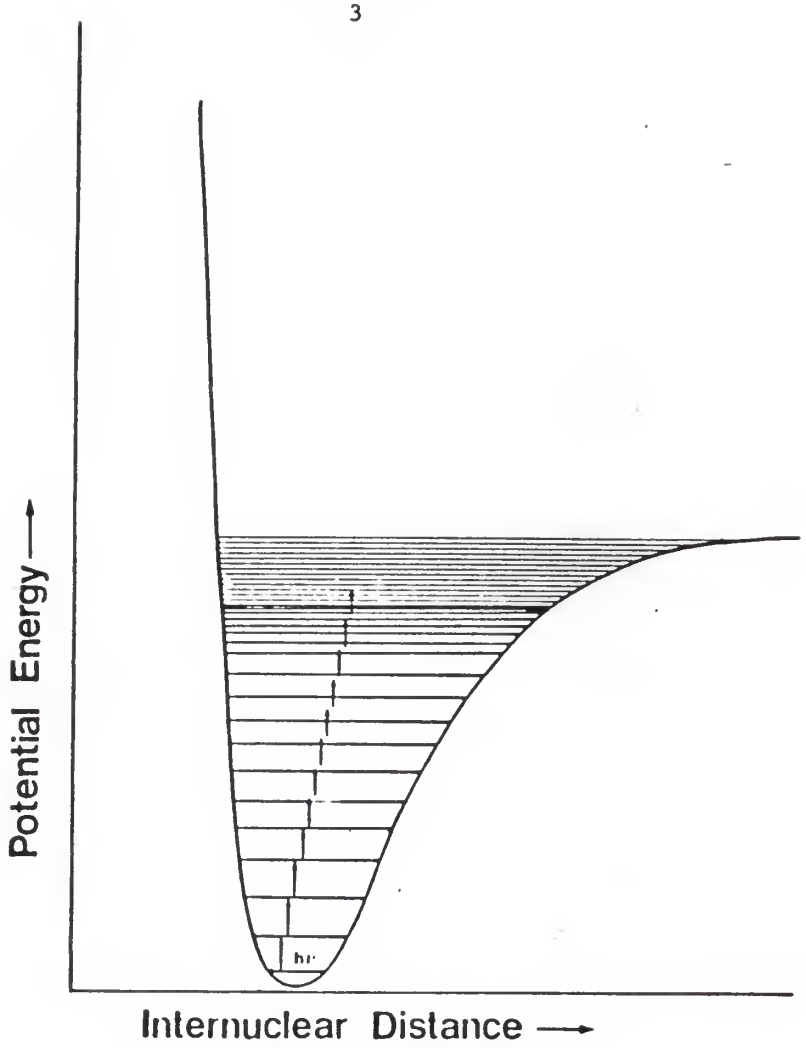

Figure 1.1 Illustration of "vibrational ladder climbing" with schematic representation of anharmonicity.

photon at 1000 cm^{-1} would only provide about 0.12 eV of internal energy. Multiphoton absorption can provide an internal energy of about 2 eV or higher depending on the absorption cross-sections, the laser intensity and various bottlenecks.

Compared to infrared laser induced unimolecular reactions, less work has been done on bimolecular processes induced or aided by vibrational energy.[28-39] In 1969 Polanyi and Wong[40] reported the results of calculations in which an increase in vibrational (internal) energy in the B-C bond effectively increased the rate of a direct A + BC --> AB + C abstraction reaction proceeding on a repulsive surface, but an increase in collision energy was markedly less effective, when the energy barrier was located in the exit channel of a potential surface. In 1971 Odiorne et.al., in a letter to the Journal of Chemical Physics[39], reported that HCl(v=1) reacted 100 times faster with K atoms to give KCl than did HCl(v=0); the excited HCl was produced by an HCl laser pulse. This was possibly the earliest reported example of vibrational excitation, provided by a laser pulse, enhancing or inducing a bimolecular chemical reaction. Since the early 1970's, experiments conducted along this line have primarily been attempts to populate low vibrational states, $v<5,6$, of di- or triatomic molecules and react the excited molecule with atoms or diatomic molecules.[28-39] Two of these attempts have provided negative results[33,34] (were unsuccessful in

enhancing the reaction). The reason for negative results might be explained by Polanyi's calculations, as he also found that a reaction with an energy barrier in the entrance channel of a potential surface was not enhanced by vibrational excitation of reactants. Table 1.1 summarizes some of the reactions and results of several of the references mentioned.

The low yields of XeCl(B,C) from the reaction of chlorofluoromethanes with $Xe(^3P_2)$ atoms provide an interesting possibility for enhancement of XeCl(B,C) formation by addition of vibrational energy to the freon. At 300K the reaction of $Xe(6s,^3P_2)$ atoms and CF_3Cl, CF_2Cl_2, and CF_2HCl (references 41,44) have very small rate constants ($1\text{-}3\times10^{-12}$ $cm^3molecule^{-1}s^{-1}$) for XeCl(B,C) formation compared to the major, quenching, pathway ($1\text{-}2\times10^{-10}$ $cm^3molecule^{-1}s^{-1}$), which is simply excitation-transfer followed by dissociation of the excited molecules.[42,43] These rate constants give branching fractions $\Gamma_{XeCl^*} < 0.05$ for these reactions. Figure 1.2 shows the potential energy sketch for formation of $XeCl^*$. The exit channel, which is the ion pair potential Xe^+Cl^- + R, is followed by radiative decay of XeCl(B,C). The B-X emission is the transition which the xenon chloride excimer laser is based. Quenching reactions in which the electronically excited reagent atom is incorporated into a product is called reactive quenching. A greater understanding of reactive quenching would be applicable to

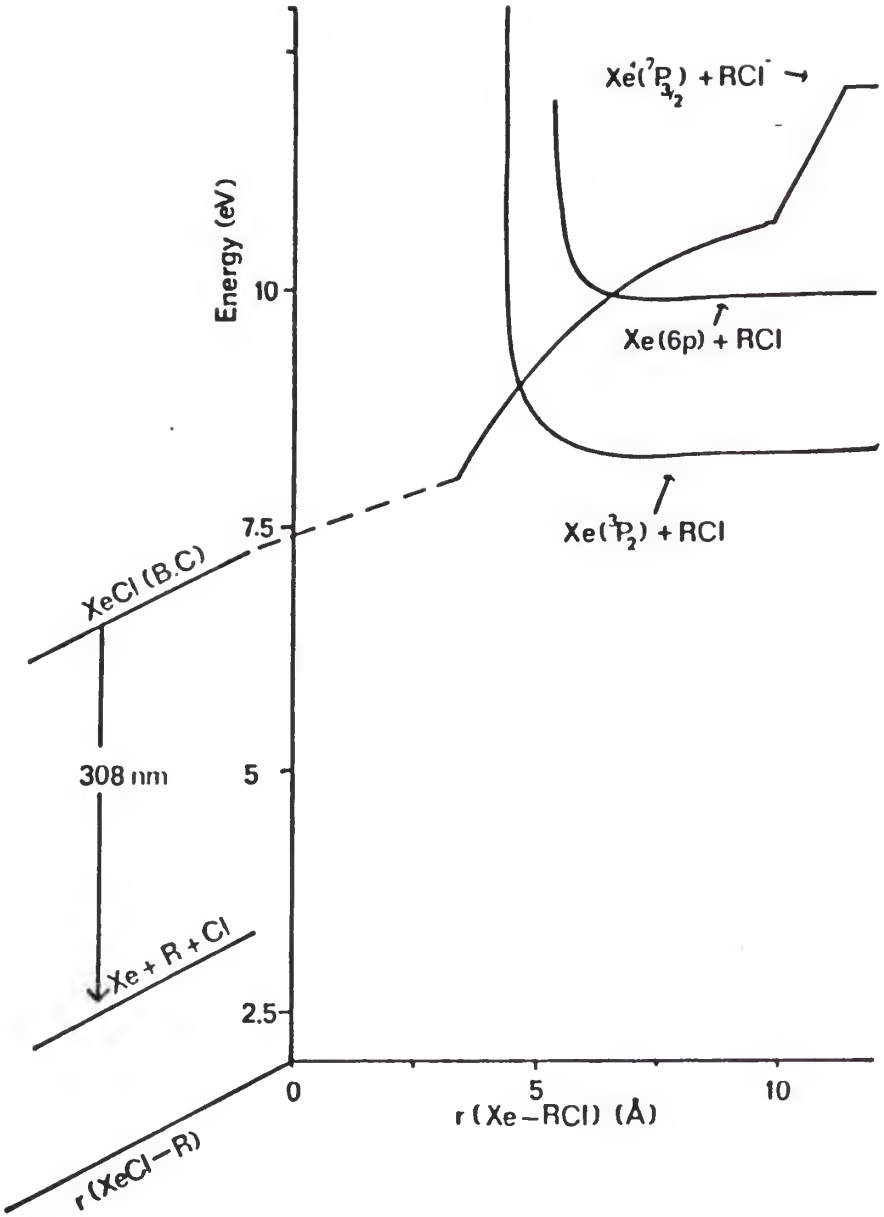

Figure 1.2 Potential energy diagram for $XeCl^*$ formed via the reaction of $Xe(^3P_2)$ with RCl. The ion pair entrance channel was drawn for I.P.(Xe) = 12.13 eV, E.A.(RCl) = 0.0 eV. $E(Xe(^3P_2))$ is 8.32 eV.

other excimer species, namely those formed from the reaction of electronically excited Ar, Kr, or Hg atoms with Cl or F atom donors.

In figure 1.2, the low $XeCl^*$ branching fraction for the freons (chlorofluoromethanes) mentioned above may be explained in terms of access to the $V(Xe^+,RCl^-)$ ion pair curve. This ion pair potential is calculated by the coulombic interaction of two charged particles; the electron affinity of RCl was taken as 0.0 eV. The non-ionic entrance channels were calculated by a Leonard-Jones 6-12 potential function.[44] The $Xe(^3P_2)$ atom has 8.32 eV of energy, so at room temperatures the $Xe(^3P_2)/RCl$ collision pair do not have enough energy to reach the ion pair potental, which leads to $XeCl^*$ (e.g. the ion pair curve crosses the Xe^*/RCl repulsive wall almost 1 eV above 8.32 eV). It is, therefore, expected that either raising the collision pair potential or lowering the ion pair potential would increase $XeCl^*$ formation. Indeed it has been shown that Xe atoms excited to 6p states (9.8 eV as opposed to the 8.32 eV 6s metastable states) gives enhanced formation of $XeCl^*$.[45,46] In the discussion at the end of this thesis, we shall see how the Xe(6p) result, as well as the experiments presented herein, support the reactive quenching mechanism based on the ionic-covalent curve crossing mechanism.

The experiments to be presented may be broken down into three types. First the 300K $XeCl^*$ branching fractions

were measured for several chlorofluoromethanes and chlorofluoroethanes with $Xe(^3P_2)$. Next the enhancement of $XeCl^*$ formation by addition of vibrational energy was measured for Xe^* with the chlorofluoromethanes. Finally the energy of the vibrationally excited freons was estimated by measuring the energy absorption under conditions representative of the $XeCl^*$ enhancement experiments.

Rererences: Chapter 1

1a.) C.K.N. Patel, Phys. Rev. Lett., 12 (1964) 588
b.) C.K.N. Patel, Phys. Rev. Lett., 13 (1965) 617
c.) C.K.N. Patel, Phys. Rev. A, 136 (1965) 1187

2.) W.W. Duley, "CO_2 Lasers, Effects and Applications". Academic Press, New York (1976)

3.) E. Grunwald, D.F. Dever, P.M. Keehn, "Megawatt Infrared Laser Chemistry". John Wiley & Sons, New York (1978)

4a.) N.V. Karlov, U.N. Petrov, A.M. Prokhorov, O.M. Stelmakh, JETP Lett. 11 (1970) 135
b.) N.V. Karlov, Appl. Opt., 13 (1974) 301

5.) W.S. Drozdoski, A. Fakhr, R.D. Bates Jr., Chem. Phys. Lett., 47(2) (1977) 309

6.) W.S. Drozdoski, R.D. Bates Jr., D.R. Siebert, J. Chem. Phys., 69(2) (1978) 863

7.) E. Grunwald, C.M. Lonzetta, K.J. Olszyna, ACS Symposium Series, No. 56, State to State Chemistry, (1977) 107

8.) E. Grunwald, K.J. Olszyna, D.F. Dever, B. Knishkowy, J. Am. Chem. Soc., 99 (1977) 6515

9.) E. Grunwald, K.J. Olszyna, D.F. Dever, B. Knishkowy, J. Am. Chem. Soc., 99 (1977) 6521

10.) S.H. Liu and E. Grunwald, 90(19) (1986) 4555

11.) S.H. Liu and E. Grunwald, 90(19) (1986) 4559

12.) A.V. Baklanov, V.V. Vizhin, A.K. Petrov, Sov. J. Quan. Elec., 12(7) (1982) 865

13.) M.P. Freeman, D.N. Travis, M.F. Goodman, J. Chem. Phys., 60(1) (1974) 231

14.) A.S. Sudbo, P.Z. Schulz, E.R. Grant, Y.R. Shen, Y.T. Lee, J. Chem. Phys., 70(2) (1979) 912

15.) R.J.S. Morrison and E.R. Grant, J. Chem. Phys., 70(10) (1981) 5679

16.) E.M. Alonso, A.L. Peuriot, V.B. Slezak, J. App. Phys. B, 40, (1986) 39

17.) J.C. Stephenson, D.S. King, M.F. Goodman, J. Stone,

J. Chem. Phys., 70(10) (1979) 4496

18.) J.C. Stephenson, J. Chem. Phys, 77(6) (1982) 3283

19.) E. Grunwald and S.H. Liu, J. Phys. Chem., 90 (1986) 4550

20.) R.E. Westen Jr., J. Am. Chem. Soc., 86(25) (1982) 4864

21.) D.S. King and J.C. Stephenson, Chem. Phys. Lett., 51(1) (1977) 48

22.) J.C. Stephenson and D.S. King, J. Chem. Phys., 69(4) (1978) 1485

23.) J.C. Stephenson, S.E. Bialkowski, D.S. King, J. Chem. Phys., 72(2) (1980) 1161

24.) M. Quack, J. Chem. Phys., 69(3) (1978) 1282

25.) I. Oref and B.S. Rabinovitch, J. Phys. Chem., 81(26) (1977) 2587

26.) B. Toselli, J.C. Ferrero, E.H. Staricco, J. Phys. Chem., 90(19) (1986) 4562

27.) R.J. Jensen, O.P. Judd, J.A. Sullivan, Los Alamos Science, 3(1) (1982) 2

28.) I.W.M. Smith in "Physical Chemistry of Fast Reactions", Vol. 2 Reaction Dynamics ed. I.W.M. Smith, Plenum Press (1980)

29.) K. Kleinermanns and J. Wolfrum, Laser Chem. 2, (1983) 339

30.) J. Wolfrum, J. Phys. Chem., 90, (1986) 375

31.) D. Klenerman and R.N. Zare, Chem. Phys. Lett., 130(3), (1986) 190

32.) I.W.M. Smith and M.D. Williams, JCS Faraday II, 82, (1986) 1043

33.) I.P. Herman and J.B. Marling, J. Chem. Phys., 71(2), (1979) 643

34.) C. Willis, R.A. Back, R. Corkum, R.D. McAlpine, F.K. McClusky, Chem. Phys. Lett., 38(2) (1976) 336

35.) R.S.F. Chang, J. Chem. Phys., 76(6), (1982) 2943

36.) R.J. Gordon and M.C. Lin, Chem. Phys. Lett., 22(2)

(1973) 262

37.) J.C. Stephenson and S.M. Freund, J. Chem. Phys., 65(10) (1976) 4303

38.) K.K. Hui and T.A. Cool, J. Chem. Phys., 68(3) (1978) 1022

39.) T.J. Odiorne, P.R. Brooks, J.V.V. Kasper, J. Chem. Phys., 55(4) (1971) 1980

40.) J.C. Polanyi and W.H. Wong, J.Chem. Phys., 51(4) (1969) 1439

41.) J.E. Velazco, J.H. Kolts, D.W. Setser, J. Chem. Phys., 69(10) (1978) 4357

42a.) J.H. Kolts, J.E. Velazco, D.W. Setser, J. Chem. Phys., 71(3) (1979) 1247

b.) D. Lin, Y.C. Yu, D.W. Setser, J. Chem. Phys., 81(12) (1984) 5830

43.) J. Balamuta, M.F. Golde, A.M. Moyle, J. Chem. Phys., 82(7) (1985) 3169

44.) J.O. Hirshfelder, C.F. Curtiss, and R.B. Bird, "Molecular Theory of Gases and Liquids" John Wiley & Sons, Inc. (1954)

45.) J.K. Ku and D.W. Setser, Appl. Phys. Lett., 48(11) (1986) 689

46.) J. Xu, A.R. Slagle, D.W. Setser, J.C. Ferrero, Chem. Phys. Lett., (In Press, 1987)

CHAPTER 2 EXPERIMENTAL TECHNIQUES

This study constisted of three types of experiments; measuring XeCl(B,C) branching fractions from $Xe(^3P_2)$ reactions at 300K, measuring the IR laser energy absorbed by the reagent molecules, and measuring the enhancement of XeCl(B,C) formation from $Xe(^3P_2)$ reactions that resulted from this absorbed energy. This chapter will describe how each of these different experiments was conducted, as well as general laboratory procedures.

2.1 Gas Handling

The Freons (Chlorofluoromethanes) were obtained from SCM Specialty Chemicals Inc. except for CF_3Cl, which came from MG Scientific Gases Incorporated. These gases had specified purities greater than 98%; however, each was further purified by vacuum distillation. Figure 2.1 shows the section of the vacuum rack relevant to loading, distilling, and storing these gases. Xenon was used directly from the tank with a specified purity of 99.995% (Research Purity) as provided by Cryogenic Rare Gas Incorporated. The argon, from a local gas company, was passed through a series of three molecular sieve traps. The first trap was at ~1 atm and was cooled to 195 K by a dry ice/acetone bath. After passing through a calibrated

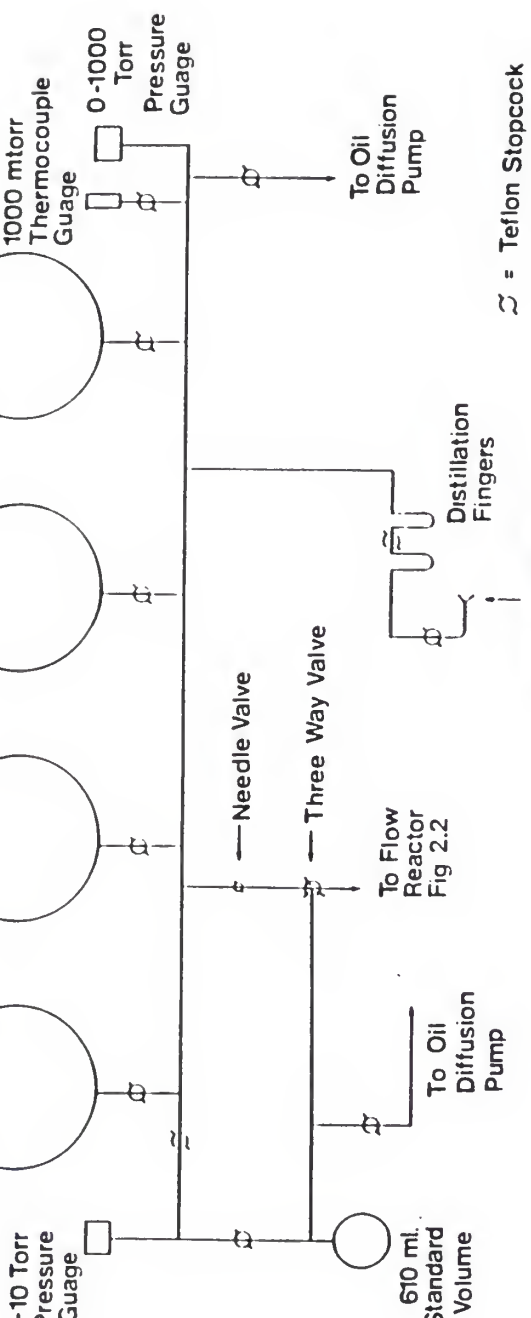

Figure 2.1 Loading and Gas Storage side of the vacuum rack. Also shown in the standard volume used to measure the reagent flow rate during an experiment.

flow meter (Fischer-Porter Catalog number 449-307, tube number FP-1/4-10-6-5, with a constant density glass float) and needle valve, the Ar (now at much lower pressure) passed through two traps cooled to 77 K by liquid nitrogen baths. From these traps the purified Ar went, via 12 mm glass tubing, through a D.C. discharge and then to the 26 mm flow reactor. The Xe was added to the Ar flow before the discharge using a needle valve attached directly to the regulator on the Xe tank. The delivey pressure gauge range on the xenon tank regulator did not allow determination of the delivery pressure. However, the needle valve after the regulator provided a method to regulate the Xe flow, which was adjusted by observation of the characteristic N_2 flames with $Ar(^3P_2)$ and $Xe(^3P_2)$. Sufficient Xe was added to remove the $N_2(C-B)$ emission, which is diagnostic of the $Ar(^3P_2)$ reaction, and replace it with the red $N_2(B-A)$ emission, which is characteristic of $Xe(^3P_2) + N_2$. Gas handling for the CO_2 laser will be discussed in Appendix II.

2.2 Flow Reactor

Figure 2.2 shows the 26 mm ID (inner diameter) flow reactor used for the $Xe(^3P_2)$ + RCl reaction studies. The two NaCl windows allow passage of the IR laser beam through the cell. These polished windows (0.5 cm thick by 4.0 cm diameter) were purchased from Optovac Incorporated. A

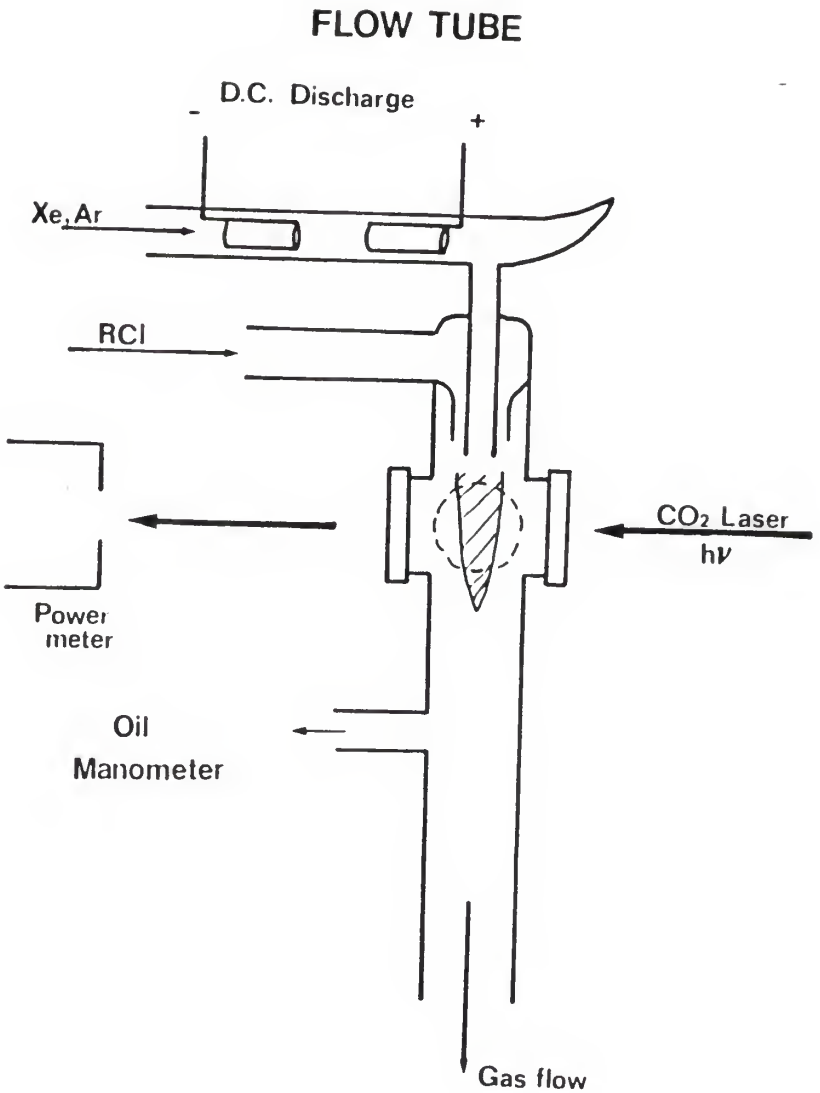

Figure 2.2 Flow reactor used for steady state and enhancement experiments.

quartz window, which allowed passage of UV radiation, was placed perpendicular to the laser path. All three windows were attached to the cell with Conap Epoxy Resin. The Ar/Xe metastable atoms entered from the top of the flow tube where they mixed with the reagent gas, which entered the flow through the outer of the two concentric inlet tubes. The outlet just below the observation region allowed the determination of the pressure in the flow cell with a silicon oil manometer (Dow Corning 704, density = 1.07g/cm^3 at 25C). The density of mercury at 25C is 13.53 g/cm^3, thus the density of silicon oil is approximately 7.9% of the density of mercury; so a 10 millimeter displacement of this fluid in the manometer is equivilent to 0.8 millimeter displacement of mercury or 0.8 Torr pressure.

Two 500 liter/minute pumps working in parallel provided a pumping capcity of about 750 liter/minute. This permitted an operating pressure range of 0.5 to 10.0 Torr. For most measurements a pressure of 1.0 Torr was used, which corresponds to an Ar flow rate of 0.06 mole/minute. This pumping speed gives a linear velocity of 2300 cm/sec in the reactor, which is probably a very good estimate at the manometer outlet where the flows have expanded to the large tube. The linear bulk flow speed depends on the square of radius of the tube (r) according to the following equation,

$$f.s.(cm/sec) = \frac{F_{Ar}RT}{P\pi r^2} = \frac{F_{Ar}}{Pr^2} \times 9.92 \times 10^4 \quad (@\ 300K)$$

where F_{Ar} is in mole/min, r in cm, and P in Torr. Since the observation region for the monochromator is near the inlet tubes for the reagent and the Ar/Xe* gases, it is possible that the bulk flow speed in the reaction region is actually faster than 2300 cm/sec, because the inlet tube for Ar is only 12 mm in diameter. For the purpose of estimating the flow speed in the reaction region, another pressure gauge was connected to the 12 mm tube carrying the argon. This permitted determination of the pressure in the smaller and larger tube simultaneously. Figure 2.3 shows the pressure in the smaller tube for a particular pressure in the larger tube. For 1.0 Torr in the large tube, the pressure in the small tube was 2.6 Torr and the flow speed in the small tube is 6400 cm/sec. See tables 2.1 and 2.2 for data on the variation in flow speeds.

Argon or xenon metastables were produced by passing the Ar or Ar/Xe flow through a hollow cathode discharge. The electrodes were constructed of rolled tantalum foil to fit snuggly into the 12 mm pyrex tube leading to the flow cell. The electrodes were each 2.0 cm in length and separated by a distance of 3.0 cm. The discharge voltage was maintained at 250 V and a current of < 20 milliampere depending on the Ar pressure (increasing Ar pressure

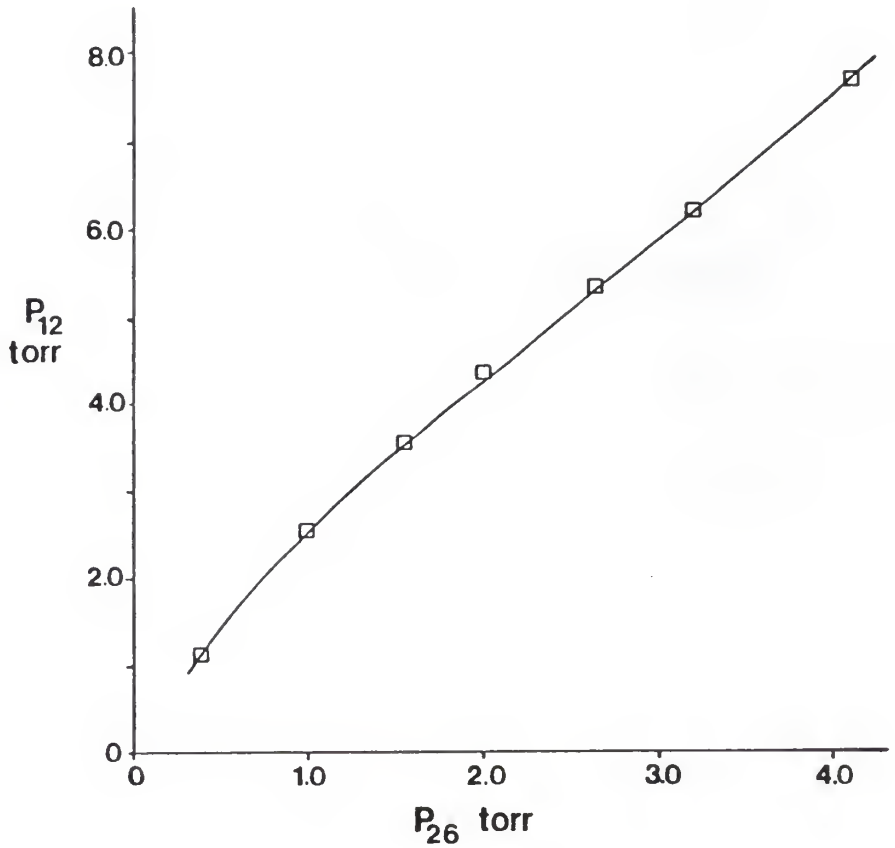

Figure 2.3 The pressure in the 12mm tube (Ar/Xe inlet) was always higher than in the 26mm tube. This is important in estimating the flow speed in the reaction zone.

Table 2.1
Flow Tube Pressure Variance
Data For Figures 2.3 & 2.4

F_{Ar} (ball position)	F_{Ar} (mole/min)	P(12mm) (torr)	P(26mm) (torr)
3.0	0.032	1.12	0.40
4.0	0.047	2.56	1.00
5.0	0.062	3.55	1.55
6.0	0.078	4.38	2.00
7.0	0.093	5.36	2.65
8.0	0.110	6.20	3.20
9.0	0.127	6.88	3.60
10.0	0.144	7.65	4.10

Table 2.2
Flow Speeds

F_{Ar} (ball position)	f.s.(12mm) (cm/s)	f.s.(26mm) (cm/s)
3.0	7870	4700
4.0	5060	2760
5.0	4810	2350
6.0	4910	2290
7.0	4780	2060
8.0	4890	2020
9.0	5090	2070
10.0	5190	2060

increased the current across the discharge). Collision of Ar^* (11.5 eV) with ground state $Xe(^1S_0)$ and direct electron collisions provide a Xe^*(8.3eV) concentration of $\sim 1 \times 10^{10}$ molecule/cm^3 (reference 1).

The flow rate of reagent was measured by observing the pressure rise in a standard volume of 610 ml over a period of 60 seconds. A three-way stopcock (see figure 2.1) was used to direct the flow of reagent to the standard volume (equiped with an MKS Baratron pressure meter with pressure range 0-10 Torr) instead of the flow reactor. Thus, the reagent flow rate is given by

$$F_R \text{ (mole/min)} = \frac{n}{t} = \frac{PV}{tRT} = \frac{P(\text{Torr})}{t(\text{min})} \times 3.23 \times 10^{-5} \quad (@\ 300K).$$

The flow of Ar was determined from the factory calibration curve (fig. 2.4.) for the tri-flat flow meter mentioned in section 2.1. The calibration was confirmed by a wet test meter. Knowing these two flow rates, the concentration of reagent relative to the total (Ar) pressure is

$$[RCl] \text{ (molecule/cm}^3) = \frac{F_{RCl}}{F_{Ar}} P_{Ar}(\text{Torr}) \times 3.24 \times 10^{16}.$$

As we shall see in chapter 4, knowing [RCl] allows determination of the relative rate constant for the formation of XeCl(B,C) under first order reaction conditions.

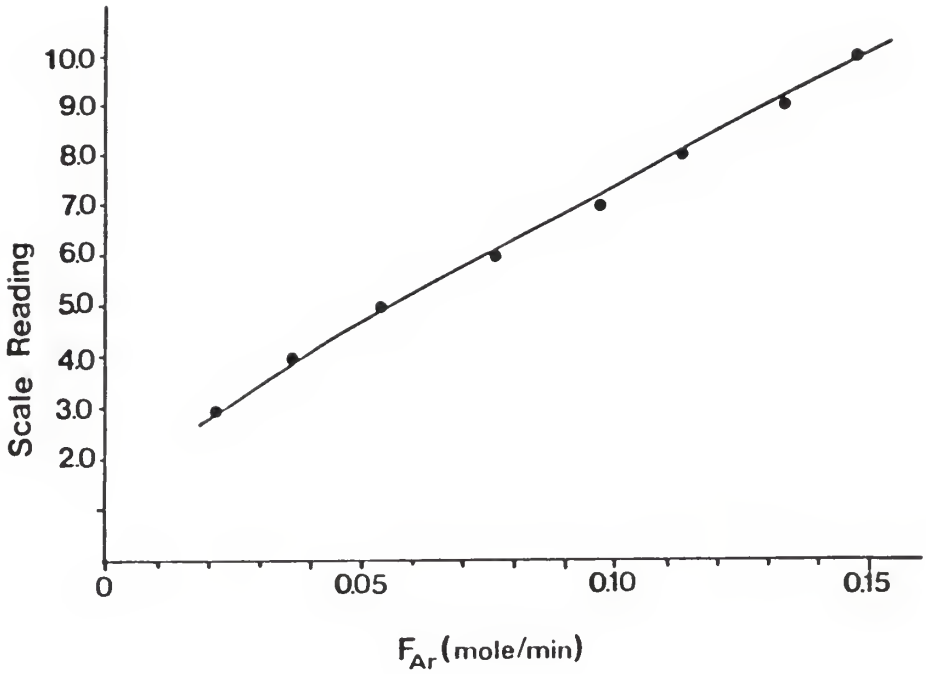

Figure 2.4 Triflat flowmeter calibration. A flow of 0.062 mole/min correspondes to a scale reading of 5.0; the pressure in the reaction zone would be approximately 1.0 torr.

2.3 Measuring the XeCl(B,C) Emission Spectra

Figure 2.5 shows the detection system used for the measurement of the steady-state emission from B-X and C-X transitions of $XeCl^*$. As mentioned previously, the light passed through the quartz window placed perpendicular to the two NaCl windows. The spectrum was recorded with a 0.3 meter McPherson (Czerny-Turner type) monochrometer. The slit widths were usually maintained at 100 um. For the enhancement experiments the monochromator was replaced by an interfenence filter to gain more signal as will be described in section 2.6. The grating in the monochrometer was blazed at 300 nm and had a groove density of 300 grooves/mm. The light, reflectively dispersed by the grating, passed through the exit slit directly to a Hamamatsu R212 photomultiplier tube. The PMT was operated at 950 V with a home made variable gain high voltage supply. The DC output of the PMT was passed through a discriminator and to an SSR Photon Counting System (Princeton Applied Research Inc.). The analog output of the SSR was sent to a strip chart recorder.

A calibrated D_2 lamp (Optronic Lab Inc., model UV-40 #268) was used to calibrate the wavelength response of the monochromater and detection system (see Appendix III for the calibration data). As shown in figure 2.6, the response is almost flat over the region where the greatest

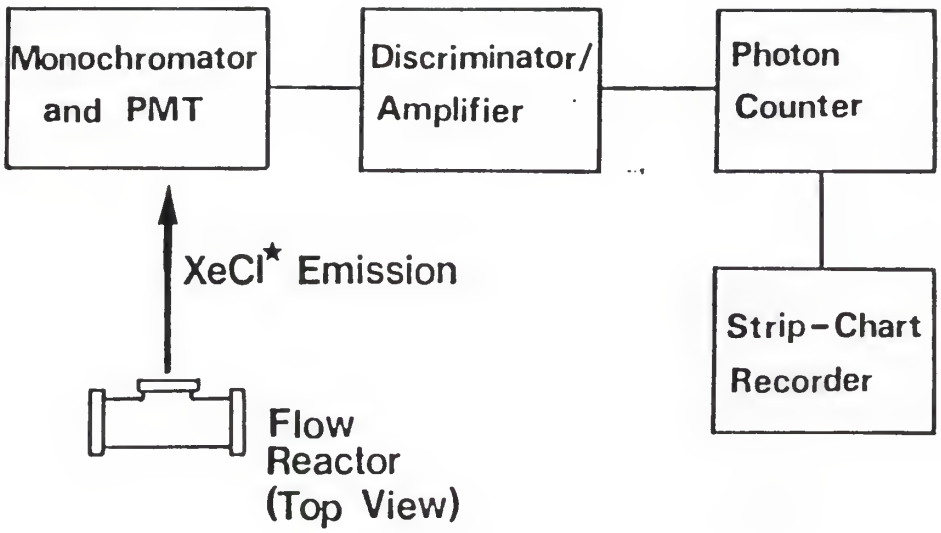

Figure 2.5 Detection system used to take steady state $XeCl^*$ emission spectra.

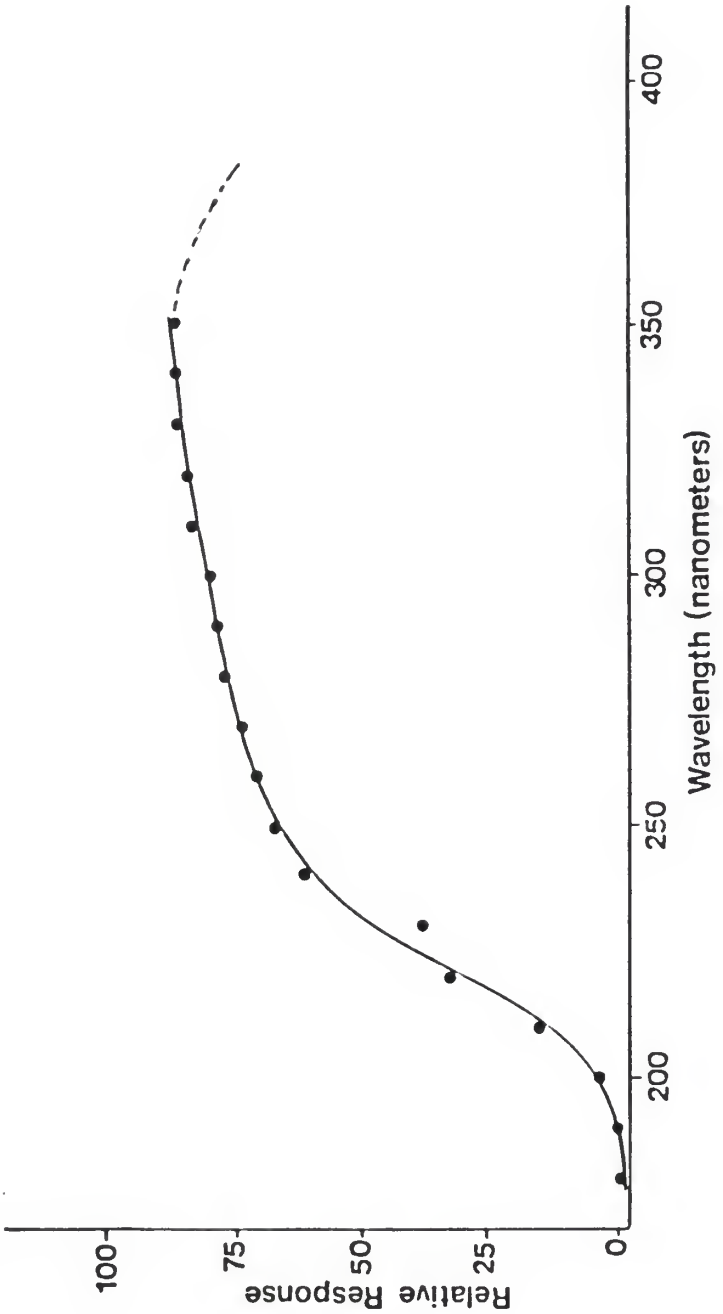

Figure 2.6 Response curve for the detection system shown in figure 2.5. (see Appendix III for data)

XeCl(B-X) and (C-A) emission occur and really only deviates seriously below 240 nm and above 380 nm, therefore the XeCl(B-X) spectra were integrated without correction. The integrated XeCl(B-X) intensities (in some cases only the peak heights at 308nm) were used for determination of the rate constant for XeCl(B,C) formation and branching fractions.

2.4 CO_2 Laser Operation

The CO_2 laser, like all lasers, operates by attaining a population inversion between certain energy levels. Unlike the more commonly known laser systems (e.g. Nd Yag, Excimer, or Dye laser) which involved electronic energy levels, the CO_2 laser emmission corresponds to transitions between vibrational energy levels of the CO_2 ground electronic state. These vibrational transitions are adequately described by the three normal modes of the CO_2 molecule. Figure 2.7 a) illustrates the motion of the carbon and oxygen atoms with respect to one another, which corresponds to ν_1, ν_2, and ν_3. The vibrational energy of the CO_2 is the sum of energies of three independent vibrational modes,

$$E(v_1,v_2,v_3) = h\nu_1(v_1 + 1/2) + h\nu_2(v_2 + 1/2) + h\nu_3(v_3 + 1/2)$$

where v_1, v_2, and v_3 correspond to the vibrational energy

Figure 2.7

a.) Representation of the vibrational modes of CO_2. Note that the second mode is doubly degenerate and another motion would be oscillation in and out of the plane of the paper.

b.) Energy level diagram illustrating population and lasing of the asymmetric stretch of the CO_2 molecule. Wavy lines represent energy transfer (non-lasing).

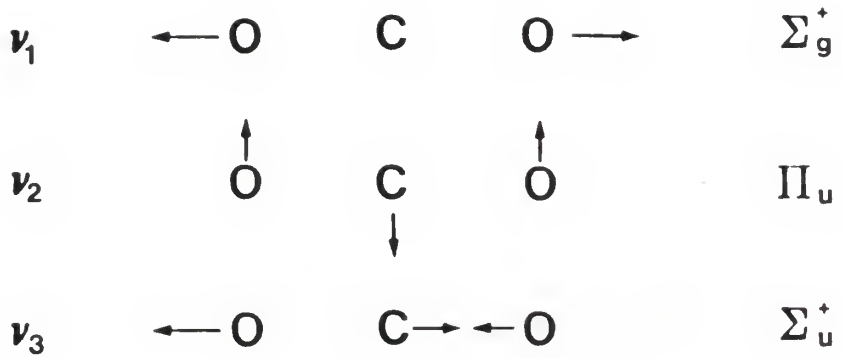
ν1
O C O
Σ+g
ν2
O C O
Πu
ν3
O C O
Σ+u

a)

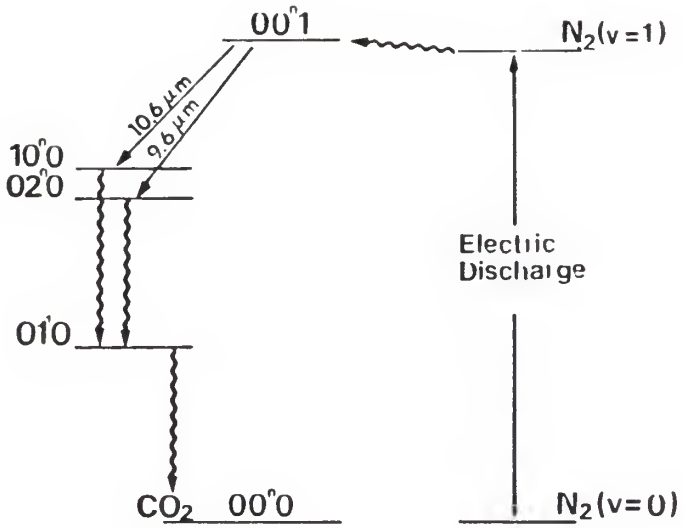
00°1
N2(v=1)
10.6 μm
9.6 μm
10°0
02°0
Electric
Discharge
01°0
CO2 00°0
N2(v=0)

b)

levels of each of the three oscillators. Thus, it is common to use the notation (v_1,v_2,v_3) to describe the energy levels of the CO_2 molecule.

The upper lasing level of the CO_2 molecule is designated (00^01) with one quanta of vibrational energy in the ν_3 non-symetric stretch oscillator. Not included in the equation above are the rotational states of the vibrational levels, which could be described by a Boltzmann distribution similar to equation 3.1. The rotational states in the (00^01) level lead to a range of wavelengths around 10.6 um (961 cm^{-1}) and 9.6 um (1063.8 cm^{-1}) corresponding to the familiar P and R branches for each of the transitions between this upper level and the (10^00) and (02^00) levels, respectvely.

Figure 2.7 b) shows the vibrational transitions relevant to the lasing process, as well as the other pertinent energy levels. Population of the (00^01) level is accomplished by two routes. One is direct excitation by electron collisions. If the laser is operated with only He and CO_2, energies of < 1 J/pulse and pulse widths of < 10 ns (fwhm) are available. When operated with a $He/N_2/CO_2$ mixture, energies of up to 15 J/pulse with a FWHM pulse width of 250 ns (fwhm) are attainable. Our laser was operated at about 3 J/pulse with a fwhm pulse width of 250 ns. (The beam diameter was almost 3 cm but was masked to 1.8 cm so that it could pass through the NaCl windows on the reaction cell.) Figure 2.8 shows the laser pulse

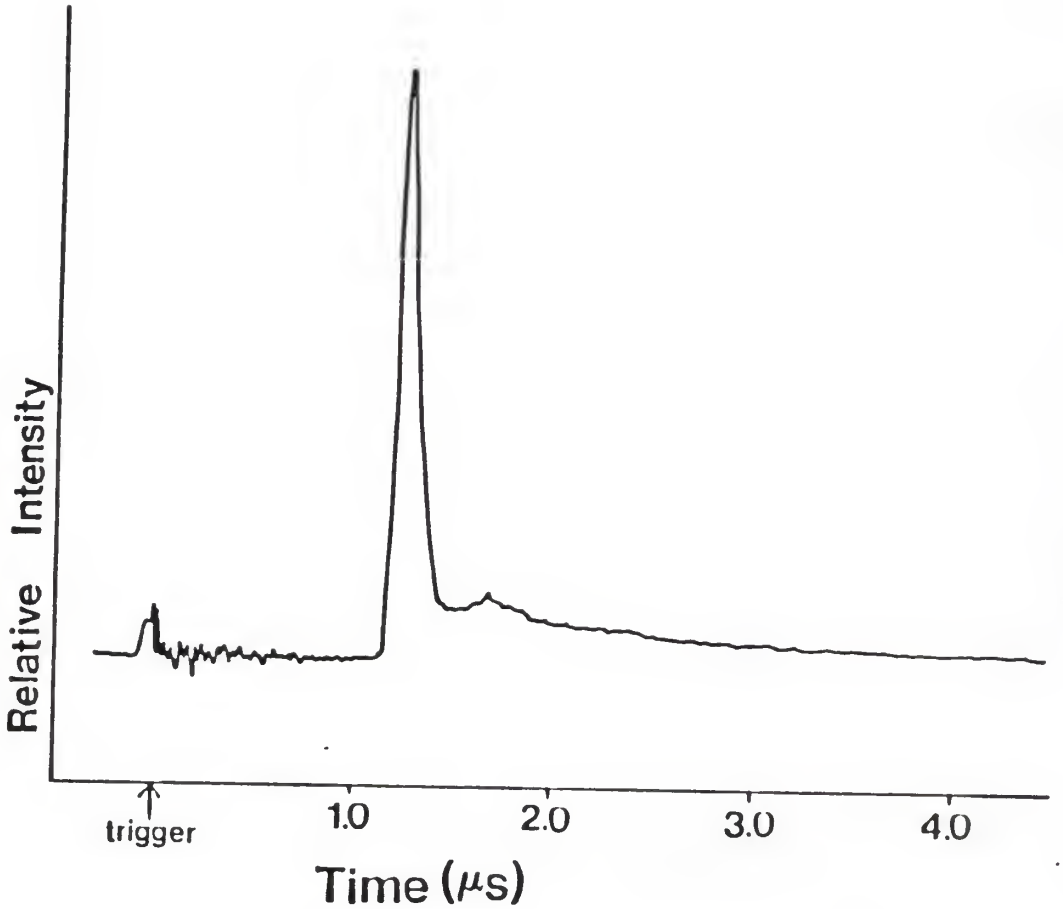

Figure 2.8 CO_2 Laser Pulse taken with a photon drag detector and LeCroy 9400 digital oscilloscope.

occured 1.2 us after the trigger with a tail extended slightly more than 1.5 us. Refering to figure 2.7 b) the increase in energy output with N_2 in the mixture is explained by the close energy match of the $N_2(v=1)$ state with the $CO_2(00^01)$ energy level. The cross-section for $N_2(v=0) + e^-$ to give $N_2(v=1)$ is much larger than the analogous reaction for CO_2. Vibrational energy transfer from collision of the excited $N_2(v=1)$ with ground state CO_2 provides a greater population inversion at the expense of having to accept a longer pulse.

The Lumonics Series 100 TEA CO_2 Lasers operate by a method known as transverse excitation at atmospheric pressure (thus TEA). The excitation is accomplished by discharging three capacitors across electrode plates, which are geometrically constructed and positioned in such a way to provide a very uniform electron plasma through the $He/N_2/CO_2$ gas mixture in the laser cavity. The electrons provide direct pumping of the upper lasing level of CO_2, as mentioned in the previous paragraph, as well as providing excited N_2. A problem typically encountered in this type of laser system, which periodically occured with our laser, is known as bright arcing. Bright arcs are the result of the unstable electron plasma, across the relatively high pressure in the cavity, constricting into thin arc channels. When this occurs, the system will not provide laser action. As the name suggests, bright arcs are readily observable as flashes. Blue light eminating from

the gaps between the protruding control knobs and the laser cover indicate bright arcs. Typically, bright arcs were observed once every 100 pulses. If they occured with higher frequency, the gas flows (pressures) were adjusted to a more appropriate range. Appendix II describes, the operation and up-keep of the laser used in these experiments.

2.5 Measuring the Absorbed IR Laser Energy

The IR absorption was measured by comparison of the laser energy passed through an empty cell to the energy passed through the same cell with an known concentration (pressure) of reagent, or reagent plus argon buffer gas. The cell was fitted with a 9 mm O-ring connector to enable attachment to the vacuum rack. As with the flow reactor, the windows were attached by Conap Epoxy Resin. The NaCl windows were polished by the manufacturer, however after extended use it was sometimes necessary to remove the windows from the cell and re-polish them. A window could be removed from the cell by slowly warming it with a heat gun and giving it a slight twist to free it from the epoxy. (The warm epoxy had a rubbery texture and could be peeled from the window easily.) The deep scratches could be removed from the windows by rubbing them on fine sandpaper and emory paper placed on a flat surface. Fine polishing was done with a ground glass plate and felt pad using #600

CeO polishing grit. Reagent gases were loaded into the cell and the pressure monitored by a 0-10 Torr range MKS Baratron pressure head. The cells were 26 mm inner diameter, which allowed easy alignment of the 18 mm diameter laser beam. The laser energy was measured directly with a Scientech calorimetric detector, which read directly in Joules. The experimental arrangement was quite simple and is shown in figure 2.9. This arrangement allowed measuring as little as 5% absorption with an uncertainty of ±10%.

When the absorbed energy was to be measured in the presence of a buffer gas, the gases were loaded into the cell in the following manner. First the reagent was loaded into the cell (usually 0.5 Torr) by expansion from a reservoir. Then the valve to the cell was closed and the reagent line evacuated. Then argon was loaded into the line (at a higher pressure than the reagent) to approximetely the desired pressure. Opening the valve to the cell, the argon rushed into the cell and when the pressure stopped falling the valve was closed quickly to insure that no reagent diffused out of the cell.

The amount of energy absorbed by the reagent is simply $E_o - E$, where E_o is the energy measured passing through the empty cell and E is the energy passing through the cell with some reagent gas present. This energy difference may be expressed as the average number of photons absorbed by each molecule

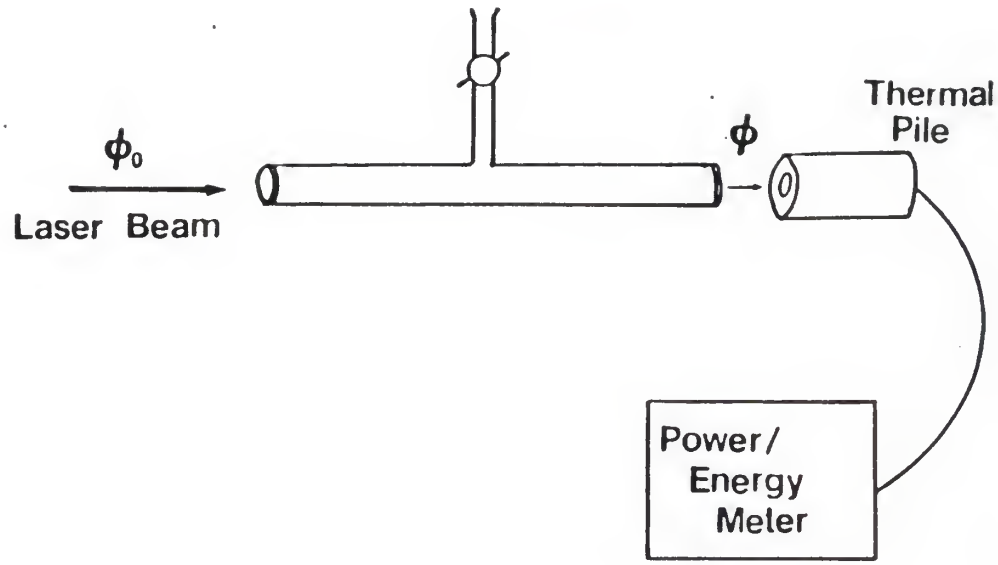

Figure 2.9 System used to measure the energy absorbed by a gas sample in the laser path. The incident fluence was actually measured with the cell evacuated but still in the beam's path.

$$\langle n \rangle = \frac{E_o - E}{h\nu N}$$

where $h\nu$ is the energy of a single photon (2.16×10^{-20} Joules at 9.2 um) and N is the number of molecules in the irradiated volume of the sample, thus implying that each molecule in the irradiated volume absorbs the same number of photons. This equation was generally used in the following form

$$\langle n \rangle = \frac{E_o - E}{h\nu (n/V) V_{irr}}$$

where n/V is the concentration of gas as calculated from he ideal gas law and V_{irr} is the volume irradiated by the laser beam

$$V_{irr} = \pi r^2 l$$

where r is the radius of the laser beam (0.9 cm) and l is the length of the cell. The cells were either 29, 49, or 115 cm in length. The cell used for a particular gas pressure was choosen such that there was no more than 50% absorption and no less than what could be measured reliably ($\leq$10%). The reason for this restriction was that the absorption cross section for some molecules may be dependent on the incident fluence, (fluence is defined as $\phi_o = E_o/A$ where A is the cross section area of the laser beam) and if the sample absorbs, for example, 50% of the energy in the first half of the cell, the molecules absorbing in the second half will not see the same incident fluence as those in the first half. If the absorption cross section for a molecule actually increases with decreasing fluence, $\langle n \rangle$ will appear larger than it should

be for the incident laser fluence. As shall be seen in the next chapter, the dependence on fluence was only important for one of the reagents (CF_3Cl), however for the sake of consistancy we used the same cell length criterion for all reagents.

Table 3.3 lists some typical data for the three freons. The <n> calculated by the energy difference method described above is compared to the <n> calculated by the cross section obtained from Beer's law. In terms of Beer's law, $\ln(\phi_o/\phi) = \sigma lc$, where l is the path length (cm), c is the concentration (molecule/cm^3), ϕ_o/ϕ is the fluence ratio, and σ is the absorption cross-section in units cm^2/molecule. In this formulation σ is assumed to be independent of fluence. Rearranging this equation and using the ideal gas relation c = n/V = P/RT gives

$$\sigma = \frac{RT}{Pl} \ln \frac{\phi_o}{\phi}.$$

The average number of photons absorbed per molecule may be calculated by

$$\langle n \rangle = \frac{\sigma \phi_o}{h\nu} \text{ (photons/molecule)}$$

where $h\nu$ is the energy of a single photon in Joules. These two equations will be used in section 3.3 in describing the dependence of absorbed energy on incident fluence.

2.6 Measuring the XeCl(B,C) Emission Enhanced by the CO_2 Laser

Detection of the XeCl(B,C) emission arising from the moleules excited by the CO_2 laser differs from the steady state observations. Since the CO_2 laser is pulsed, the vibrationally excited RCl, RCl^{**}, are produced rapidly by the 1.5 us laser pulse and then decay exponentially as the vibrational energy was relaxed by argon collisions, as the vibrationally excited molecules flow out of the field of view and, of course, as these molecules react with Xe^*. The enhancement ratio is defined as the ratio of the $XeCl^*$ emission intensity (I_e) enhanced by the CO_2 laser relative to the $XeCl^*$ steady-state emission intensity (I_{XeCl^*}) without the laser pulse.

Due to the low repetiton rate of the CO_2 laser, it was not possible to obtain a XeCl(B-X) emission spectrum (230-320nm) from the CO_2 laser experiment. However, the emission at 308nm will have the save fraction of the B-X emission for the laser enhanced reaction as for the steady state reaction because the XeCl(B-X) 308nm emission includes some emission from all vibrational levels.[4] As shown in figure 4.3, the $XeCl^*$ emission is strongest around 308nm. Therefore, a filter which observed from 295 to 355nm was used to monitor the enhanced XeCl(B,C) formation.

In order to observe the $XeCl^*$ signal change after the laser pulse, it was necessary to use a detection system

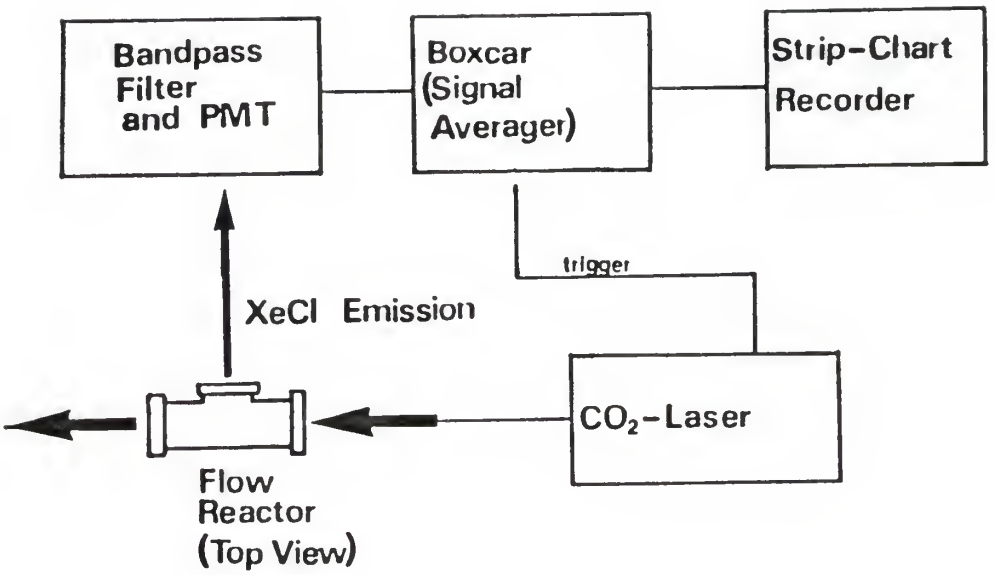

Figure 2.10 Detection system used to measure $XeCl^*$ enhanced by the addition of vibrational energy to RCl. See the text for an explanation of the changes made relative to the observation of steady state $XeCl^*$ emission (figure 2.5).

with adequate response time and one that permitted signal averaging. With the monochromator set at 100 um slits a typical count rate for the steady state XeCl(B) emission was $3x10^4$ counts/s. Since the $XeCl^*$ following the laser pulse lasts only 100-200us and we wanted to define the time profile, we needed time resolution of at least 5 μs. During a 5 μs period the number of counts was less than one. Replacing the monochromator with a filter centered at 320±25 nm increased the signal by 50-100 times depending on the voltage to the PM tube. With the filter the signal level was several counts per 5 μs time interval. The response time of the PMT is on the order of 0.1 ns, so the time response of the PM tube was not a limiting aspect. The output of the PMT was terminated by a 10 Kohm resistor at the PM tube base, and then passed to the 1 Mohm input of the PAR Boxcar (model 162 boxcar with model 164 gated integrator). The output of the boxcar is a 10 V full scale signal, which was sent to a strip chart recorder.

The boxcar was triggered by the sync output of the CO_2 laser power supply, which occured 1.0 us prior to the onset of the laser pulse (see figure 2.8). Figure 2.10 shows this detection system. The response time of this detection scheme was compared to a 125MHz digital oscilloscope (LeCroy model 9400) with 50 ohm termination throughout the signal path and 50 ohm termination at the PM tube base. The enhancement profile was the same with both detection systems. A gate width of 5 μs for the boxcar was

found to be best for the available signal level. A count rate of 200,000 (typical $XeCl^*$ steady state signal level with the bandpass filter) on the photon counter corresponded to a current of 1000 nA from the PM tube. With the 10 Kohm terminator at the base this provided a voltage of 10 mV. With this voltage level it was not necessary to use an amplifier before the boxcar (the boxcar input range is ±500mV). Figure 4.6 shows a time profile for the enhancement of the reaction of RCl^{**} with $Xe(^3P_2)$. The 5 μs gate was positioned at varying times after the laser pulse and the signal was summation averaged for a time long enough to give a significant pen deflection on the strip chart recorder. For CF_2Cl_2 the background ($XeCl^*$ steady-state) was averaged for ten to twenty laser pulses which provided about 0.2 to 1 V deflection on the chart recorder (10 V is full scale). With the laser enhancing the reaction, ten pulses provided a deflection of 6 to 7 volts. The enhancement ratio is simply the ratio of these two signals.

Prior to using this detection system, no terminator was at the base of the PM tube and the the 1 Mohm input of a wideband preamp was used before the boxcar. This caused serious distortion in the enhancemed $XeCl^*$ signal, giving a maximum enhancement ratio of 2.0 for CF_2Cl_2 occuring 50 us after the laser pulse, and a tail extending to 1000 us. The main cause of the distortion was the RC time constant encountered at the 1 Mohm terminator of the preamp. Since

this input had a specfied input capacitance of 20 pF, the RC time constant was 20 us which was far too slow for the signal change indicated in the enhancement profiles of chapter 4, with maximums at 15 us. Another problem was that the length of the cable leading from the PM tube base to the preamp was about 4 inches long. Due to intrinsic impedence of the cable and the electrical noise that was picked up in that length, this was a poor way to connect the PM tube base and the pre-amp. To measure signal from the PM tube, the base should be terminated with a resistance before passing the signal to a cable of any significant length. It was determined that with a 1 inch cable between the base and the discriminator to the photon counter there was very little change in the signal level with/without a 50 ohm terminator; a longer cable gave decreased signal without the terminator at the base.

References: Chapter 2

1.) J.H. Kolts and D.W. Setser, Reactive Intermediates in the Gas Phase, Chapter 3, Academic Press, Inc., New York, 1979.

2.) D.W. Setser, D.H. Stedman, and J.A. Coxon, J.Chem.Phys., 53, 1004, 1970.

3.) Amnon Yariv, Optical Electronics, pp. 211-214, CBS College Publishing, New York, 1985.

4.) T.D. Dreiling and D.W. Setser, J. Chem. Phys., 75(9), (1981) 4360

CHAPTER 3 INFRARED ABSORPTION BY POLYATOMIC MOLECULES

3.1 IR Multiphoton Absorption (IRMPA) Model

The phenomenon of IRMPA for polyatomic molecules has been studied at various levels of sophistication (references 16-26, chapter 1). For our purpose we will follow the simplest approach and divide the 300 K Boltzmann sample into two groups; those molecules which absorb the laser energy and those which do not[1-3] This approach allows estimation of the amount of energy absorbed by the fraction participating in IRMPA from measurement of the bulk energy absorption, which is expressed as the average number of photons per molecule, $\langle n \rangle$, as described in section 2.5.

At 300 K most of the molecules will be in their ground vibrational state, as may be shown by the Boltzmann equation for a harmonic oscillator, which represents the vibrational mode envisioned as the pump mode.

$$N_v/N = (1/q)e^{-h\nu v/kT}$$

N_o/N is the fraction of molecules in state v=0 of the mode of interest, h is Planck's constant, k is the Boltzmann constant, T the temperature in degrees Kelvin, and q is the vibrational partition function $q = \sum \exp(-h\nu v/kT)$ (sum over

all v's). For example, CF_3Cl at ν = 1090 cm^{-1} for the C-F stretching frequency gives q = 1.005377 and N_o/N = .995. Even at low temperatures, many rotational states for v=0 will be populated. To calculate the distribution for a symmetric top model,[4] values for $A = h/8\pi^2cI_a$ and $B = h/8\pi^2cI_b$, the rotational spacing constants, are needed. I_a and I_b are the moments of inertia, c = speed of light and h = Plancks constant. It can be shown that the rotational distribution for a given J,K level this prolate symetric top is approximated by

$$N_{J,K}/N = (2J + 1)g_K\exp(-E_{J,K}/kT)/Q_r$$

where k is the Boltzmann constant in, T the temperature in degrees Kelvin, g_K is the degeneracy for a given K level (described in Appendix II), and the energy levels are given by

$$E_{J,K} = BJ(J + 1) + (A - B)K^2$$
$$J = 0,1,2,3,.... \qquad K = 0,\pm1,\pm2,....,\pm J$$

To calculate the distribution for each value of J, it is necessary to sum over the possible values of K. Figure 3.1 shows the rotational distribution function for each J for CF_3Cl up to J=150 for T=300K. (The details and a listing of the program used for this calculation are in the appendix.) Also shown in figure 3.1 is a representation of

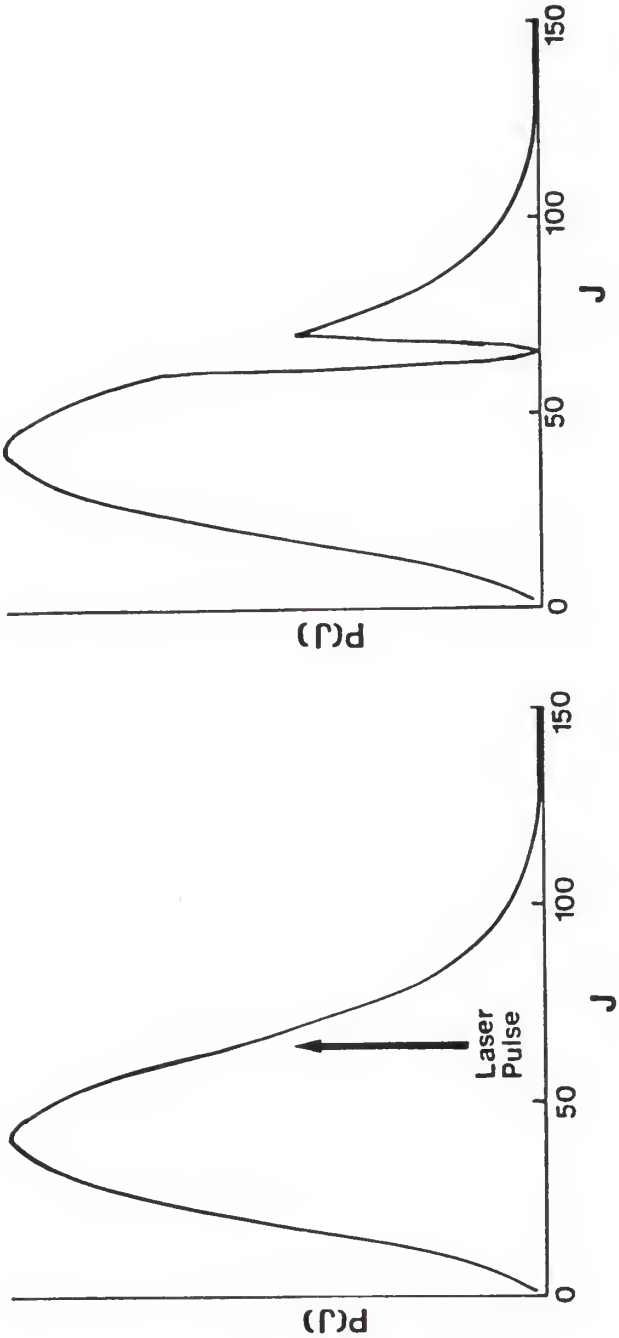

Figure 3.1 Illustration of the CO_2 laser pulse removing a fraction of the v=0, 300K rotational population. The position of the laser pulse is only schematic.

Figure 3.2

a.) Infrared absorption spectra taken on the Perkin-Elmer 180 Spectrometer at a resolution of 1.0-2.0 cm^{-1}. The RCl pressure was 4.0 Torr for each and the cell length was 10.0 cm.

b.) Relative Gain Curve for some vibrational-rotational transitions of CO_2, resembling a typical CO_2 laser output range.

c.) High resolution (0.013 cm^{-1}) IR spectra for the CF stretching band of CF_2Cl_2. Provided by K.C. Kim, Los Alamos National Lab.

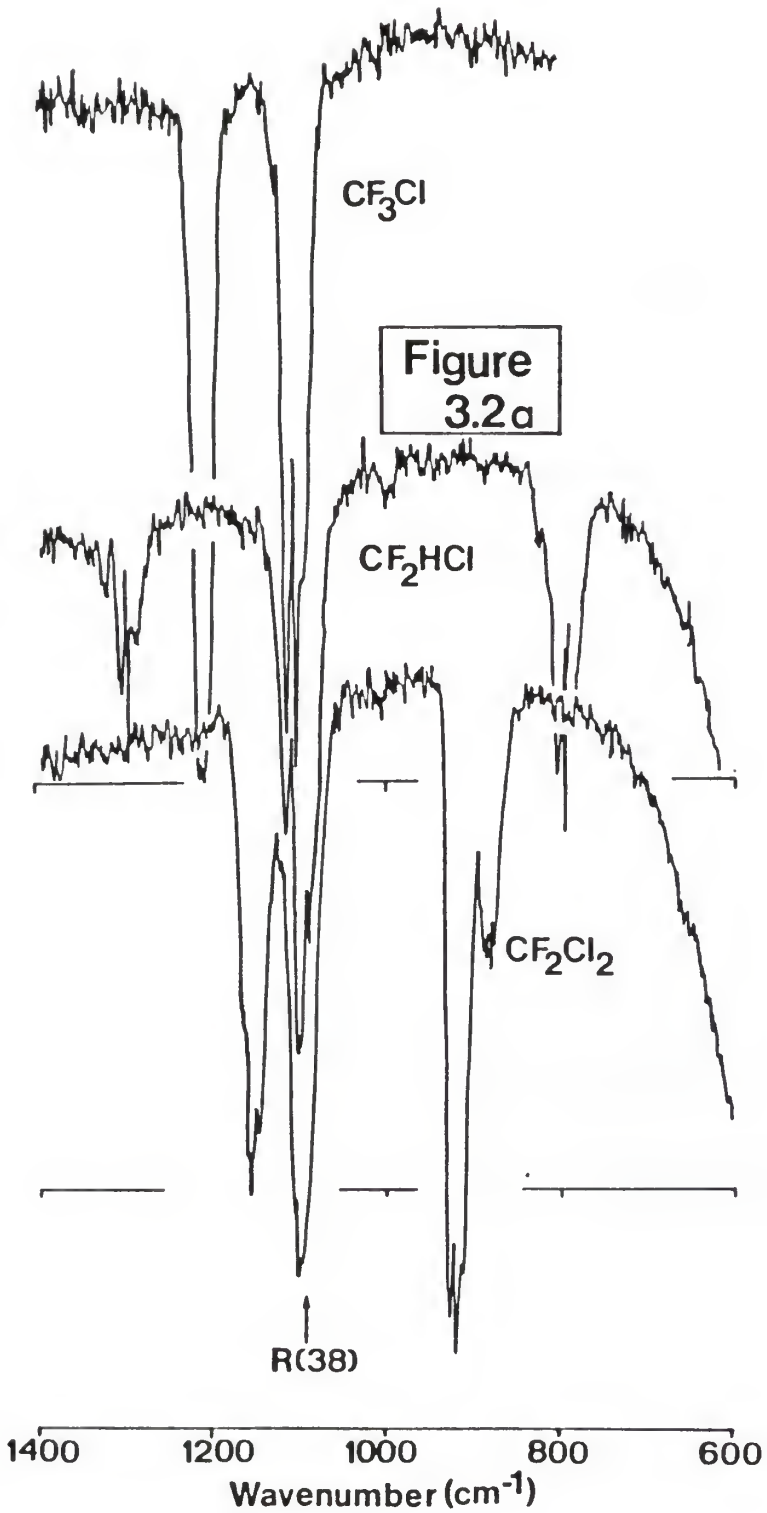
CF3Cl
CF2HCl
CF2Cl2
R(38)
1400
1200
1000
800
600
Wavenumber (cm-1)

Figure 3.2a

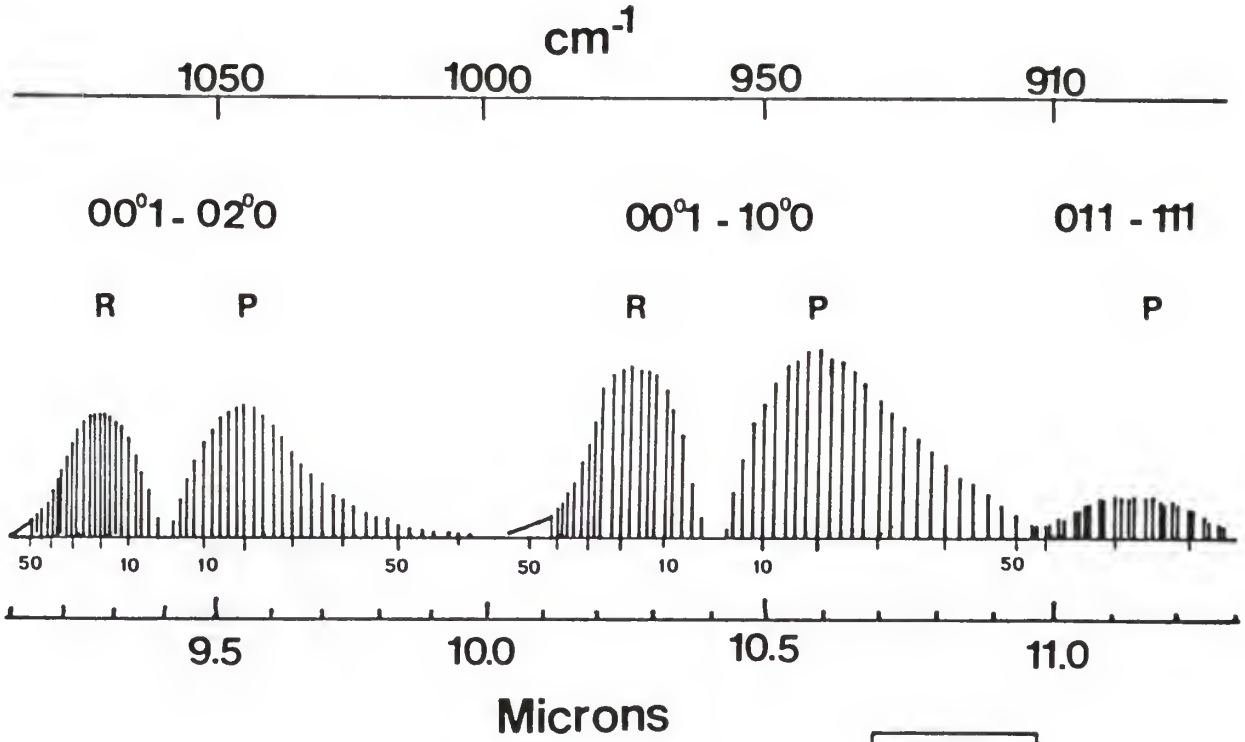
cm-1
1050
1000
950
910
00°1 - 02°0
00°1 - 10°0
011 - 111
R
P
R
P
P
50
10
10
50
50
10
10
50
9.5
10.0
10.5
11.0
Microns

Figure 3.2b

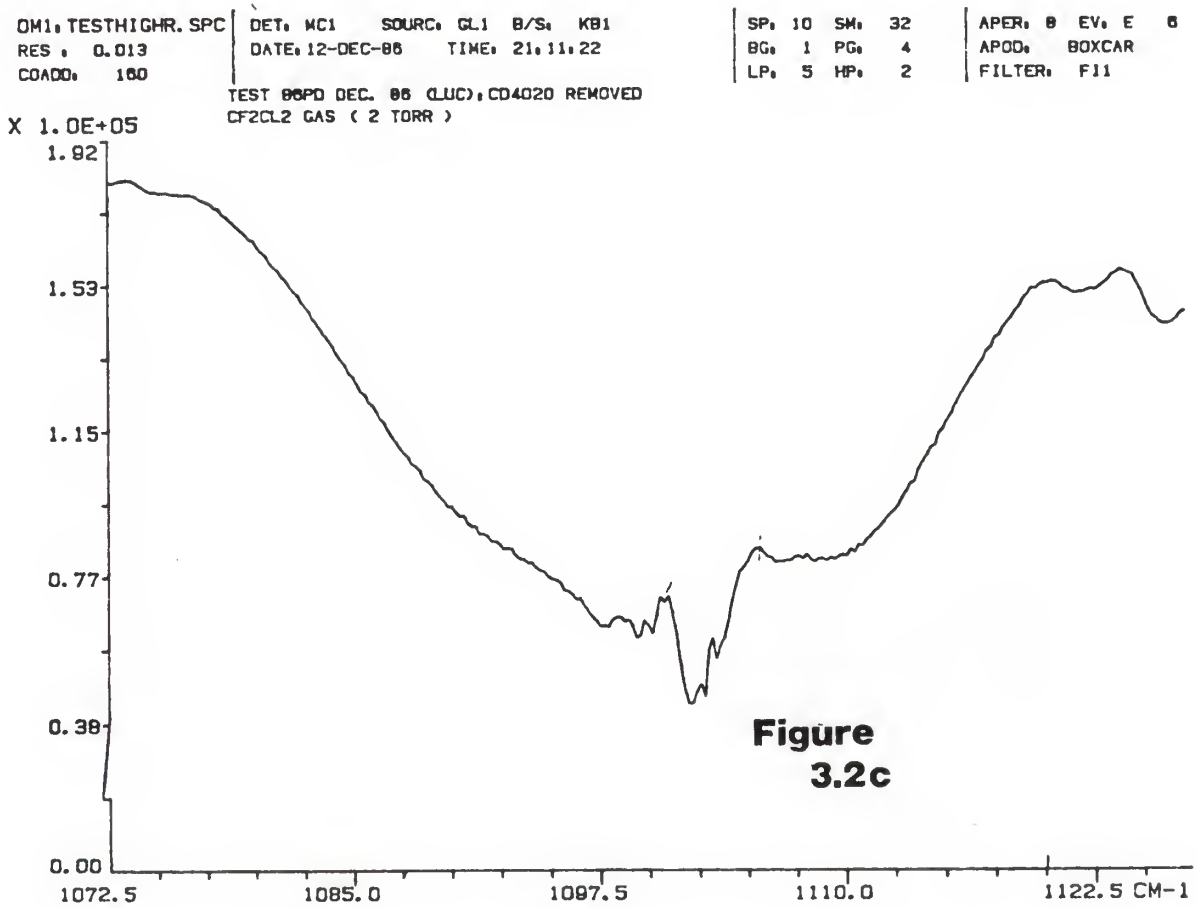
OM1: TESTHIGHR. SPC
RES : 0.013
COADD: 160
DET: MC1 SOURC: GL1 B/S: KB1
DATE: 12-DEC-86 TIME: 21:11:22
SP: 10 SM: 32
BG: 1 PG: 4
LP: 5 HP: 2
APER: 8 EV: E 6
APOD: BOXCAR
FILTER: F11
TEST 86PD DEC. 86 (LUC): CD4020 REMOVED
CF2CL2 GAS (2 TORR)
X 1.0E+05
1.92
1.53
1.15
0.77
0.38
0.00
1072.5
1085.0
1097.5
1110.0
1122.5 CM-1

Figure 3.2c

a pulse from the CO_2 laser. The laser band width reported by the manufactuer is 0.03 cm^{-1}. This suggests that only a fraction of the molecules in v=0 will absorb laser enrrgy, i.e. that fraction of the sample with occupied rotational states in resonance with the laser band width. This energy match requisite results in the "Rotational Bottleneck" as identified by Letokhof.[5] (For asymmetric tops such as CF_2Cl_2 or CF_2HCl the calculation of a rotational energy distribution is considerably more involved because the energy levels cannot be expressed as simply as for the symmetric top for which two of the three moments of inertia are equal.[4]) Various broadening mechanisms actually bring more rotational states into resonance with the laser frequency than predicted by this simple argument but for small molecules such as these, the fraction absorbing is less than 0.5.

3.2 Broadband IR Absorption Spectra and Absorption Coefficients

Absorption spectra were taken on a Perkin-Elmer 180 dual beam IR spectrophotometer operated with a resolution of 1.0-2.0 cm^{-1}. Samples were loaded into the 10.0 cm cell from the vacuum rack as described in section 2.5. Survey scans over the range 4000 to 600 cm^{-1} were taken for each sample to verify absence of water and other manufacturing impurities. Absorption spectra of CF_2Cl_2, CF_3Cl, and

CF_2HCl are shown in figure 3.2a in the range 1400 to 600 cm^{-1}. Figure 3.2b shows the available output of the CO_2 laser lines. The match of the R_{38} line with the strong C-F stretching frequency at 1090 cm^{-1} makes this a viable choice for pumping the the freon molecules.

The IR absorption spectra also provide data for calculating the broadband absorption cross section.[6] Expressing Beers Law in the following form

$$\ln(I_o/I) = \sigma lc$$

where l is the path length, c is the concentration, and I_o/I is the usual intensity ratio, and σ is the absorption coefficient. Taking absorption spectra at several pressures in the range of 0.5-5.0 torr, plots of $\ln(I_o/I)$ vs lc are linear (figure 3.3) with slope of σ_o, the broadband absorption cross section. The subscript "o" will be used, σ_o, to signify that this is the broadband absorption cross section. The dependence of absorbed energy and absorption cross section on fluence will be described in the next section. Table 3.2 lists the σ_o as calculated from the linear least square slope of the data in figure 3.3.

3.3 Absorbed Energy as a Function of Incident Fluence

The equations at the end of section 2.5 show that $\langle n \rangle$ has a

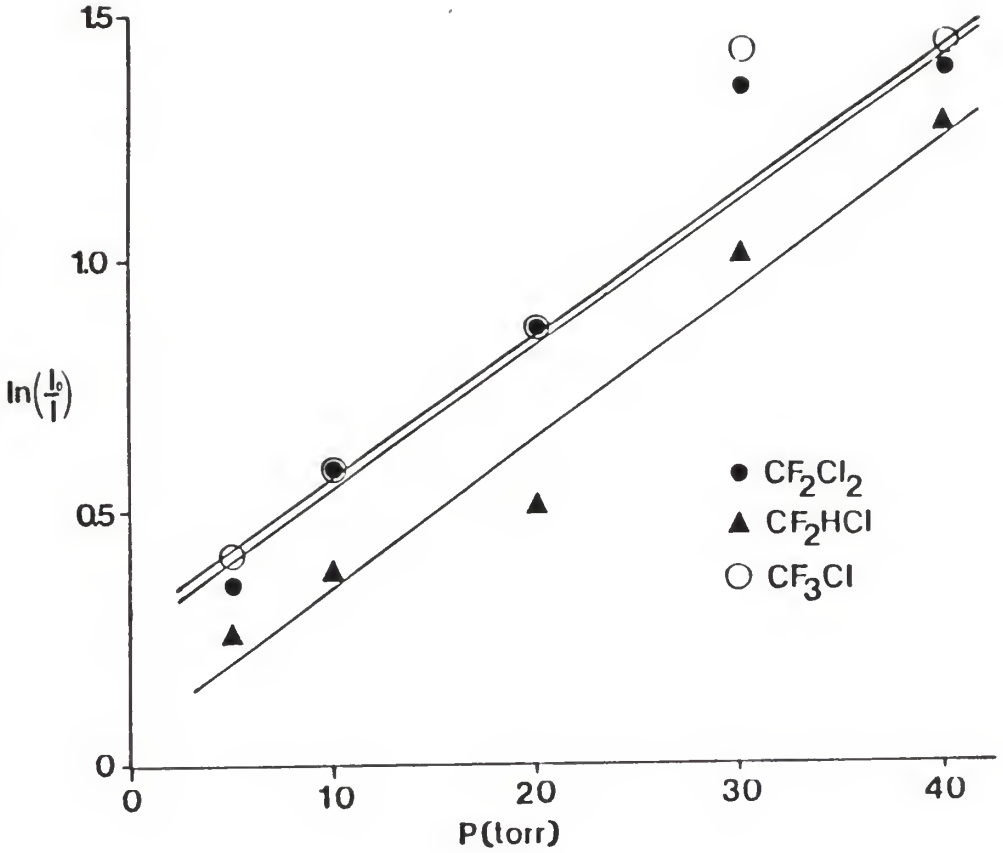

Figure 3.3 Broadband (2.0 cm^{-1}) absorption cross sections were calculated from the slopes of these lines. Data for these plots are in table 3.1 and was taken from IR spectra like those in figure 3.2a.

Table 3.1
Broadband Absorption
and Cross Sections

P_{RCl} (torr)	I/I_o	$\ln(I_o/I)$	
40	0.25	1.386	CF_2Cl_2
30	0.26	1.347	
20	0.42	0.867	$\sigma_o=(8.9\pm0.94)\times10^{-19}$
10	0.56	0.580	cm^2/molecule(d)
5	0.70	0.357	
40	0.28	1.273	CF_2HCl
30	0.36	1.022	
20	0.60	0.511	$\sigma_o=(9.2\pm0.80)\times10^{-19}$
10	0.68	0.386	cm^2/molecule(d)
5	0.77	0.261	
40	0.24	1.427	CF_3Cl
30	0.24	1.427	
20	0.42	0.867	$\sigma_o=(8.8\pm1.10)\times10^{-19}$
10	0.55	0.598	cm^2/molecule(d)
5	0.66	0.416	

a.) I/I_o values were taken from the IR absorption spectra at 1089 cm^{-1}
b.) All gasses were prepared as a 10% RCl/Ar mixture
c.) Cell length was 10.0 cm
d.) The error limits are from the standard deviation from the linear least squares analysis[10]

linear dependence on ϕ_o, the incident fluence, if σ, the laser absorption cross-section, for a particular molecule is independent of ϕ_o. Figure 3.4 shows the σ of CF_3Cl, CF_2HCl, and CF_2Cl_2 vs ϕ_o ranging from 0.05 to 0.7 J/cm^2. Also shown in this figure are the values of σ_o, the broadband absoption cross-sectin described in the previous section. For CF_2HCl and CF_2Cl_2 σ is independent of ϕ_o, however the absorption cross section for CF_3Cl decreases with increasing fluence. To compare $\langle n \rangle$ from $\sigma(\phi_o)$ figure 3.5 shows $\langle n \rangle$ calculated from σ for all three gasses. The $\langle n \rangle$ for CF_2Cl_2 and CF_2HCl increased linearly with ϕ. That for CF_3Cl appears to be linear because of the small scale, but comparison of the data in Table 3.2 shows that the increase of $\langle n \rangle$ was less than the ϕ, i.e. a 20 fold increase in ϕ gave only a 10 fold increase in $\langle n \rangle$. In order to measure the energy absorbed by the gas sample without inducing error from "nonlinear" absorption, provisions were made (see section 2.5) so that the fluence did not vary by more than 50% over the length of the cell.

3.4 Absorbed Energy as a Function of Pressure

The absorption is dependent, not only on the intrinsic absorption cross section and fluence, but also on the rotational and vibrational relaxation occuring during the laser pulse. In collisionless conditions (no collisions in the time frame of the laser pulse) the model descibed in

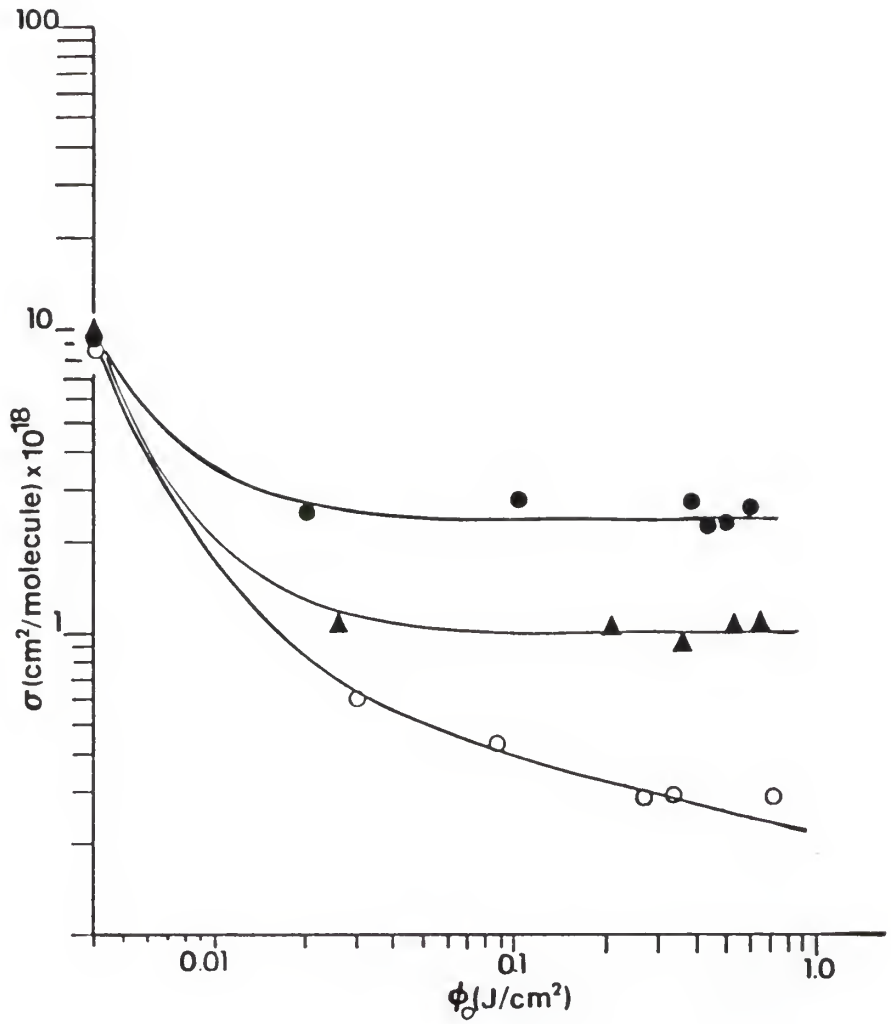

Figure 3.4 Absorption cross section as a function of incident fluence. The intercepts are the broadband cross sections. CF_2Cl_2(●), CF_2HCl(▲), CF_3Cl(○).

Table 3.2
Absorption Cross Section and <n>
for Varying ϕ_o
Data for figure 3.4 & 3.5

ϕ_o J/cm^2	ϕ J/cm^2	P torr	σ cm^2/molecule	<n>[a] photon/molecule	<n>[b] photon/molecule
			CF_2Cl_2		
0.601	0.179	5.0	2.58×10^{-19}	7.18	4.18
0.507	0.169	5.0	2.34 "	5.49	3.35
0.488	0.160	5.0	2.38 "	5.37	3.25
0.445	0.118	5.0	2.83 "	5.83	3.24
0.108	0.028	5.0	2.85 "	1.42	0.79
0.021	0.007	5.0	2.46 "	0.24	0.14
			CF_2HCl		
0.618	0.417	3.8	1.10×10^{-19}	3.15	2.62
0.532	0.327	5.0	1.04 "	2.55	2.03
0.354	0.252	3.8	0.95 "	1.56	1.33
0.211	0.148	3.8	0.99 "	0.97	0.82
0.026	0.017	3.8	1.19 "	0.14	0.12
			CF_3Cl		
0.705	0.614	5.0	0.294×10^{-19}	0.96	0.90
0.311	0.295	2.0	0.281 "	0.41	0.40
0.258	0.226	5.0	0.382 "	0.34	0.32
0.083	0.069	5.0	0.394 "	0.15	0.14
0.029	0.022	5.0	0.589 "	0.08	0.07

a.) As calculated by Beer's Law
b.) As calculated by energy difference
c.) Cell length for all measurements was 29 cm.

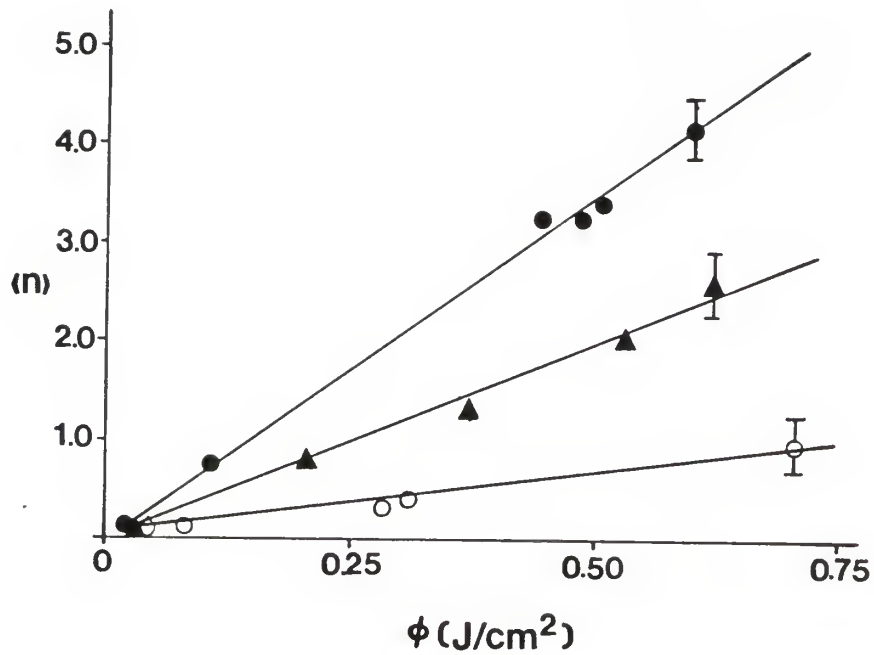

Figure 3.5 The average number of photons absorbed per molecule appears to increase linearly with fluence for all three methanes; CF_2Cl_2(●), CF_2HCl(▲), and CF_3Cl(○).

section 3.1, in which only a small fraction of the molecules in the path of the laser beam will actually absorb the energy, is quite valid. After this fraction of molecules has been raised to a higher energy, what remains is a "hole" in the Boltzmann rotational distribution of the v=0 population,[7] i.e., the laser pulse transfered a fraction of the molecules from the v=0 level for which the photon energy was resonant or near resonant to rotational states of the next higher level. However, as the gas pressure is increased more photons/molecule are absorbed, because collisions transfer molecules into the "hole" and they then absorb. At even higher pressures vibrational relaxation of the higher levels may inhibit the vibrational ladder climbing, but the molecules still absorb energy from the radiation field.

Grunwald et.al[8] have accurately (within 5%) been able to model the absorption process for CF_2HCl by taking a kinetic approach in which rotational and vibrational (collisional) relaxation were considered. The results indicate that vibrational relaxation occurs at a very high rate for collisions between the excited CF_2HCl and an unexcited molecule. In fact the relaxation rates indicate that relaxation occurs faster than gas-kinetic collision frequencies ($1.5 \times 10^7 s^{-1} torr^{-1}$) and relaxation accelerates with increasing vibrational energy.[9] Rotational relaxation in the ground state, filling the hole produced by the laser pulse, is also extremely efficient ($3 \times 10^8 s^{-1} torr^{-1}$).

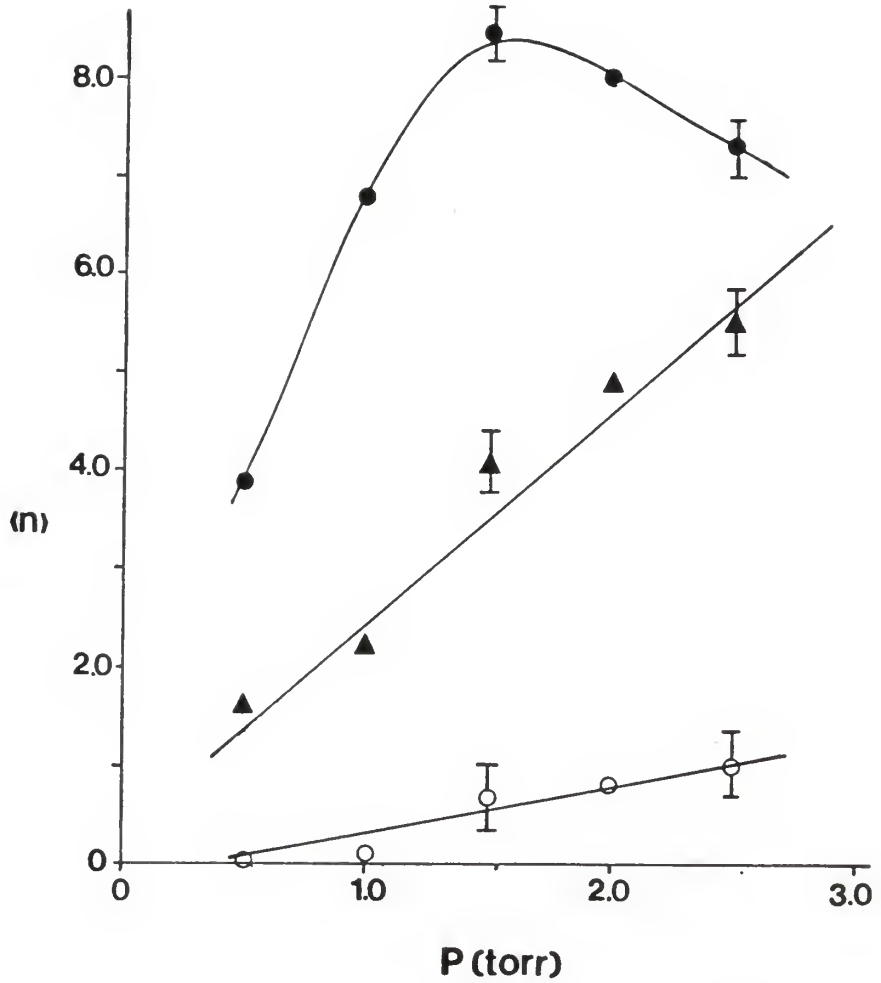

Figure 3.6

The average number of photons absorbed per molecule as a function of RCl pressure and fluence about 1 J/cm^2. CF_2Cl_2(●), CF_2HCl(▲), and CF_3Cl(○)

Table 3.3
<n> For Increasing RCl Pressure

P[a] (torr)	ϕ[b] (J/cm^2)	<n>[c] photon/molecule	<n>[d] photon/molecule
	CF_2Cl_2		
0	0.934	-	-
0.5	0.814[e]	3.9	4.2
1.0	0.702	6.8	7.8
1.5	0.499	8.5	11.4
2.0	0.389	8.0	11.9
2.5	0.310	7.3	11.9
	CF_2HCl		
0	1.140	-	-
0.5	0.906[e]	1.6	1.7
1.0	1.066	2.2	2.2
1.5	0.932	4.1	4.5
2.0	0.805	4.9	5.8
2.5	0.674	5.5	7.0
	CF_3Cl[e,f]		
0	0.971	-	-
0.5	0.971	0.00	0.00
1.0	0.965	0.07	0.07
1.5	0.886	0.7	0.7
2.0	0.836	0.8	0.9
2.5	0.774	1.0	1.0

a.) P=0 was used to determine ϕ_o and cell length was 49 cm.
b.) Fluence values are the average of at least 3 (usually 5) measurements. Standard deviation was typically $\pm 0.04 J/cm^2$. Cell length=49cm.
c.) <n> as calculated by the energy difference method described in section 2.5 with uncertainty of ±15%
d.) <n> as calculated by the Beer's Law method described in section 2.5 with error of ±15%
e.) ϕ_o=0.971 for this measurement and cell length 115cm.
f.) These values are very uncertian but are used to estimate f in section 3.4.

Figure 3.6 shows the result of increasing the pressure of all three of the molecules for ϕ=0.8 J/cm^2. It is readily apparent from these data that the absorption process depends on reagent pressure, i.e. the absorption cross section is pressure dependent. While these results provide useful insight to the absorption process, for our purpose it is more important to obtain data that more closely parallel the experimental conditions for the XeCl* enhancement experiments. In the enhancment experiments, a typical Ar pressure was about 1 torr and RCl pressure was about 10^{-4} torr ($3x10^{12}$ molecule/cm^3). It is impossible to measure the amount of energy absorbed by such a small amount of sample by the direct technique used in this work. In fact the lowest pressure for which the amount of absorption could be measured was about 0.5 torr for CF_2Cl_2 and CF_2HCl and 1.0 torr for CF_3Cl. Thus absorption data in which the RCl pressure is low (0.5 to 1.0 torr), and constant, compared to the argon buffer gas are shown in figure 3.7. As with increasing RCl pressure, increasing Ar pressure gave a higher number of photons absorbed per molecule. However, it is important to realize the distinction between the cause of the two 'increasing' absorption processes. Increasing the reagent gas pressure caused an increase in the absorbed energy because rotational <u>and</u> vibrational relaxation processes were important, because collision with another RCl provided the opportunity for transfer of vibratinal energy not only to

translation (as with Ar collisions) but also transfer to rotation and vibrations of the unexcited RCl. In the case of increasing argon pressure, the rotational relaxation is much important than vibrational relaxation.[10] Therefore, the increased absorption with increasing pressure is due mostly to the filling of the hole (or rotational bottleneck) produced by the laser pulse. Thus, at high Ar pressure there are enough collisions occuring during the 1.5 us laser pulse to remove the bottleneck in v=0 because molecules occupying the otner rotational states of this level relax to replace the sample pumped out, and are subsequently being pumped out also.

The CF_2Cl_2 and CF_2HCl reached a plateau where no more photons were absorbed at high pressure, i.e. the absorption was saturated. Reaching this saturation point necessarily implies that collisions have removed all relevant bottlenecks. The average number of photons absorbed may be calculated as before and $\langle n' \rangle$ is now defined as the saturation number of photons absorbed. The $\langle n' \rangle$ value may be used as a reference point for comparison to the $\langle n \rangle$ calculated for 1.0 torr (or 0.5 torr) to estimate the fraction of molecules

$$f = \langle n \rangle / \langle n' \rangle,$$

absorbing at 1 torr of Ar for the enhancement experiments.

One of the gases, CF_3Cl, did not seem to saturate

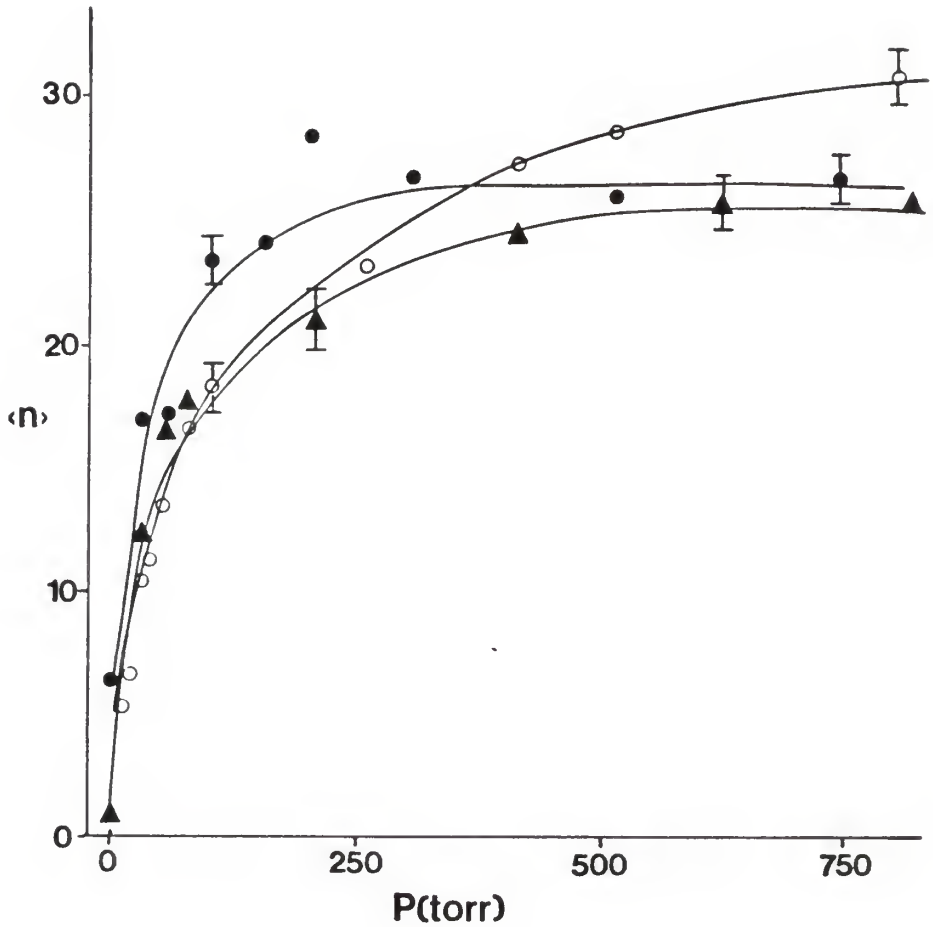

ure 3.7 The average number of photons absorbed per molecule as a function of increasing argon pressure These plots were used to determine f, the fraction of molecules absorbing under near collisionless conditions. CF_2Cl_2(●), CF_2HCl(▲), and CF_3Cl(○)

Table 3.4
<n> For Increasing Ar Pressure

P[a] (torr)	ϕ[b] (J/cm^2)	<n>[c] photon/molecule	<n>[d] photon/molecule
	CF_2Cl_2		
0	0.965	-	-
0.5	0.856	6.4	6.7
27.2	0.667	16.9	19.9
53.4	0.671	17.2	20.4
101.5	0.564	23.5	30.2
153.0	0.551	24.2	31.5
204.0	0.479	28.5	39.3
305.2	0.507	26.8	36.1
516.2	0.521	26.0	34.6
747.0	0.508	26.8	36.0
	CF_2HCl		
0	0.958	-	-
0.5	0.942	0.94	0.94
26.5	0.744	12.5	14.1
51.5	0.669	16.9	20.0
74.8	0.652	17.9	21.5
101.0	0.656	17.7	21.1
206.0	0.597	21.1	26.4
417.2	0.538	24.6	32.1
621.0	0.518	25.8	34.3
815.7	0.518	25.8	34.3

a.) P=0 was used to determine ϕ_o.
b.) Fluence values are the average of at least 3 (usually 5) measurements. Standard deviation was typically $\pm 0.04 J/cm^2$
c.) <n> as calculated by the energy difference method described in section 2.5 with an uncertainty of ±10%
d.) <n> as calculated by the Beer's Law method described in section 2.5 with an uncertainty of ±10%

Table 3.4 (cont'd)

p[a] (torr)	ϕ[b] (J/cm^2)	$\langle n \rangle$[c] photon/molecule	$\langle n \rangle$[d] photon/molecule
	CF_3Cl		
0	0.941	-	-
0.5	0.919	e	e
10.6	0.849	5.36	5.60
20.8	0.827	6.6	7.04
31.0	0.701	10.5	11.6
41.3	0.748	11.3	12.5
50.9	0.709	13.6	15.5
77.6	0.656	16.7	19.7
101.1	0.630	18.2	21.9
260.6	0.542	23.3	30.2
367.6	0.472	27.4	37.7
565.0	0.451	28.7	40.2
800.0	0.411	31.0	45.3

a.) P=0 was used to determine ϕ_o.

b.) Fluence values are the average of at least 3 (usually 5) measurements. Standard deviation was typically $\pm 0.04 J/cm^2$

c.) $\langle n \rangle$ as calculated by the energy difference method described in section 2.5 with an uncertainty of $\pm 10\%$

d.) $\langle n \rangle$ as calculated by the Beer's Law method described in section 2.5 with an uncertainty of $\pm 10\%$

e.) A value of 0.2 is used, as approximated from table 3.3, to calculate the fractional absorption, f, in section 3.4

under high pressure conditions. It also absorbed the least number of photons, $\langle n \rangle = 0.2$, under 1 torr conditions. In order to estimate f, however, a saturation point was still choosen and, at least, an approximate value of the fraction is provided in table 3.5 along with CF_2HCl and CF_2Cl_2.

Table 3.5
Fractional Absorption Data for the Freons

reagent	<n> photons/molecule	<n´>	f=<n>/<n´>
CF_2Cl_2	6.5	26.5	0.03
CF_2HCl	1.0	25.5	0.04
CF_3Cl	0.2	30.0	0.007

References: Chapter 3

1.) J.C. Jang-Wren, D.W. Setser, J.C. Ferrero, J. Phys. Chem. 89(3) (1985) 414

2.) B. Toselli, J.C. Ferrero, E.H. Staricco, J. Phys. Chem., 89(8) (1985) 1492

3.) Y.R. Kolomilskii, V.S. Marchuk, E.A. Rayabov, Sov. J. Quant. Elec., 12( ) (1982) 1139

4.) Gerhard Herzberg, "Molecular Spectra and Molecular Spectra, II. Infrared and Raman spectra of Polyatomic Molecules", Van Nostrand Reinhold Company, New York, (1945)

5.) V.S. Letokhov, "Nonlinear Laser Chemistry, Multiple-Photon Excitation, Chemical Physics 22", Springer-Verlag, New York, (1983)

6.) Reference 1

7.) see for example R.T.V. Kung and H.W. Friedman, J. Chem. Phys., 72(1) (1980) 337

8.) E. Grunwald and S.H. Liu, J. Phys. Chem., 90(19) (1986) 4550

9.) S.H. Liu and E. Grunwald, J. Phys. Chem., 90(19) (1986) 4555

10.) J.L. Copeland, "Experimental Errors and Their Treatment", unpublished handout for Physical Chemistry Lab students, Revised January 1978.

CHAPTER 4 KINETIC STUDIES OF XeCl(B,C) FORMATION

4.1 Kinetics of XeCl(B,C) Formation from $Xe(^3P_2)$ + RCl

The following reactions describe the XeCl(B,C) formation, in a discharge flow reactor operating at 300K.

$$Xe^* + RCl \xrightarrow{k_{XeCl^*}} XeCl(B,C) + R\cdot$$

$$Xe^* + RCl \xrightarrow{k_{Other}} \text{other products}$$

$$XeCl(B) \xrightarrow{\tau_B^{-1}} Xe + Cl + h\nu$$

$$XeCl(C) \xrightarrow{\tau_C^{-1}} Xe + Cl + h\nu$$

Here, Xe^* represents $Xe(^3P_2)$ which has a lifetime of 149.1 seconds.[1] RCl is the chlorine containing reagent; either Cl_2 or the chlorofluoromethanes in these experiments. There are two $XeCl^*$ states, $XeCl(B,^2\Sigma^+)$ and $XeCl(C,^2\Pi_{3/2})$ formed from reactive quenching of Xe^* by RCl with rate constant k_{XeCl^*}, with lifetimes of 11 and 121 ns, respectively.[4] The rate constant k_{Other} represents the "non-reactive" quenching channel, which is mostly excitation-transfer followed by dissociation of the excited molecules.[2,3] The branching fraction for $XeCl^*$ formation is defined as $\Gamma_{XeCl^*} = k_{XeCl^*}/k_Q$, where k_Q is the total

quenching rate constant.

The rate of change of $XeCl^*$ may be written as

$$\frac{d[XeCl^*]}{dt} = k_{XeCl^*}[Xe^*][RCl] - \tau_{eff}^{-1}[XeCl^*].$$

Since the XeCl(B) and XeCl(C) lifetimes (τ_B and τ_C) are very short, the rate at which they are formed will be equivalent to the rate at which they are lost. Since Ar collisions mix the B and C states, the rate equation may be approximated by including the total $XeCl^*$ concentration with an effective lifetime $\tau_{eff}^{-1} = f_B\tau_B^{-1} + f_C\tau_C^{-1}$ where f_B and f_C are the fractions of XeCl(B) and XeCl(C). Thus $d[XeCl^*]/dt = 0$, giving a steady state $XeCl^*$ concentration of

$$[XeCl^*]_{ss} = \frac{k_{XeCl^*}[Xe^*][RCl]}{\tau_{eff}^{-1}}.$$

The rate of emission of photons from $XeCl^*$ is

$$\frac{d[photons]}{dt} = I_{XeCl^*} = \tau_{eff}^{-1}[XeCl^*].$$

where the photons emitted per unit time (intensity) is directly proportional to the steady state concentration. Using the steady state expression for $XeCl^*$ gives

$$I_{XeCl^*} = k_{XeCl^*}[Xe^*][RCl].$$

From this equation we see that by changing [RCl] and monitoring the intensity, a plot of I vs [RCl] will be linear with slope = $k_{XeCl}*[Xe^*]$. For a constant $[Xe^*]$, comparison of these $I_{XeCl}*$ plots give relative $k_{XeCl}*$.

It was possible to find a range of RCl concentration for which first order conditions hold true. This was done by holding $[Xe^*]$ constant and varying the flow of an RCl/Ar mixture through a needle valve. (The needle valve permitted varying the flow of the RCl/Ar mixture and thus the [RCl] in the flow reactor; see section 2.2). If the I vs [RCl] plots were not linear, the RCl was diluted by more Ar and run again. Eventually it was determined that a 10% RCl/Ar mixture produced first order plots in a range of [RCl] = $0.1\text{-}2.0\times10^{13}$ molecule/cm^3. Figure 4.1 (data from table 4.1) shows the results of various [RCl]/Ar mixtures over a wide concentration range, the first order domain only exists below ~$1\text{-}2\times10^{13}$ molecule/cm^3.

Figure 4.2 shows some typical $XeCl^*$ spectra taken as described in section 2.3. The C-A emission band is shown, although it was not used in obtaining the integrated intensities because the B/C ratio was assumed to be constant for all reagents at the same Ar pressure (as has been found in numerous cases).[5] The relative $XeCl^*$ intensities were obtained by integrating the area under the XeCl(B-X) band.

While the plots of $I_{XeCl}*$ vs [RCl] give a relative measure of the pseudo first order rate constant, $k' =$

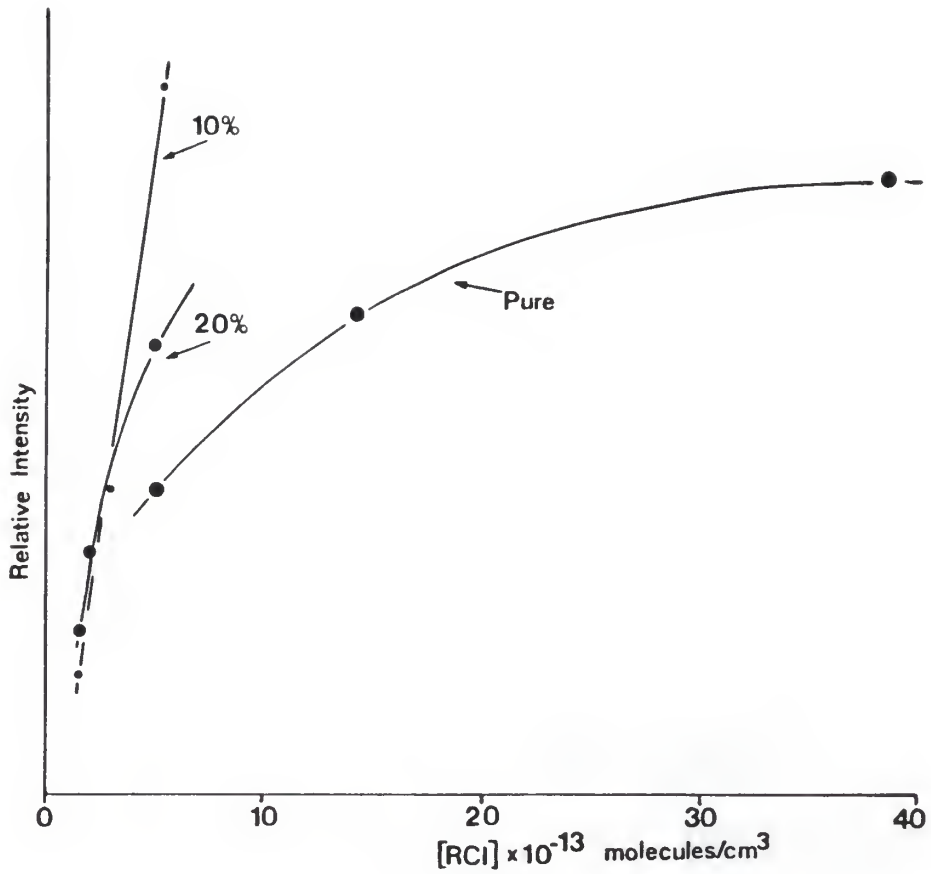

Figure 4.1 Plots used to determine the first order regime for CF_2Cl_2 at several dilutions. The approximate range was selected as $0.1\text{-}2.0\times10^{13}$ molecules/cm^3.

Table 4.1
$XeCl^*$ Formation for
Several $[CF_2Cl_2]$ Ranges
Data for figure 4.1

Relative Intensity	$[RCl] \times 10^{-13}$ molecule/cm^3	comments
	Pure CF_2Cl_2	
10.5	5.06	not linear
15.3	14.3	
19.2	38.5	
	20% CF_2Cl_2/Ar	
6.1	1.62	almost linear
8.6	2.00	
14.6	4.87	
	10% CF_2Cl_2/Ar	
1.4	0.15	linear
3.5	0.31	
8.1	0.54	
12.3	1.10	

Figure 4.2 Typical XeCl(B-X,C-X) emission spectra for several of the reagents used in these experiments. Concentrations are about 5×10^{12} molecules/cm^3, and the pressure in the reactor was 1.0 torr. At 320 nm there is a x3 scale change on the photon counter.

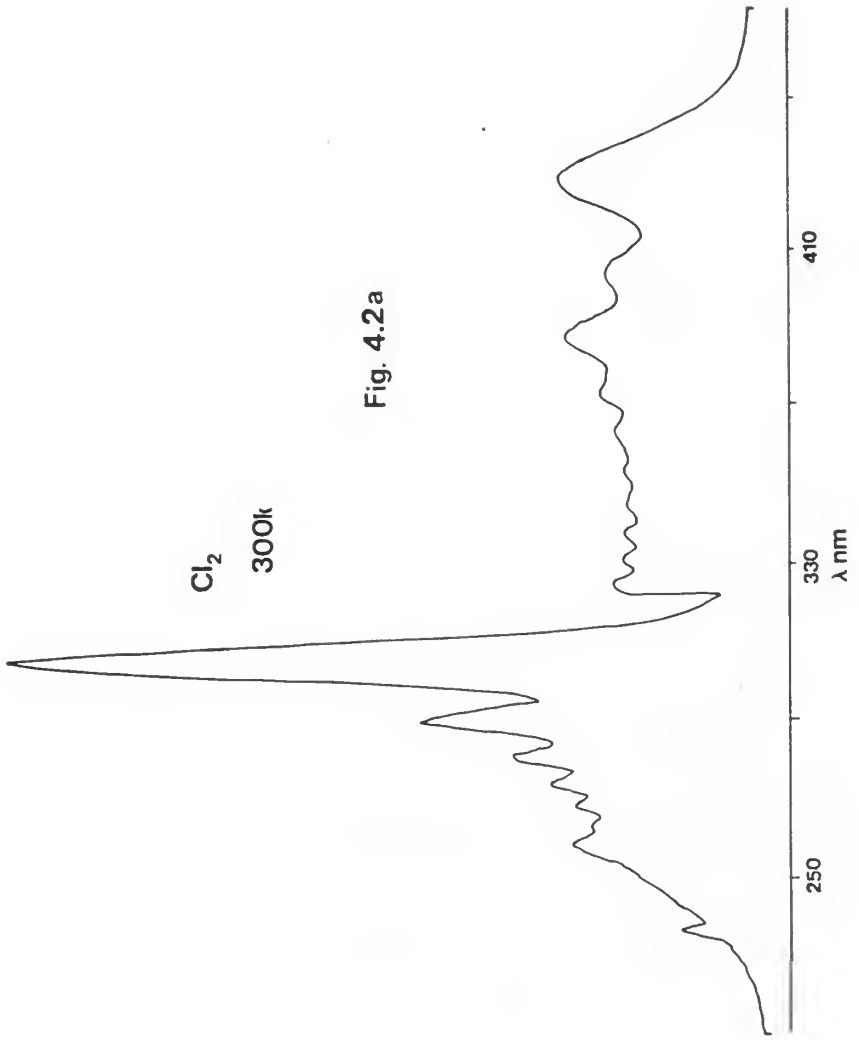

Fig. 4.2a

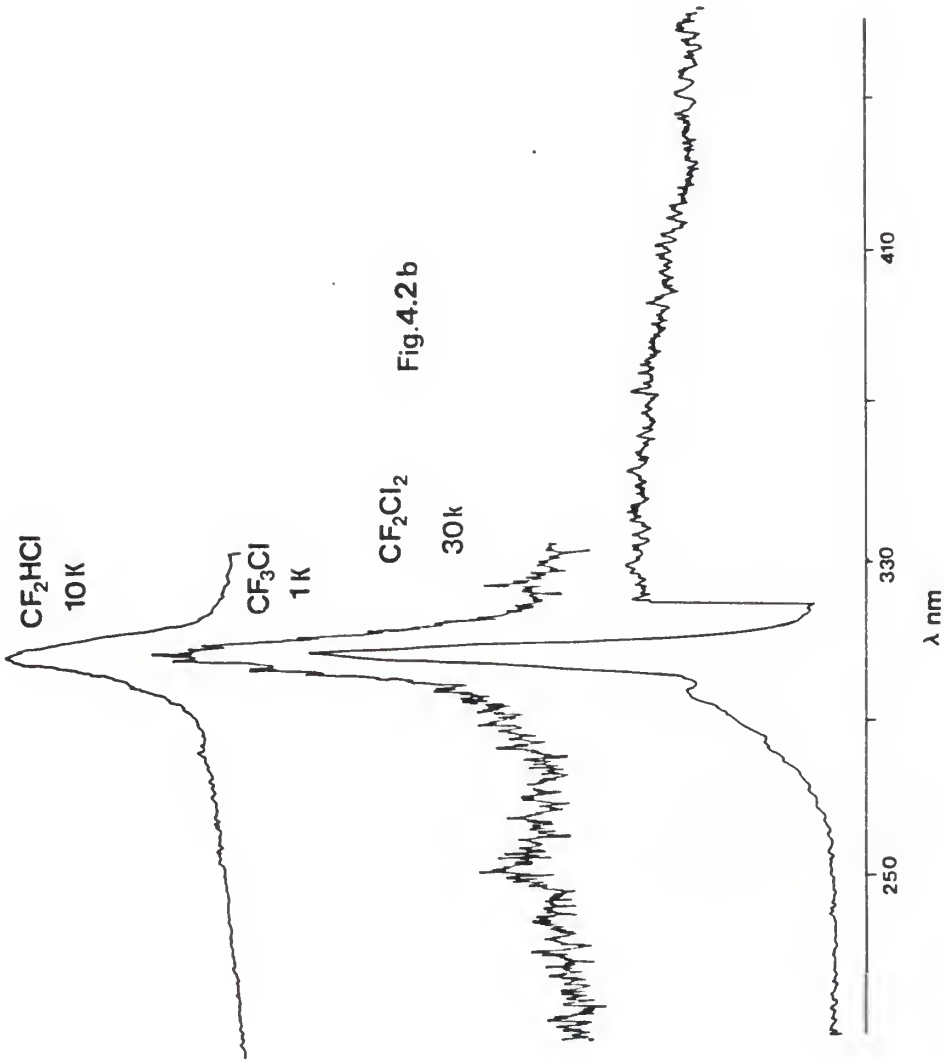

Fig.4.2b

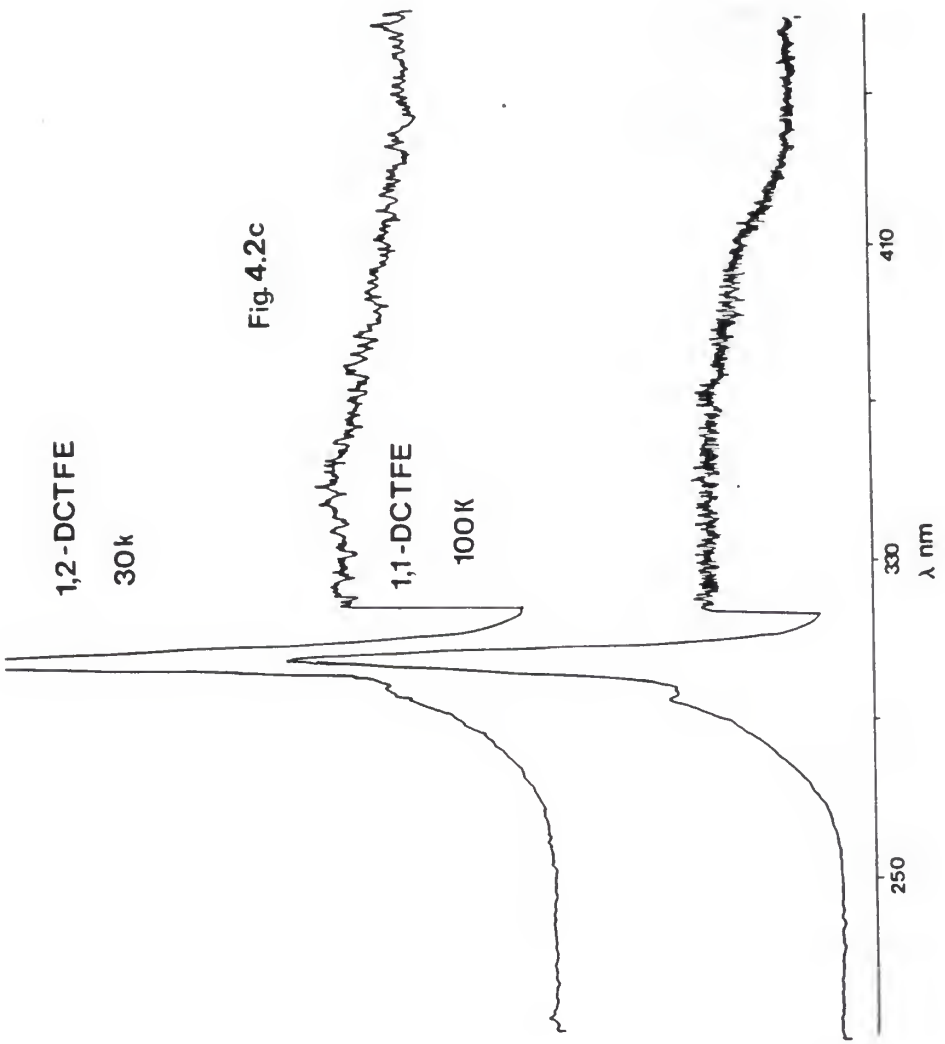

Fig. 4.2c

$k_{XeCl^*}[Xe^*]$, it is not possible to find the true rate constant, k_{XeCl^*}, because $[Xe^*]$ is not accurately known. It was, however, possible to use a reference reaction to obtain k_{XeCl^*}. The reference of choice was Cl_2 since $k^{Cl_2}_{XeCl^*}$ is known ($7.2 \times 10^{-10} cm^3 molecule^{-1} s^{-1}$) and the reaction of Xe^* with Cl_2 is assumed to occur with $\Gamma_{XeCl^*} = 1.0$, i.e. $k^{Cl_2}_{XeCl^*} = k_Q$.[7] Taking the ratio of the rate constant for RCl vs Cl_2 gives

$$\frac{k^{RCl}_{XeCl^*}}{k^{Cl_2}_{XeCl^*}} = \frac{I^{RCl}_{XeCl^*}/[Xe^*][RCl]}{I^{Cl_2}_{XeCl^*}/[Xe^*][Cl_2]}$$

and rearranging this equation gives

$$k^{RCl}_{XeCl^*} = \frac{I^{RCl}_{XeCl^*}/[RCl]}{I^{Cl_2}_{XeCl^*}/[Cl_2]} \times 7.2 \times 10^{-10}$$

Table 4.3 in the next section lists values of k_{XeCl^*} for a variety of chlorofluoromethanes and chlorofluroethanes calculated in this manner. The I/[RCl] ratio was actually taken as the slope of the plot of I vs [RCl] like those in figures 4.3 a-d. Values of k_{XeCl^*} compare with previous estimates of <0.5, <0.3, and <0.2 for CF_2Cl_2, CF_2HCl, and CF_3Cl respectively.[2]

4.2 Determination of Branching Fraction for $XeCl^*$ Formation

The branching fraction, Γ_{XeCl^*}, is defined as the fraction of Xe^* + RCl collisions leading to excimer

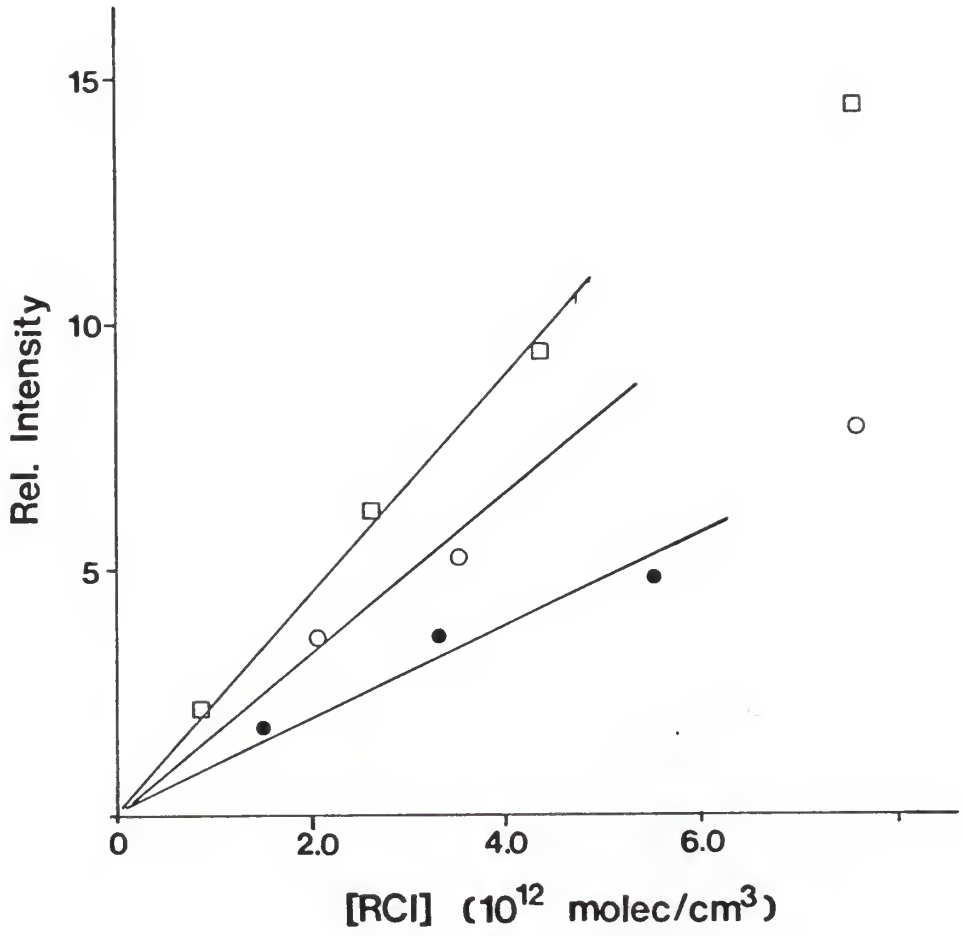

Figure 4.3a Plots used to determine k_{XeCl}*. CF_2Cl_2(●), CF_3Cl(○), Cl_2(□).

Table 4.2a
$XeCl^*$ Formation vs [RCl]
Data for figure 4.3a

Relative $XeCl^*$ Intensity[#]	$[RCl] \times 10^{-12}$ molecule/cm^3	comments
	CF_2Cl_2	
1.80x10	1.55	slope=(7.67±1.20)$\times 10^{-12}$
3.70x10	2.66	cm^3/molecule
4.86x10	5.50	
	CF_3Cl	
3.66	2.13	slope=(1.50±0.14)$\times 10^{-12}$
5.21	3.53	cm^3/molecule
7.92	7.70	
	Cl_2	
2.15x10^3	0.89	slope=(2.12±0.08)$\times 10^{-9}$
6.1910^3	2.66	cm^3/molecule
9.3710^3	4.29	

[#]The x10 and x10^3 factors on CF_2Cl_2 and Cl_2 represent scaling factors used on the photon counter.

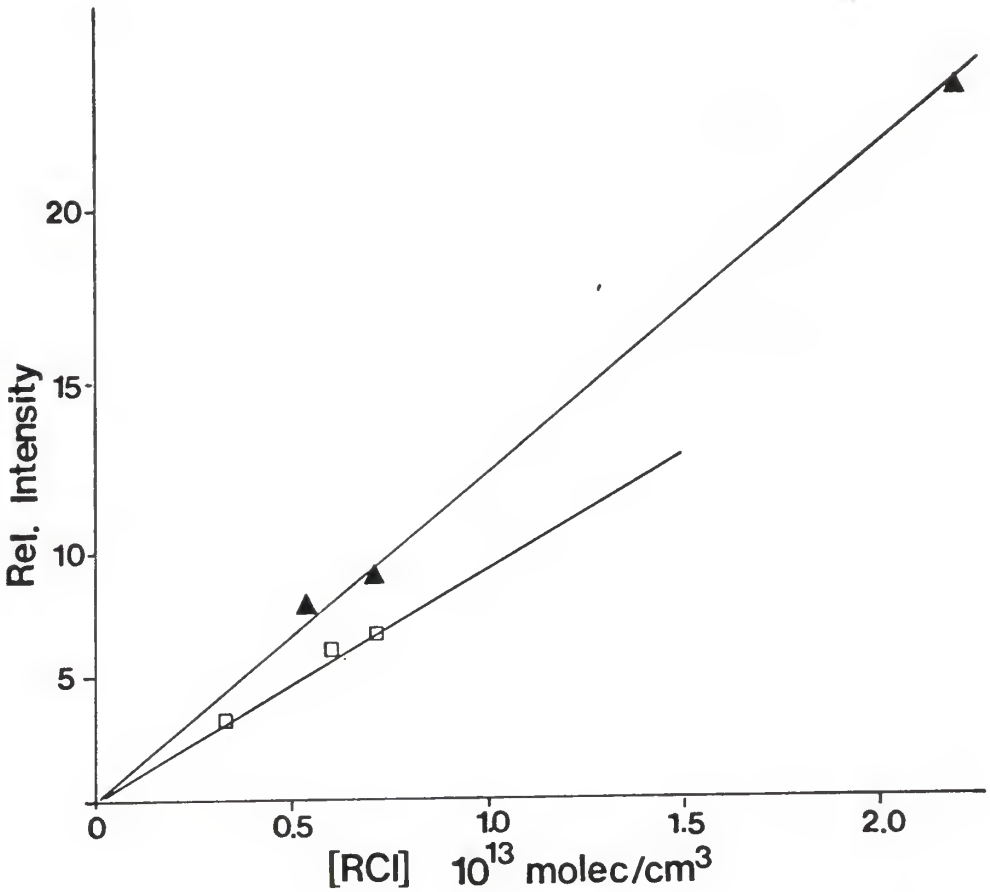

Figure 4.3b Plots used to determine k_{XeCl}*. CF_2HCl(▲), Cl_2(□).

Table 4.2b
$XeCl^*$ Formation vs [RCl]
Data for figure 4.3b

Relative $XeCl^*$ Intensity[#]	$[RCl] \times 10^{-13}$ molecule/cm^3	comments
	CF_2HCl	
12.3	1.20	slope=$(6.52 \pm 0.01) \times 10^{-13}$
9.1	0.71	cm^3/molecule
8.0	0.54	
	Cl_2	
6.8×10^3	0.71	slope=$(6.67 \pm 0.73) \times 10^{-10}$
6.1×10^3	0.65	cm^3/molecule
4.7×10^3	0.32	

[#]The $\times 10^3$ factors on and Cl_2 represents scaling factors used on the photon counter.

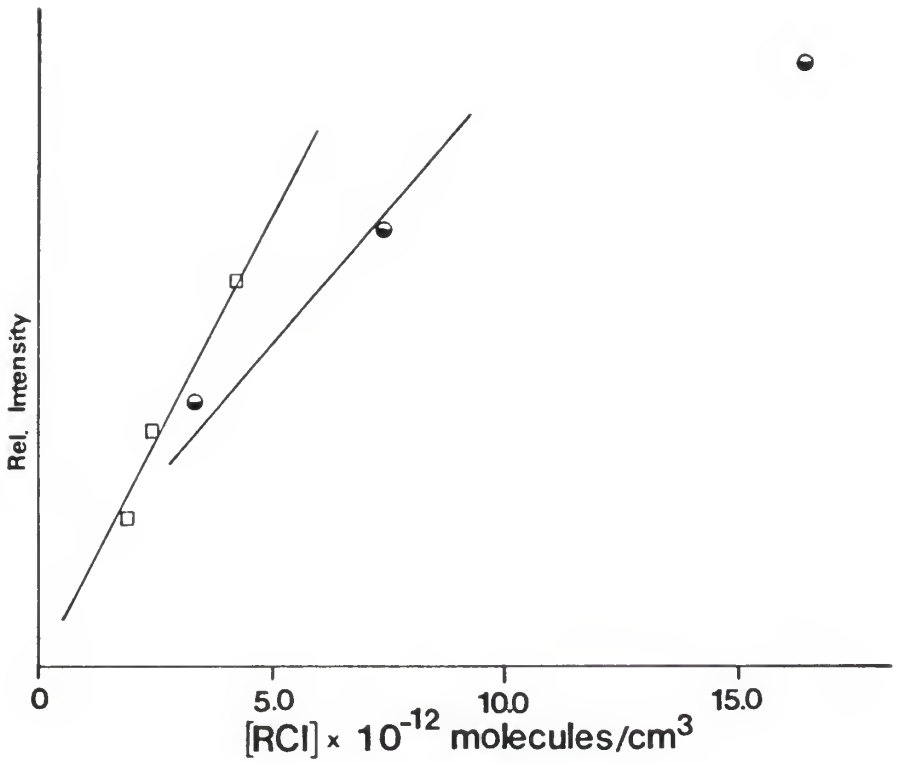

Figure 4.3c Plots used to determine k_{XeCl^*}. CF_2ClBr(◒), Cl_2(□).

Table 4.2c
$XeCl^*$ Formation vs $[CF_2ClBr]$
Data for figure 4.3c

Relative $XeCl^*$ Intensity#	$[RCl]\times10^{-12}$ molecule/cm^3	comments
	CF_2ClBr	
12.8	16.4	slope=$(5.23\pm0.94)\times10^{-13}$
9.3	7.53	cm^3/molecule
5.7	3.44	
	Cl_2	
8.2	4.06	slope=$(2.20\pm0.30)\times10^{-12}$
5.0	2.34	cm^3/molecule
3.1	1.86	

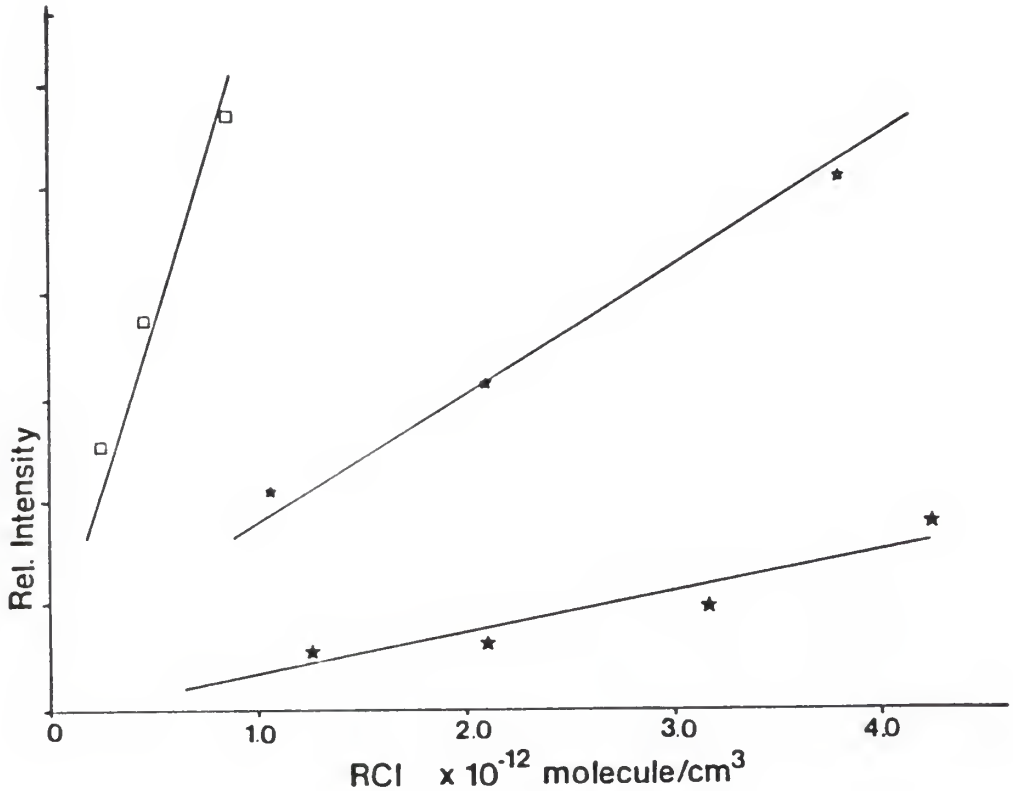

Figure 4.3d Plots used to determine k_{XeCl}*.
1,1-DCTFE(☆), 1,2-DCTFE(★), Cl_2(□).

Table 4.2d
$XeCl^*$ Formation vs [Ethanes]
Data for figure 4.3d

Relative $XeCl^*$ Intensity[#]	$[RCl] \times 10^{-12}$ molecule/cm^3	comments
	1,1-DCTFE	
2.12	1.06	slope=$(1.09 \pm 0.02) \times 10^{-12}$
3.19	2.11	cm^3/molecule
5.10	3.80	
	1,2-DCTFE	
0.55	1.27	slope=$(4.60 \pm 0.64) \times 10^{-13}$
0.61	2.11	cm^3/molecule
1.19	3.17	
1.86	4.23	
	Cl_2	
2.52x10	0.27	slope=$(5.09 \pm 0.68) \times 10^{-11}$
3.79x10	0.42	cm^3/molecule
5.72x10	0.87	

[#]The x10 factors on Cl_2 represents a scaling factor used on the photon counter.

Table 4.3
$XeCl^*$ Rate Constants
and Branching Fractions with $Xe(^3P_2)$

compound[e]	k_{XeCl^*} ($\times 10^{-10}$ $cm^3 molecule^{-1} s^{-1}$)	k_Q	Γ_{XeCl^*}
CF_2Cl_2	0.026±0.005	1.9±0.2[a]	0.014
CF_2HCl	0.001±0.0005	2.0±0.4[b]	0.0005
CF_3Cl	0.0051±0.0020	1.0±0.1[a]	0.0051
CF_2ClBr	0.17±0.03	4.0±2.0[b]	0.043
1,1-DCTFE	0.15		
1,2-DCTFE	0.065		

a.) Taken directly from reference 1 and 2.
b.) These k_Q values were extimated by comparison to values of this reagent with $Ar(^3P_2)$ or $Kr(^3P_2)$ from a table in reference 7.
c.) Error limits are from the standard deviation of plots like those in figures 4.3-4.5.
d.) The major quenching channel for CF_2ClBr is $XeBr^*$.
e.) 1,1- and 1,2-DCTFE are 1,1- and 1,2-Dichlorotetrafluoroethane.

formation ($XeCl^*$) relative to the total quenching rate constant

$$\Gamma_{XeCl^*} = \frac{k^{RCl}_{XeCl^*}}{k^{RCl}_{Q}}$$

The previous section described how to obtain values for $k^{RCl}_{XeCl^*}$. Values of k_Q were not measured in these experiment, but were taken from the literature (see table 4.3).

Although k_Q's were not measured in these experiments, a brief description of a method for determining values of k_Q is given here. (This method was used by Velazco et. al.[6]) Since the lifetime of the $Xe(^3P_2)$ state is quite long (149.5 s) it is not possible to observe emission from this state. Instead of monitoring emission from the metastable state, an absorption technique is employed in which the intensity of a metastable diagnostic line is monitored as a function of distance down the length of a flow tube. A plot of intensity vs distance down the tube is linear with a slope equal to $-k_Q[Q]/v$, where v is the velocity of the gas in the flow tube. Since the flow velocity in the flow tube can be calculated, the slopes can be multiplied by v to give simply $k_Q[Q]$. These values are determined for several quencher concentrations and plotted against [Q] to yield a straight line with slope k_Q.

Previous estimates of Γ_{XeCl^*} for CF_2Cl_2, CF_2HCl, and CF_3Cl are <0.03, <0.02, and <0.02 respectively,[2] where k_Q were estimated in the same manor used in table 4.3. Some

k_Q values were taken directly from reference 6 and unpublished work, if a value had not been measured for a particular reagent, it was estimated by comparison to quenching results of that reagent and/or similar RCl molecules with $Ar(^3P_2)$ and $Kr(^3P_2)$. (For the remainder of this paragarph k_Q values are in units $x10^{-10}$ $cm^3molecule^{-1}s^{-1}$) The k_Q for CF_2Cl_2 was measured as 1.9. For CF_3Cl, k_Q for $Ar(^3P_2)$ and $Kr(^3P_2)$ were 2.2 and 1.4 respectively, and the series of reagents CCl_4-CCl_3F-CCl_2F_2 has values 6.3-3.3-1.9, thus k_Q is estimated as 1.0. k_Q for CF_2HCl is taken as 2.0 by similar comparison. These estimated k_Q values are used in table 4.3 to calculate the branching fractions..

4.3 Enhancement of XeCl(B,C) Formation by IR Laser Energy

The kinetic scheme for $XeCl^*$ formation from the Xe^* with vibrationally excited RCl (RCl^{**}) is more complicated than the steady state $XeCl^*$ production discussed in section 4.1. This is due to the fact that the RCl^{**} produced by the laser pulse,

$$RCl + mh\nu \rightarrow RCl^{**},$$

is subject to several loss steps that occur on a time scale which is competitive with the time RCl^{**} is resident for view by the detection system. We assume that RCl is

homogeneously mixed in the zone that is irradiated by the laser, although this will be questioned later. The $XeCl^*$ removal and formation processes are shown here

$$Xe^* + RCl^{**} \xrightarrow{k_1} XeCl^* + R\cdot$$

$$Ar + RCl^{**} \xrightarrow{k_2} Ar + RCl^*$$

$$RCl + RCl^{**} \xrightarrow{k_3} 2\ RCl^*$$

$$Xe^* + RCl^{**} \xrightarrow{k_4} \text{other products}$$

$$RCl^{**} \xrightarrow{\tau_p^{-1}} \text{pump out}$$

$$XeCl^* \xrightarrow{\tau^{-1}} Xe + Cl + h\hat{}$$

where τ_p^{-1} is the rate constant for the flow of RCl^{**} out of the observation zone. The symbol RCl^*, represents vibrationally excited states with insufficient energy to lead to enhanced $XeCl^*$ formation. The Xe^* are produced in a steady supply upstream from the reaction zone and do not change their concentration during or after the laser pulse, i.e. the reaction rate constant for RCl^{**} with Xe^* does not significantly differ from that for RCl.

As in section 4.1, the intensity of emission from $XeCl^*$ is equivalent to the formation rate

$$I_{XeCl^*} = k_1[Xe^*][RCl^{**}].$$

In order to describe the time dependent $XeCl^*$ emission intensity following the laser pulse, we need $[Xe^*]$ and $[RCl^{**}]$. The rate of removal of $[RCl^{**}]$ is

$$\frac{d[RCl^{**}]}{dt} = -[RCl^{**}]((k_1 + k_4)[Xe^*] + k_2[Ar] + k_3[RCl] + \tau_p^{-1}).$$

The rate of production of RCl^{**} is given by the interaction of the laser pulse with the [RCl], which can be considered as a delta function. This provides $[RCl_o^{**}]$, which is some fraction, f, of [RCl] (e.g. $[RCl_o^{**}] = f[RCl]$). Rearranging the above equation gives

$$\frac{d[RCl^{**}]}{-[RCl^{**}]} = ((k_1 + k_4)[Xe^*] + k_2[Ar] + k_3[RCl] + \tau_p^{-1})dt$$

$$= k_{eff}dt$$

Integration of this equation (from time = 0 to t) gives $-\ln([RCl^{**}]/[RCl_o^{**}])$ for the left hand side and $\exp(-k_{eff}t)$ for the right hand side. It is possible to simplify k_{eff} with some approximations. Since Ar is the buffer gas and is always in extreme excess (3.2×10^{16} molecule/cm^3 at 1 torr), [Ar] is constant. Xe^* and RCl are present in low concentrations; $[Xe^*]$ is estimated to be about 10^{10} molecule/cm^3 (reference 8) and [RCl] was typically 10^{13}

molecule/cm^3. Values of rate constants for k_2 and k_3 have been published for molecules similar to the freons we used. The V-T/R (vibration to translation/rotation) relaxation rate of CF_2Cl_2 in Ar has been measured as 8.6 $ms^{-1}torr^{-1}$ ($2.7x10^{-13}$ $cm^3molecule^{-1}s^{-1}$).[9] The same reference provides a value for the quenching rate of $CF_2Cl_2^{**}$ by CF_2Cl_2 as 21.4 $ms^{-1}torr^{-1}$ ($6.6x10^{-13}$ $molecule^{-1}s^{-1}$). If the total quenching constant is not significantly different from k_Q ($\triangleq k_1 + k_4$), a representative value is about 10^{-10} $cm^3molecule^{-1}s^{-1}$ (table 4.3). Now using these as representative values, the right hand side of the above equation gives $(k_1 + k_4)[Xe^*] \triangleq 10^1$, $k_2[Ar] \triangleq 10^3$, and $k_4[RCl^{**}] \triangleq 10^1$. From section 2.2, τ_p^{-1} is $5x10^3$ s^{-1}. Thus, neglecting the first and third term in the right hand side is justifiable since the order of magnitude of these two terms is smaller than $k_2[Ar]$ and τ_p^{-1}. The time dependence of $[RCl^{**}]$ becomes

$$-\ln\frac{[RCl^{**}]}{[RCl_o^{**}]} \cong (k_2[Ar] + \tau_p^{-1})t$$

or

$$[RCl^{**}] = [RCl_o^{**}]\exp(-(k_2[Ar] + \tau_p^{-1})t),$$

and the concentration of the vibrationally excited RCl is expected to show a exponential decay in time with the time constant depending on the pressure of the buffer gas and

the pumping speed in the flow reactor. In this treatment we have neglected the fact that relaxation by Ar collisions will be multistep in nature and also that the vibrationally excited molecules probably can not be placed into only two categories, i.e. the ratio k_1/k_4 will depend on the level of vibrational energy.

Since the $XeCl^*$ emission intensity follows $[RCl^{**}]$

$$(I_{XeCl^*})_t = k_1[Xe^*][RCl_o^{**}]\exp(-(k_2[Ar] + \tau_p^{-1})t)$$

where 't' is the time after the laser pulse (the instantaneous production of $[RCl_o^{**}]$). From this point on the $XeCl^*$ emission resulting from enhancement by the laser pulse will be refered to as I_e.

In the experimetal section the enhancement ratio, R, was defined as the ratio of the $XeCl^*$ signal enhanced by the laser pulse I_e, $(Xe^* + RCl^{**})$ to I_{XeCl^*}, the $XeCl^*$ emission intensity without the laser $(Xe^* + RCl)$. In terms of the kinetic expressions for the $XeCl^*$ intensities, the enhancement ratio is expressed as $R = I_e/I_{XeCl^*}$, or

$$R = \frac{I_e}{I_{XeCl^*}t} = \frac{k_1[Xe^*][RCl_o^{**}]\exp(-(k_2[Ar] + \tau_p^{-1})t}{k_{XeCl^*}[Xe^*][RCl]}$$

Now using $[RCl_o^{**}] = f[RCl]$, canceling the $[Xe^*]$ and $[RCl]$, and rearranging this equation gives

$$k_1 = \frac{I_e}{fI_{XeCl^*}} k_{XeCl^*}\exp((k_2[Ar] + \tau_p^{-1})t)$$

and at early times ($t \leq 10$ us) this gives

$$k_1 \cong \frac{I_e}{f I_{XeCl^*}} k_{XeCl^*}$$

because the exponential term in the previous expression is close to unity at short times. Thus, we have an expression for the rate constant for the formation of $XeCl^*$ in terms of experimentally determined parameters; the f values are associated with the fraction of RCl molecules interacting with the laser pulse and they were listed in table 3.5, I_e/I_{XeCl^*} are the enhancement ratios available in tables 4.4, 4.5 and 4.6, and k_{XeCl^*} are the rate constants for the formation of $XeCl^*$ from RCl also listed in table 4.3.

Figure 4.4 shows the time profile for production of the $XeCl^*$ from vibrationally excited CF_2Cl_2, CF_2HCl, and CF_3Cl at $\phi \cong 1$ J/cm^2. The data are given in table 4.4. The shape of the enhancement profiles are similar for all three molecules, but the enhancement was largest for CF_2Cl_2.

The decay times for the profiles showed a dependence on the Ar pressure as was predicted by the expression I_e/I_{XeCl^*} above. Figure 4.5 illustrates the effect of doubling the Ar pressure on the enhancment ratio. The ratio of R_1 (1 torr) to R_2 (2 torr) by the above equation

$$\frac{R_1}{R_2} = \frac{f_1}{f_2} \exp(k_2[Ar]t)$$

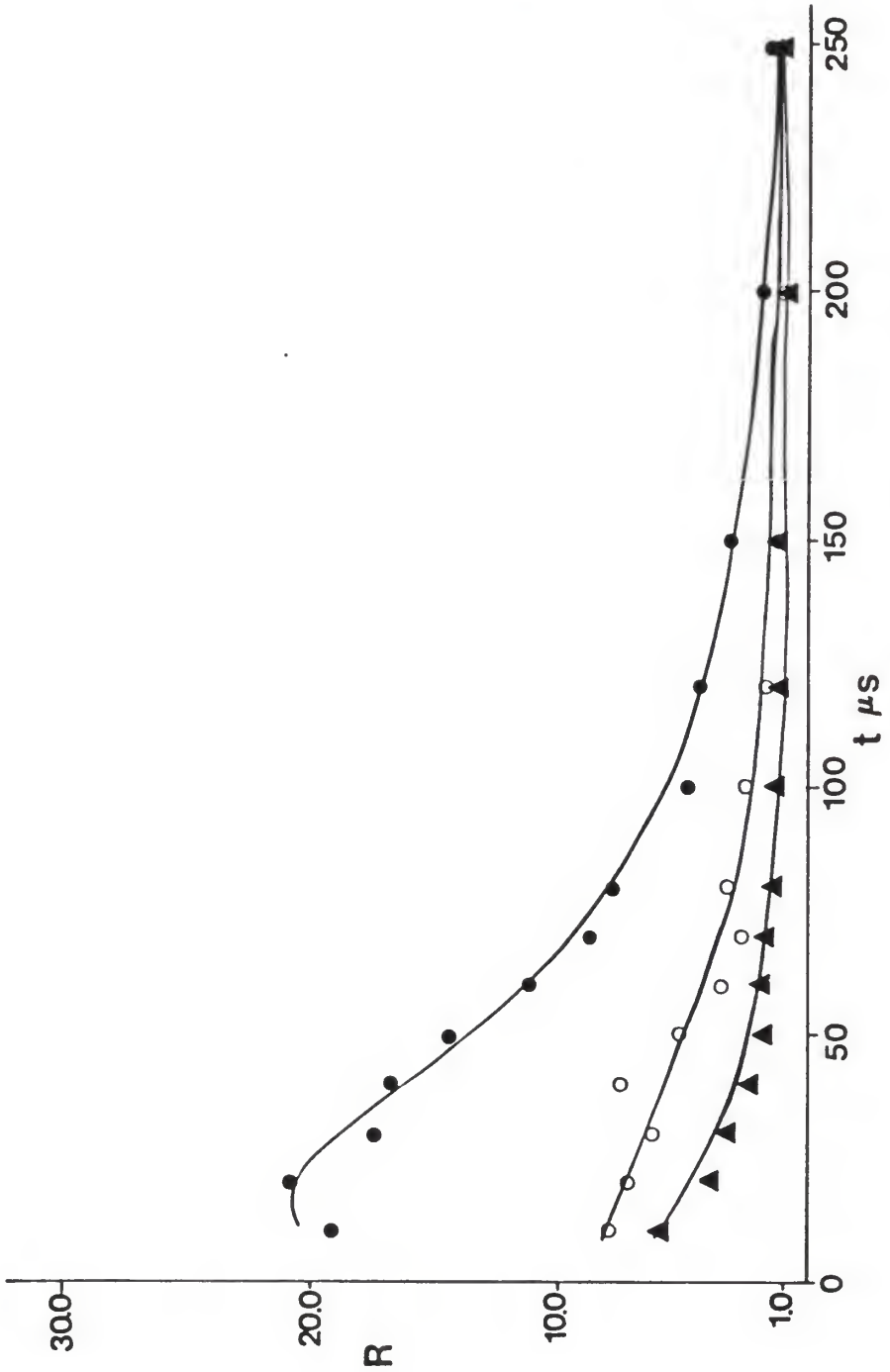

Figure 4.4 Enhancement profile for CF_2Cl_2(●), CF_2HCl(▲), and CF_3Cl(○).

Table 4.4
Enhancement Profile Data for the Freons

time[a] (us)	I, beam blocked[b]	I_e, beam not blocked[b]	R = I_e/I
	$[CF_2Cl_2]$ = 3.34x10^{12} moleule/cm^3, P_{Ar} = 1 torr		
10	0.38(/10)	7.15(/10)	19.1
20	"	7.80	21.8
30	"	6.55	17.5
40	"	6.35	16.9
50	"	5.40	14.4
60	"	4.20	11.2
70	"	3.30	8.80
80	"	3.00	8.00
100	"	1.85	4.93
120	"	1.60	4.27
150	"	1.15	3.07
200	"	0.70	1.87
250	"	0.65	1.73
	$[CF_2HCl]$ = 7.64x10^{12} moleule/cm^3, P_{Ar} = 1 torr		
10	0.60(/50)	4.80(/50)	8.00
20	"	4.30	7.17
30	"	3.70	6.17
40	"	4.50	7.50
50	"	3.15	5.25
60	"	2.15	3.58
70	"	1.60	2.67
80	"	2.00	3.33
100	"	1.50	2.50
120	"	1.10	1.83
150	"	0.70	1.17
200	"	0.60	1.00
250	"	0.70	1.17

a.) This is the time at which the aperature was opened after the laser pulse. For all measurements the gate width was 5 us.
b.) The number in parenthesis represents the number of pulses required to reach this level.

Table 4.4 (cont'd)
Enhancement Profile Data for the Freons

time[a] (us)	I, beam blocked[b]	I_e, beam not blocked[b]	$R = I_e/I$
	$[CF_3Cl] = 8.40 \times 10^{12}$ moleule/cm^3, P_{Ar} = 1 torr		
10	0.56(/50)	3.35(/50)	6.00
20	"	2.20	3.93
30	"	1.90	3.39
40	"	1.30	2.32
50	"	1.10	1.96
60	"	1.10	1.96
70	"	1.00	1.79
80	"	0.80	1.43
100	"	0.75	1.34
120	"	0.60	1.07
150	"	0.40	0.71
200	"	0.60	1.07
250	"	0.60	1.07

a.) This is the time at which the aperature was opened after the laser pulse. For all measurements the gate width was 5 us.
b.) The number in parenthesis represents the number of pulses required to reach this level.

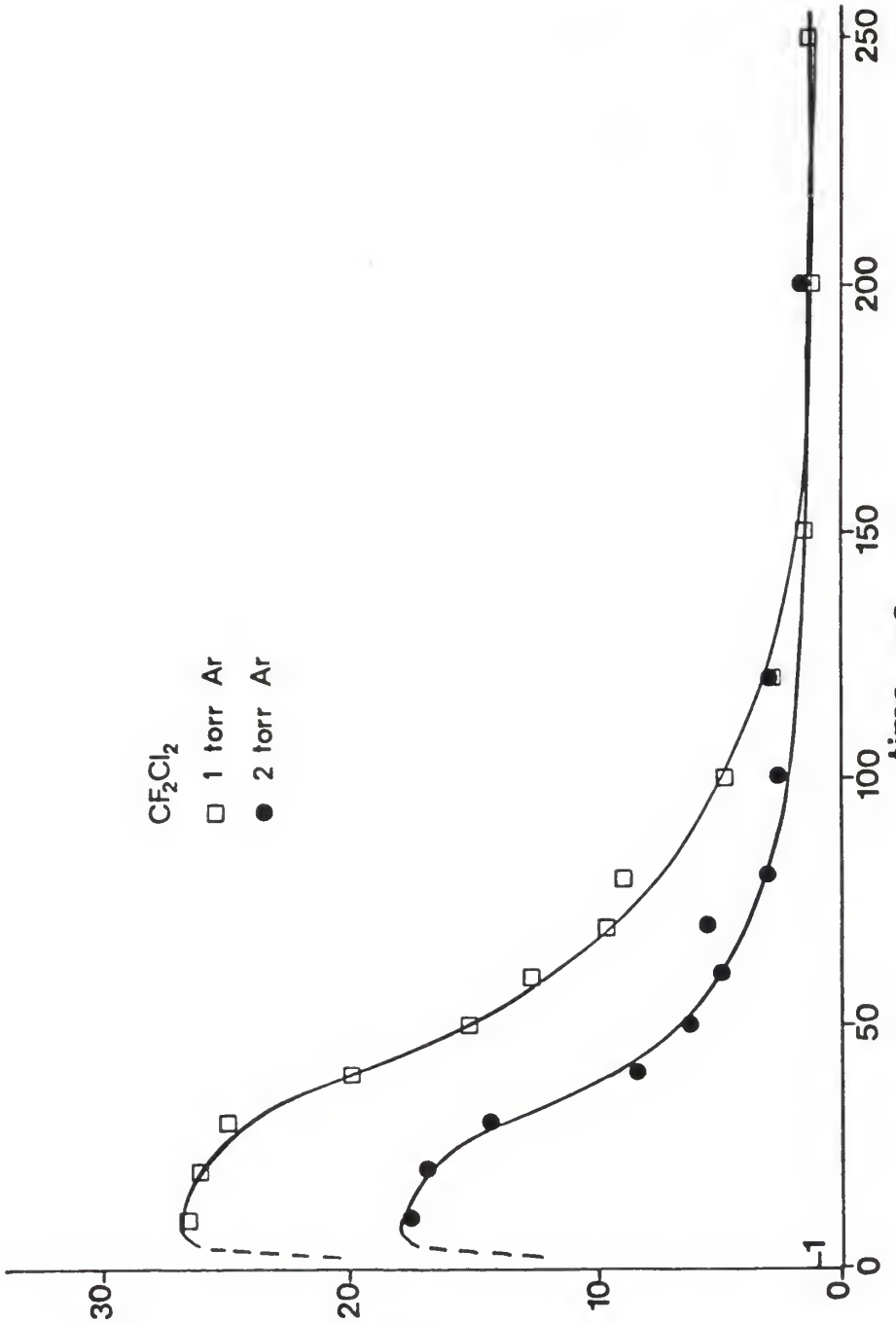

Figure 4.5 Enhancement profiles illustrating the dependence of R, the enhancement ratio, on Ar pressure. At higher pressure RCl^{**} is depleted by collisional deactivation.

Table 4.5
Enhancement Profile Data for CF_2Cl_2
for Different Ar Pressures.

time[a] (us)	I, beam blocked[b]	I_e, beam not blocked[b]	R = I_e/I ratio
	CF_2Cl_2 (3.6×10^{12} molecule/cm^3) in 1.0 torr Ar		
10	0.27(/10)	7.20(/10)	26.7
20	"	7.05	26.1
30	"	6.75	25.0
40	"	5.40	20.0
50	"	4.10	15.2
60	"	3.40	12.6
70	"	2.60	9.60
80	"	2.40	8.90
100	"	1.30	4.80
120	"	0.75	2.80
150	"	0.43	1.60
200	"	0.45	1.70
250	"	0.38	1.40
	CF_2Cl_2 in 2.0 torr Ar		
10	0.21(/10)	3.70(/10)	17.6
20	"	3.55	16.9
30	"	3.00	14.3
40	"	1.75	8.30
50	"	1.35	6.40
60	"	1.05	5.00
70	"	1.15	5.50
80	"	0.65	3.10
100	"	0.55	2.60
120	"	0.65	3.10
150	"	--	--
200	"	0.28	1.30
250	"	0.21	1.00

a.) This is the time at which the aperature was opened after the laser pulse. For all measurements the gate width was 5 us.

b.) The number in parenthesis represents the number of pulses required to reach this level.

cannot be expected to accurately model the experimental results since f_1 and f_2 are only very crude estimates of the actual fraction absorbed energy and, also because k_2 may not be true under our experimental conditions (i.e., 10^{-4} torr RCl as opposed to the pressure at which k_2 was actually measured). In fact k_2 is probably 10-100 times larger, thus our calculations give a larger R_2/R_2. However using values given earlier ($k_2 = 2.7\times10^{-13}$, t = 10us, [Ar] = 3.22×10^{16}, and assuming $f_1/f_2 = 1.0$) gives $R_1/R_2 = 1.09$. This value is not very close to the experimental value of 26.7/17.6 = 1.52 (using data from table 4.5 at 10us). However it does follow the predicion of decreasing R with increasing Ar pressure.

Other experimental variables indicated in table 4.6, affeted the enhancement. The maximum enhancement increased with increasing fluence as shown in figure 4.6 (due to increasing <n>). The ratio of R_1 (low ϕ) to R_2 (high ϕ) is

$$\frac{R_1}{R_2} = \frac{f_1 \exp(-k_2[Ar]t)}{f_2 \exp(-k_2[Ar]t)}$$

For a small change in ^ it is probably valid to assume that k_2 does not change much (i.e., the collisional relaxation will not change appreciably for increasing vibrational energy), suggesting that R_1/R_2 might be directly proportional to f_1/f_2, the ratio of the fraction of molecules absorbing at lower/higher fluence. It was shown in section 3.3 that increasing ϕ_o increases the amount of

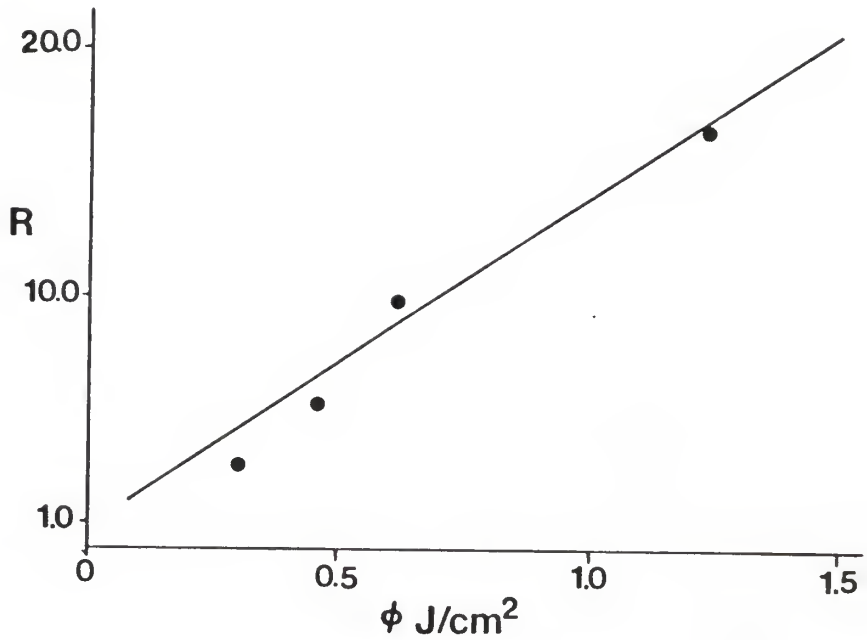

Figure 4.6 Maximum enhancement (R at the maximum of the enhancement profile) for CF_2Cl_2 as a function of incident fluence.

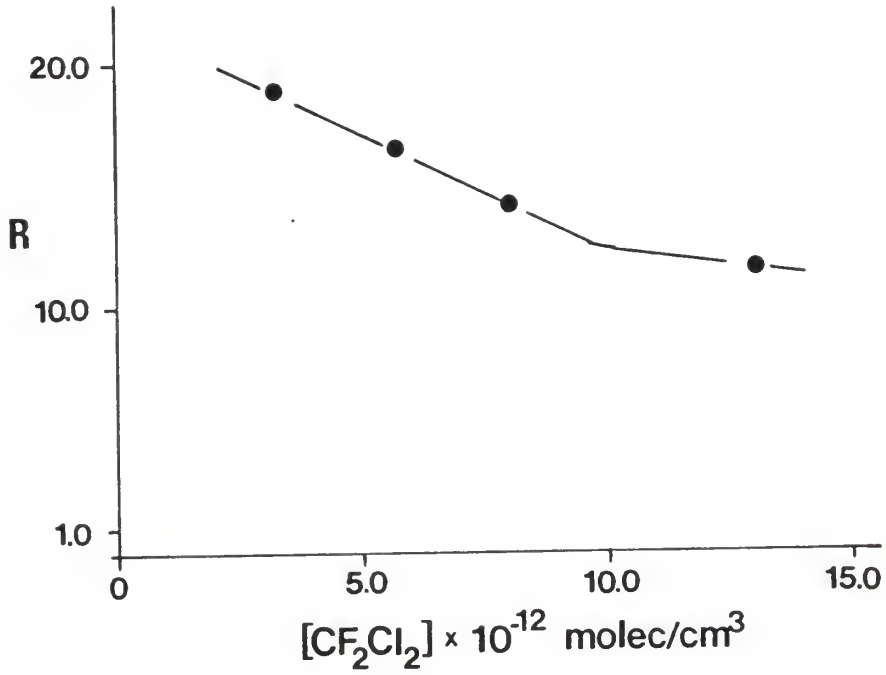

Figure 4.7 Maximum enhancement (R at the maximum of the enhamcement profile) as a function $[CF_2Cl_2]$. The decrease in R is attributed to collisional deactivation of RCl^{**} by cold RCl.

Table 4.6

Enhancement Maximum[a] Data for CF_2Cl_2 for Different Fluences.

ϕ_o (J/cm^2)	I, beam blocked[b]	I_e, beam not blocked[b]	R = I_e/I ratio
	CF_2Cl_2 5.70x10^{12} molecules/cm^3, 1 torr Ar		
1.23	0.50(/10)	8.19(/10)	16.4
0.62	"	4.97	9.94
0.46	"	2.91	5.32
0.30	"	1.69	3.38

a.) The maximum in the enhancement profile was monitored by setting the aperature 12us after the laser pulse.
b.) The number in parenthesis represents the number of pulses required to reach this level.

****

Table 4.7
Enhancement Maximum[a] Data for varying $[CF_2Cl_2]$.

$[CF_2Cl_2]$ molecule/cm^3	I, beam blocked[b]	I_e, beam not blocked[b]	R = I_e/I ratio
	CF_2Cl_2 in 1 torr Ar		
3.3x10^{12}	0.38(/10)	7.15(/10)	18.8
5.7 "	0.50	8.19	16.4
8.0 "	0.53	7.54	14.2
13.1 "	0.77	8.90	11.6

a.) The maximum in the enhancement profile was monitored by setting the aperature 12us after the laser pulse.
b.) The number in parenthesis represents the number of pulses required to reach this level.

energy absorbed (<n>) by RCl. However, determination of f in section 3.4 was only done for one fluence. Thus it does not seem possible to say from the model whether R_1/R_2 would increase with increasing fluence, but intuitively since <n> increases with increasing fluence (figure 3.5), it is not unexpected that the $XeCl^*$ enhancement increases "functionlly" with <n>. Furthermore, it was determined previously that σ is constant with ϕ and so should be f. From Figure 4.6 this functionality appears to be linear.

The enhancement maximum showed a weak inverse dependence on $[CF_2Cl_2]$ in the range $0.3\text{-}3.0\times10^{13}$ molecule/cm^3. This reflects the vibrational deactivation of $CF_2Cl_2^{**}$ by cold CF_2Cl_2 molecules. This also indicates that the assumption made previously, concerning neglecting this type of relaxation, is not quite correct. The data for the effect of increasing [RCl] is provided in table 4.6 and figure 4.9.

The finite rise time (about 12 us) of the enhancement profile is not what was expected. The CO_2 laser pulse lasts only 1.5 us, and the production of RCl^{**} should follow (rise with) the laser pulse. If the Xe^* and RCl are well mixed prior to the laser pulse, the $XeCl^*$ emission should also follow the rise of the laser pulse since the $XeCl^*$ lifetime is on the order of nanoseconds while the RCl^{**} lasts hundreds of microseconds. In a similar experiment with $XeCl^*$ production from $Xe(^3P_2)$ + HCl(v>0), Chang[10] accredited the finite rise time to a mixing time.

Inspection of the $XeCl^*$ flame in the laser irradiation zone indicates that incomplete mixing is also the explanation for a delayed rise time in our experiments.

As indicated in the time dependent expression for $I_{e/I_{XeCl}}*$, the enhancement ratio is also predicted to depend on the time the RCl^{**} is available (in the observation zone) for reaction with Xe^*. Unfortunately it was not possible to alter the rate at which RCl^{**} was flowing past the observation zone without significantly changing the pressure in the reactor. An attempt was made to mask the top half of the laser beam such that only the RCl directly in front of the PM tube mask was irriadiated. Apparently the PM tube mask has a wider field of view than the 0.2 mm indicated in chapter 2 thus instead of just inducing a faster decay time, as was expected, the overall signal was decreased.

References: Chapter 4

1.) J.E. Velazco, Ph.D. Thesis, p18, Chem. Dept., Kansas State University, Manhattan, KS, 1977

2.) J.H. Kolts, J.E. Velazco, D.W. Setser, J. Chem. Phys., 71(3) (1979) 1247; D. Lin, Y.C. Yu, D.W. Setser, J. Chem. Phys., 81(12) (1984) 5830

3.) J. Balamuta, M.F. Golde, A.M. Moyle, J. Chem. Phys., 82(7) (1985) 3169

4.) P.J. Hay and T.H. Dunning Jr., J. Chem. Phys., 69(5) (1979) 2209

5.) T.D. Dreiling and D.W. Setser, J. Chem Phys., 75(9) (1981) 4360

6.) ref. 1, p148

7.) J.E. Velazco, J.H. Kolts, D.W. Setser, J. Chem. Phys., 69(10) (1978) 4357; also ref. 1, pp107-129

8.) J.H. Kolts and D.W. Setser in Reactive Intermediates in the Gas Phase, ed. D.W. Setser, Academic Press (1979)

9.) Ma Xing-Xiao and Xu Zhu-De, Chem. Phys. Lett., 98(6) (1983) 563

10.) R.S.F. Chang, J. Chem. Phys., 76(6) (1982) 2943

CHAPTER 5 Discussions and Conclusions

5.1 Model for Xe^* + RCl Quenching

The branching fractions at 300K for CF_2Cl_2, CF_3Cl, and CF_2HCl with $Xe(^3P_2)$ are all quite low indicating that the major channel is non-reactive quenching. The non-reactive quenching is attributed to energy transfer followed by dissociation of the excited species.[1-3] Figure 1.2 illustrated the potential energy diagram relavent to the reactive quenching channel. Access to the XeCl(B,C) states is provided via a crossing with the Xe^+/RCl^- ion pair curve; a mechanism discussed by Setser and King in 1976.[4]

Golde[1] has discussed non-reactive quenching mechanisms. For CF_3Cl, CF_2Cl_2, and CF_2HCl with Xe^* the dominant events are

$$Xe^* + CF_2Cl_2 \text{ --> } Xe + CF_2 + 2Cl$$

$$Xe^* + CF_3Cl \text{ --> } Xe + CF_3 + Cl$$

and

$$Xe^* + CF_2HCl \text{ --> } Xe + CF_2H + Cl$$

$$\text{ --> } Xe + CF_2Cl + H.$$

The branching (fraction) for Cl-atom production is 1.96, 0.97, 0.85, and 0.35 (H atoms), respectively, for these

reactions (relative to 2.00 for Cl_2 and H_2). Thus, the k_Q for Xe^* + CF_2Cl_2 and CF_3Cl is associaed with the above reactions, while k_Q for Xe^* + CF_2HCl involves elimination of H and Cl, a process which is not as energetically permissable as the the former two. The quenching reactions are similar to Xe resonance (147 nm) photolysis in that larger Cl atom yields from chlorofluoromethanes occur for molecules with more Cl atoms.

Thus the reactions occur by excitation transfer to an electronically excited RCl state which subsequently dissociates. Since the k_Q values are less (see table 4.3) than the gas kinetic value ($3\text{-}4 \times 10^{-10}$ $cm^3 molecule^{-1} s^{-1}$), the excitation transfer occurs at short range. This is represented by the cross-hatched area around the entrance channel potential in figure 5.1.

5.2 IR Absorption

The three freons (chlorofluoromethanes) were found to have an absorption band (C-F stretch) corresponding to the R_{38} line of the $00^01\text{-}02^00$ band of the CO_2 laser. In addition, CF_2Cl_2 showed an overlap of the ν_8 rocking frequency with the P_{26} line of the $00^01\text{-}10^00$ CO_2 band. IR absorption spectra of several chlorofluoroethanes were also taken (1,2-DCTFE, 1,1-DCTFE, 1,1,2-TCTFE, and 1,1,1-TCTFE), and 1,2-dichlorotetrafluoroethane and 1,1,1-trichlorotrifluoroethane had a strong overlap (with the

CO_2 laser output) in the range 1030-1060 cm^{-1} which overlaps the P-branch of the 00^o1-02^o0 transition which extends from 1015-1055 cm^{-1}. The broadband absorption cross section was measured for the three freons (see section 3.2) and determined to be almost the same for all three. And all were considerably larger (10x) than the absorption cross section for CO_2 laser absorption even for a fluence as low as 0.1 J/cm^2. this is typical for small molecules.

The average energy absorbed was found to depend linearly on the incident fluence for the two asymmetric top molecules (CF_2Cl_2 and CF_2HCl) and the σ are constant over the range of fluence investigated (0.05-0.70 J/cm^2). The σ for CF_3Cl decreases with increasing fluence in the same range (see figure 3.4).

Our results can be compared to other studies in the literature. Duperex and van den Bergh[5] reported that increasing ϕ from 1.6-10.9 J/cm^2 (R(40) of the 9.2 um band) changed $\langle n \rangle$ for CF_2HCl at 0.3 torr in a linear way from about 2.0 to 12.0 photons/molecule; this correlates with the results in section 3.3 were $\langle n \rangle$ increased linearly from 0.1 to 2.6 photons/molecule with increasing ϕ from 0.05 to 0.7 J/cm^2. The discrepancy between our value at 0.7 J/cm^2 and their value at 1.7 J/cm^2 is due to the different pressures at which the $\langle n \rangle$ was measured (ours were measured at 4 torr) since σ depends on pressure. They also showed that $\phi > 10$ J/cm^2 was required for significant (14%/pulse)

laser induced dissociation of CF_2HCl. Grunwald et.al.[6] indicate that at 1.6 torr CF_2HCl and ϕ=.65 J/cm^2 (at 9.2 um), the fractional reaction to CF_2 + HCl is about 10^{-2}, and the energy of activation is 234 kJ/mole (equivalent to 18 photons at 9.2 um). King and Stephenson[7] predicted (from thermodynamic data) that $\langle n \rangle \geq 26$ (338 kJ/mole) is required for dissociation of CF_2Cl_2; they found that CF_2Cl_2 dissociation is $<10^{-2}$ for $\phi \leq 4$ J/cm^2.[8] Mevergniew[9] has shown that in the range ϕ=0.5-2 J/cm^2 and pressure from 0.5 to 60 torr, the fractional dissociation of CF_3Cl is less than 10^{-4}.

In chapter 3 (table 3.5) the $\langle n' \rangle$ for CF_2Cl_2 was 26.5, for this energy unimolecular reaction could possibly be occuring but this energy is near the threshold. However this $\langle n' \rangle$ must be an upper limit on the true value since there are relaxation processes occuring during these measurements which are not taken into account. And $\langle n' \rangle$ for CF_2HCl and CF_3Cl are 25.5 and 30.0, respectively. As mentioned before the value for CF_3Cl is much more uncertain than the others. Our experiments were conducted at ϕ<1.0 J/cm^2 and P<1 torr, there is no indication from the literature that laser induced unimolecular reaction is occuring to any significant extent. This is particularly important for the $XeCl^*$ enhancement experiments since dissociation induced by the laser pulse would produce unpredictable results in k_Q and k_{XeCl^*}. This is also the reason no attempt was made on $XeBr^*$ enhancement from

vibrationally excited CF_2ClBr (i.e., trying to measure the <n> for this compound resulted in coating of the NaCl windows on the absorption cell with Br_2 as was evidenced by a yellow color).

5.3 Enhancement

The enhancement in $XeCl^*$ formation was found to occur when the RCl molecule was irradiated by the CO_2 laser pulse (figure 4.8). The dependence on fluence for CF_2Cl_2 indicated that the enhancement increased with the level of vibrational energy. In the model used, the RCl molecules were divided into to groups, those which absorb energy from the field and those which did not (due to a broad rotational distribution in the ground vibrational level). The fraction, f, of molecules absorbing energy from the IR field was estimated by comparing the energy absorbed at 0.5 torr to the energy absorbed when "all of the molecules in the sample were able to absorb the energy," because of high collision frequency (near 1 atm Ar). This means that the average energy absorbed, under collisionless conditions, by the fraction, f, of the sample is approximately <n>/f.

The ionic-covalent curve crossing mechanism for the production of $XeCl^*$ from $Xe(^3P_2)$ + RCl explains the low branching yields of $XeCl^*$. Setser et.al.,[10,11] have illustrated that increasing the energy of the entrance channel, by using Xe(6p,9.8eV) instead of Xe(6s,8.3eV),

increases the production of $XeCl^*$. Raising the electronic energy of the entrance channel allows the ion pair potential to cross the entrance channel around 5 angstroms and reactive quenching becomes more efficient than the competing excitation transfer which is followed by dissociation at shorter range.

The enhancement observed in the experiments presented in this thesis may also be qualitatively explained in terms of the competition between excitation transfer and the covalent-ionic curve crossing. Since the energy provided for enhancement was in the form of vibrational rather than electronic energy, the enhancement is not necessarily explained by raising the energy of the potential entrance channel (i.e., the potentials are calculated in the Born-Oppenheimer approximation from the motion of the electrons, not the nuclei). Nevertheless, it may be relevant that the Xe(6p) electronic energy and the added vibrational energy are comparable. The enhancement of $XeCl^*$ formation also correlates with electron attachment cross sections. Electron attachment experiments for the methanes mentioned above[12a] provided results which initially made these molecules particularly interesting for enhancement studies, i.e., the thermal (300K) dissociative electron attachment rate constant increased consistently in the order $k(CF_4) \leq 10^{-17}$, $k(CF_3Cl) = 7 \times 10^{-14}$, $k(CF_2Cl_2) = 7 \times 10^{-10}$, $k(CFCl_3) = 1 \times 10^{-7}$ $cm^3 molecule^{-1} s^{-1}$. Christophorou et.al.[12b] have shown that the dissociative

electron attachment cross section for CF_3Cl increases almost a factor of x3 with increasing temperature from 300K to 750K. Also the energy of the onset of dissociative electron attatchment decreases from 1.55 eV to 1.1 eV in the same temperature change. Thus, it is plausible to expect that increasing the vibrational energy concomitantly increases the propensity for electron attachement for electrons to be provided by Xe^*. It is difficult to understand the exact mechanism as it relates to the potential diagram in figure 1.2. For the 300K Xe^*/RCl reaction pair, the incoming trajectories are within a very small Boltzmann distribution around the entrance channel. Increasing the vibrational energy of the RCl creates a new energy population, illustrated by the schematic higher energy distribution in figure 5.1. This new energy distribution must lead to the enhanced formation of $XeCl^*$ because the vibrational energy aids the long range coupling of the entrance channel to the ion pair potential. The vibrational energy probably allows the RCl molecule to reach the RCl^- potential, via internal coordinaties not easy to show on the potential diagram.

The values of k_Q for all of the methanes in table 4.3 are of the same magnitude as the gas kinetic rate constant for these reactions, and the non-reactive quenching occurs almost unit branching over reactive quenching. Thus, the enhancement of the $XeCl^*$ branching fraction is most probably not due to a change in the total quencing rate

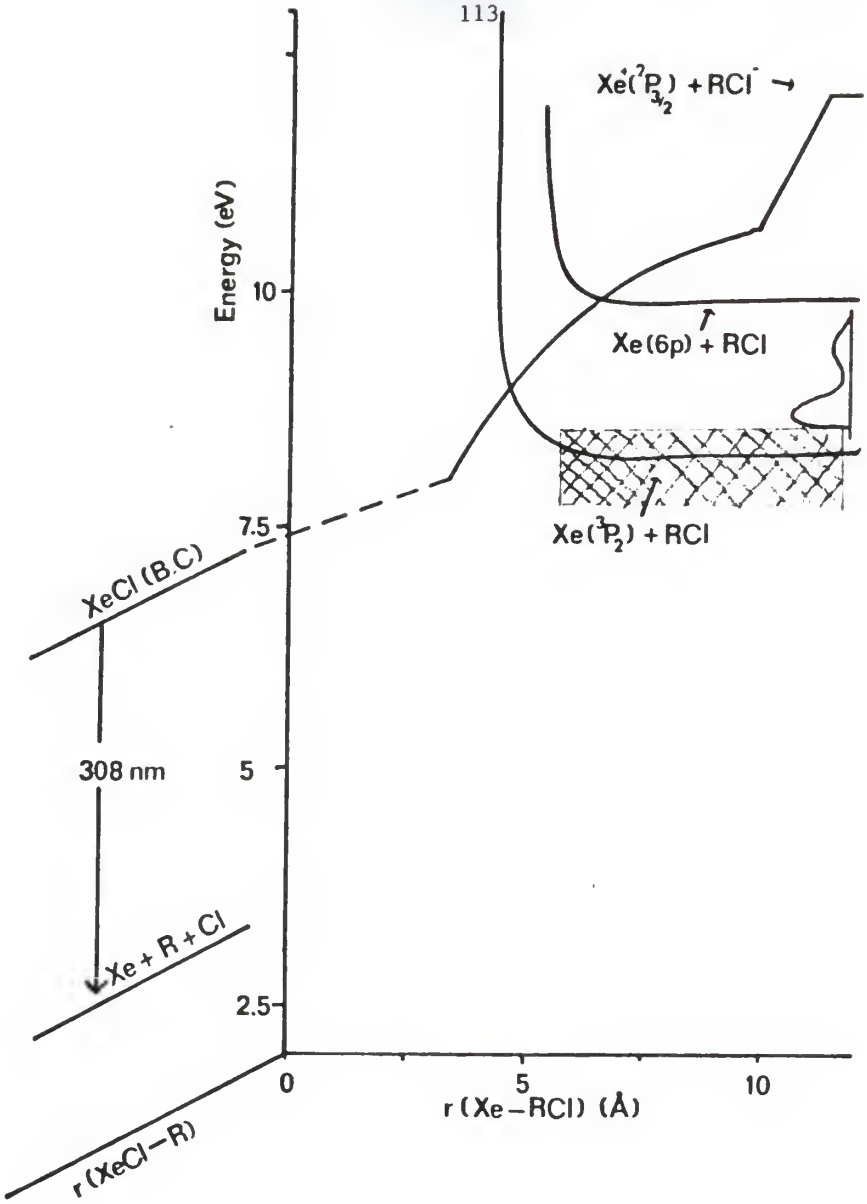

Figure 5.1 Potential energy diagram for $XeCl^*$ formed via reaction of $Xe(^3P_2)$ with RCl. Also shown on this plot is a schematic representation of a Boltzmann vibrational distribution and a vibrationally excited RCl, RCl^{**}, distribution. See chapter 1 for method of drawing the potentials.

constant, but rather an increase in the reactive quenching rate constant (k_1 in section 4.3). The following equation

$$\Gamma^{**}_{XeCl^*} = \frac{k_1}{k_Q} = \Gamma_{XeCl^*}\frac{R}{f}$$

and data from tables 4.5 (R at 10 us), 3.5 (f), and 4.3 (Γ_{XeCl^*}) give the enhanced (adjusted for the fraction of molecules absorbing the energy) branching fractions, $\Gamma^{**}_{XeCl^*}$, for the vibrationally excited molecules as 1.33, 0.54, and 0.94 for CF_2Cl_2, CF_2HCl, and CF_3Cl, respectively. The large value for CF_2Cl_2 is not readily explainable. Since f is expected to be an upper limit on the actual fraction of molecules absorbing the radiation, it can not be the source of error. As mentioned above, the $XeCl^*$ steady state branching fractions agree well with previous results. The measurement of R, the enhancement ratio, could lead to error since it is dependent on an acurate measure of the $XeCl^*$ steady state emission signal which is generally not as strong as the enhanced signal and could give an over estmate of R, and thus the enhanced branching fraction.

5.4 Conclusions

The production of $XeCl^*$, from the reactive quenching of $Xe(^3P_2)$ by CF_2Cl_2, CF_3Cl, and CF_2HCl, is significantly enhanced by addition of vibrational energy to the 300K

reaction pair (Xe^*/RCl). There is a large uncertainty in the enhanced branching values due mostly to the uncertainty in the f values. However, the $XeCl^*$ branching is obviously increased by the addition of vibrational energy. The inherently low $XeCl^*$ formation from the 300K reaction is explained by the $V(Xe^+,RCl^-)$ being inaccessible to thermal trajectories on the $Xe(^3P_2)/RCl$ entrance potential. Addition of vibrational energy effectively couples the two potentials so that the ion pair curve is more accessible to the incoming collision pairs. While there have been a number of publications (see chapter 1) concerning enhancement of bimolecular reactions via addition of vibrational energy, this is believed to be the first involving infrared multi-photon absorption (IRMPA) as the source of vibrational excitation.

There are possibilities for further experiments regarding reaction enhancement by IRMPA with metastable systems. Enhancement of $XeCl^*$ production from Xe^* + chlorofluoroethanes is a prime example although of the several molecules considered, only $1,2\text{-}C_2Cl_2F_4$ and $1,1,2\text{-}C_2Cl_3F_3$ were found to have significant vibrational absorption in the range of the CO_2 laser. Experiments with CF_3CH_2Cl would be useful because the IR absorption cross sections are known.[13] Repetition of the work here with $Kr(^3P_2)$ would be of interest because the higher energy changes the electronically excited RCl states involved in the ion potential. Study of the production of XeO^* and

XeS* is also a prospect, since Γ_{XeO}* and Γ_{XeS}* are small (Γ_{XeO}*$\leq$0.10)[14] and the output of the CO_2 laser has been found to populate at least the O_3(010) vibrational level.[15]

References: Chapter 5

1.) J. Bulamuta, M.F. Golde, A.M. Moyle, J. Chem. Phys., 82(7) (1985) 3169

2a.) J.H. Kolts, J.E. Velazco, D.W. Setser, J. Chem. Phys., 71(3) (1979) 1247
b.) D. Lin, Y.C. Yu, D.W. Setser, J. Chem. Phys., 81(12) (1984) 5830

3.) J.E. Velazco, J.H. Kolts, D.W. Setser, J. Chem. Phys., 69(10) (1978) 4357

4.) D.L. King and D.W. Setser in "Annual Review of Physical Chemistry, Reactions of Electronically Excited-State Atoms", 27 402-447, Annual Reviews Inc., (1976)

5.) R. Duperrex and H. van den Bergh, J. Chem. Phys., 75(7) (1981) 371

6.) E. Grunwald, K.J. Olszyna, D.F. Dever, B. Knishkowy, J. Am. Chem. Soc., 99(20) (1977) 6515

7.) D.S. King and J.C. Stephenson, Chem. Phys. Lett., 51(1) (1977) 48

8.) R.J.S. Morrison, R.F. Loring, R.L. Farley, E.R. Grant, J. Chem. Phys., 75(1) (1981) 148

9.) M. Neve de Mevergues, "Topical Meeting on Multiphoton Processes, Miramare (Trieste)", 18-22 March, 1985, Belgium

10.) J.K. Ku and D.W. Setser, Appl. Phys. Lett., 48(11) (1986) 689

11.) J. Xu, A.R. Slagle, D.W. Setser, J.C. Ferrero, Chem. Phys. Lett., (submitted March 1987)

12a.) R. Schumacher, H.R. Sprunken, A.A. Christodoulides, R.N. Schindler, 80(20) (1978) 2248
b.) S.M. Spyrou and L.G. Christophorou, J. Chem. Phys., 82(6) (1985) 2620
c.) S.M. Spyrou and L.G. Christophorou, J. Chem. Phys., 83(6) (1985) 2829

13.) D.W. Setser, T.S. Lee, W.C. Danen, J. Phys. Chem., 89(26) (1985) 5799

14.) J. Xu, D.W. Setser, J.K. Ku, Chem. Phys. Lett., 132(4,5) (1986) 427

15.) R.J. Gordon and M.C. Lin, Chem. Phys. Lett., 22(2) (1973) 262

APPENDIX I SYMMETRIC TOP ROTATIONAL DISTRIBUTION

In order to try and obtain a better understanding of the rotational energy levels of polyatomic molecules the author is adding this appendix. Most of the discussion herein is taken from Herzberg (Molecular Spectra and Moleular Structure, II Infrared and Raman Spectra of Molecules, Van Norstrand Reinhold Co., 1945 pp13-29). The program listing at the end of this appendix was used to calculate the rotational distribution for CF_3Cl in figure 3.1.

The formula for the energy levels of a polyatomic moleule may be derived in a semiclassical way by considering the kinetic energy of rotation about all three rotation axis x, y, and z

$$E = \frac{1}{2}I_x w_x^2 + \frac{1}{2}I_y w_y^2 + \frac{1}{2}I_z w_z^2 = \frac{P_x^2}{2I_x} + \frac{P_y^2}{2I_y} + \frac{P_z^2}{2I_z}$$

where I_i are the moments of inertia, w_i are the angular velocities, P_i the angular momentum about the x, y, and z axis, and the relation $P_i = w_i \Sigma_i mr$ was used. For a prolate symetric top P_z is taken as the C_3 rotation axis or the principle rotation axis and $P_A \equiv P_z^2 = K^2$ gives K as the angular momentum quantum number for rotation about the figure axis as shown below. Also as defined for a prolate symmetric top $I_x = I_y \equiv I_B$.

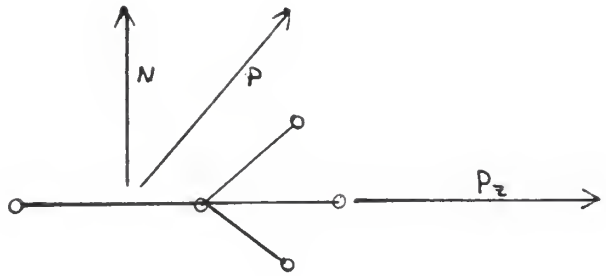

The sum of the squares of the angular momentum of the P_x and P_y axis gives N^2, $P_x^2 + P_y^2 = N^2$. While K is given by the rotation of the three identical nuclei about P_z, P_z is also rotating about P, which is the resultant of the P_x and P_y with P_z, i.e. $P^2 = P_x^2 + P_y^2 + P_z^2$. Rotation about P occurs with frequency $P/2\ I_B$ which is the same frequency as the rotation of a diatomic moleule with moment of inertia I_B and angular momentum P = J. Thus $J^2 = P_x^2 + P_y^2 + K^2$ or $P_x^2 + P_y^2 = J^2 - K^2$ and the total kinetic rotational energy is now given as

$$E = \frac{J^2}{2I_B^2} - K^2\left(\frac{1}{2I_B^2} - \frac{1}{2I_A^2}\right)$$

and using the magnitude of the total angular momentum

$$E = \frac{J(J+1)h^2}{2I_B^2} + K^2\left(\frac{h2}{2I_A} - \frac{h2}{2I_B}\right)$$

And now using the rotational spacing constants $A = h^2/2I_A^2$ and $B = h^2/2I_B^2$ gives

$$E_{J,K} = BJ(J+1) + K^2(A-B)$$

as the formula for the energy levels of a prolate (rigid rotor) symmetric top. For a given J value, the value of K may vary since K represents the rotation of P_z about P thus J is always at least as big or bigger than K

$$J = K,K+1,K+2,.....$$

or K can take values less than J

$$K = J,J-1,J-2,....-J.$$

And according to the $E_{J,K}$ expression above, states of a particular J>0 are doubly degenerate in K since K takes on + and - values. The + and - values coorespond to two different directions of P_z rotation about P.

Using this energy level formula it is possible to calculate a thermal distribution of rotational levels according to the equation

$$N_{J,K} \sim g_{J,K}e^{-E_{J,K}/kT}.$$

The degeneracy factor, $g_{J,K}$, is 2J+1 for J=0 (since K=0 only) but is 2(2J+1) for J>0 (since $K=\pm J$). These two degeneracies are taken into account in lines 380 and 410 of

the program listing. The above equation differs from the equation for a diatimic or linear molecule by a factor $e^{(-(A-B)K^2/kT)}$ as well as by a statistical weighting factor. The statistical weighting factor arises due to the nuclear spin of the three identical nuclei for molecules with threefold rotation axis such as a C_{3v} symetric top like CF_3Cl. This leads to levels with K=0,3,6,9,... having larger statistical weights than those with K=1,2,4,5,7,8,... In general it is given that for K divisible by 3 (including zero) the weight is $1/3(2I+1)(4I^2+4I+3)$ and for K not divisible by 3 the weight is $1/3(2I+1)(4I^2+4I)$ where I is the spin of the three identical nuclei. For ^{19}F, I=1/2 giving a weight of 4:2 for K divisible by 3:K not divisible by 3. These weights are considered in lines 380 and the decision in line 420 of the program listing.

The program calculates the moments of inertia I_A and I_B by equations from P.W. Atkins (Physical Chemistry, Oxford University Press, 1982, p574) at lines 190-240. The rotatinal spacing constants were calculated (lines 290,300) to be A=0.129 cm^{-1} and B=0.115 cm^{-1}. These values are used to calculate the distribution from the double loops at lines 370-470. The distribution is calculated by summing the "sub-distributions" for all +K's at a particular J value and including weighting for the degeneracy as well as weighting for nuclear spin mentioned in the previous paragraph.

```
10  REM  *** CALCULATE ROTATIONAL DISTRIBUTION ***
20  REM  *** FOR CF3CL ***
30  DIM X(151),Y(151)
40  H = 6.6262E - 34:AN = 6.02E23:PI = 3.1415927
50  REM  H is Plancks constant
60  REM  AN is Avogadros´ number
70  REM  PI is the obvious
80  KT = 1.3807E - 23 * 300 * 5.034E22
90  REM  KT is the Boltzmann constant times the temperature
    (300 K)
100  REM  KT is converted to wavenumbers
110  M1 = 18.998:M2 = 12.011:M3 = 35.453: REM g/mole
120  REM    M1,  M2,  and  M3  are  the masses of Fluorine,
    Carbon, and Chlorine
130  M = 3 * M1 + M2 + M3
140  R1 = 1.6:R2 = 1.4: REM angstroms
150  NP = 150
160  TH = 110: REM  degrees
170  REM  TH  is roughly the angle between Cl and the three
    F´s
180  TH = TH * PI / 180: REM  machine needs radians
190  IA = 2 * M1 * R1 ^ 2 * (1 -  COS (TH))
200  T1 = IA / 2
210  T2  =  (M1  /  M) * (M2 + M3) * R1 ^ 2 * (1 + 2 *  COS
    (TH))
220  T3 = (M3 / M) * R2 * ((3 * M1 + M2) * R2 + 6 * M1 * R1
    * ((1 + 2 *  COS (TH)) / 3) ^ (1 / 2))
230  IB = T1 + T2 + T3
240  IA = IA / 1E3:IB = IB / 1E3
250  REM IA AND IB are the moments in kg/mole Ang^2
260  REM    the  equations  for the moments were taken from
    P.W. Atkins Physical Chemistry
270  PRINT "Ia = ";IA;" kg Ang^2"
280  PRINT "Ib = ";IB;" kg Ang^2"
290  RK  = H * AN / (8 * PI ^ 2) * 1E20 / 3E10: REM   cm^-1
    kg Ang^2
300  A = RK / IA:B = RK / IB: REM  cm^-1
310  PRINT "A = ";A;" cm^-1"
320  PRINT "B = ";B;" cm^-1"
330  REM  A and B are the rotational spacing constants
340  MJ = 0
350  REM MJ is the maximum of the distribution
360  REM The following J,K loops calculate the distribution
370  FOR J = 0 TO NP
380  X(J) = J:Y(J) =  EXP ( - (B * J * (J + 1)) / KT) * 2 *
    (2 * J + 1): REM K=0
390  FOR K = 1 TO J
400  EJ = B * J * (J + 1) + (A - B) * K ^ 2
410  YA =  EXP ( - EJ / KT) * 2 * (2 * J + 1)
420  IF  INT (3 / K *  INT (K / 3) + .001) = 1 THEN YA = YA
    * 2
430  Y(J) = Y(J) + YA
440  NEXT K
```

```
450  IF Y(J) > MJ THEN MJ = Y(J)
460  PRINT J;" ";
470  NEXT J
480  FOR J = 0 TO NP:Y(J) = Y(J) / MJ: NEXT J
490  REM  Create  a  data  file  to  be  read by a plotting
     program
500  F$ = "CF3CL ROT DIST"
510  XT$ = "J"
520  YT$ = "P(J)
530  PRINT
540  PRINT  CHR$ (4)"OPEN ";F$
550  PRINT  CHR$ (4)"WRITE ";F$
560  PRINT XT$","YT$","NP
570  FOR J = 0 TO NP: PRINT X(J),Y(J): NEXT J
580  PRINT  CHR$ (4)"CLOSE"
```

APPENDIX II DETAILED DESCRIPTION OF LASER OPERATION AND MAINTENANCE

The Lumonics model 103-2 CO_2 laser (S.N. 1689) used in these experiments requires four gas cylinders for operation. One He tank (medium grade), one CO_2 tank (medium grade), and two N_2 tank (high purity). One of the N_2 tanks is for the gas mix and the other is for the spark gap. Although the operating manual specifies that the spark gap may be operated with dry air, it was determined that the standard air cylinders available through the chemistry department contained too much H_2O. This was evidently the cause of a blue-green powder buildup in the spark gap cavity and on the brass electrodes which led to poor or no discharge in the laser cavity. The spark gap was cleaned on several occasions by the procedure in the operating manual. Thus, N_2 is recommended for the spark gap.

With the gas cylinders conected the following series of steps are required for power up;

1.) Switch the key on (turn clockwise)

2.) Press the gas flow switch (green light)

2a.) Open the gas regulators and adjust delivery pressure (described below).

2b.) Adjust the flow meters on the power supply. (The

startup flows suggested in the operation manual are $He/CO_2/N_2$ = 90/6/4%, see flow calibrations in the manual to determine the flow settings.)

2c.) Allow the system to purge about 30 minutes if it has not been operated for about a week.

3.) With the hign voltage knob turned to zero press the H.V. switch. (If the white interlock light is on the high voltage will not come on; be sure the cover is down tight.) Now turn the high voltage knob up gradually until the laser is firing regularly. With the startup flow rates H.V. could be between 25 and 40 kV.

In general the laser should not be operated with the top off, but if it is necessary the interlock switch at the rear of the laser may be held down by hand. Under no circumstances should one reach across or stand next to the laser with the cover off and the High Voltage on. Read the precautions in the operation manual carefully before removing the cover for any kind of maintenance. The capacitors carry a lethal charge. A grounding stick may be constructed by attatching a 3 inch piece of copper tube to the end of a 2 foot wooden stick and attatching a grounding cable between the cooper and a water pipe in the room. This grounding stick should be used every time prior to working inside the laser to assure that any residual charge is drained, even though the interlock circuit is supposed

to draw off any charge when the top is removed.

Each of the four gas cylinders was fitted with appropriate two stage regulators and the delivery pressures were maintained at the following values;

He	10.0 psig
CO_2	10.0 psig
N_2	10.0 psig
N_2(spark gap)	18.0-24.0 psig (variable)

The spark gap N_2 pressure was adjusted by setting the trigger at the single position and gradually increasing the delivery pressure from the regulator (from 18.0 psig) so the laser did not fire. Then switching the trigger to repetitive the laser fired at the selected rate. With the rate knob turned completely counter clockwise, the rate was 0.5 Hz. If the pressure was too low the laser fired randomly rather than with the trigger. When the pressure was high enough the laser fires with the trigger from the power supply. If it is too high the laser would mis-fire or not fire at all.

The laser gas mix was controled at the power supply front panel by three seperate flow meters, one for each gas $He/CO_2/N_2$. The gas ratio was altered from the start up values to obtain optimum laser output. For example, holding CO_2 constant and increasing the N_2 increases the output energy, but also increases the pulse length.

Increasing the He pressure may help keep the pulse length down. Completely eliminating N_2 provides the shortest pulse but lowest energy. Clara Jang's thesis (chapter 2, page 25) shows the pulse profile at several $He/CO_2/N_2$ ratios.

Tuning the laser to a particular output CO_2 line was most easily accomplished as follows, assuming there is only one person to do the tuning. With the laser triggering and firing properly (as described before) a block of wood was placed about 1 foot in front of the output aperture. From the rear of the laser the tuning knob is turned 1/8 turn per trigger until the loud snapping of the laser beam stricking the wood was heard. The line was identified by removing the block of wood and permitting the beam to enter the CO_2 spectrum analyzer. Aligning the spectrum analyzer is simply a matter of adjusting the two rear screw legs and positioning it left and right so that the beam enters almost linearly. The beam, passing through the entrance slit, strikes a viewing monitor about 2 inches inside the analyzer. The viewing monitor is seen by opening the lid on top of the analyzer as much as possible and looking straight down into the unit. The monitor is yellow and a dark spot the shape of the slit will be observed each time the laser beam strikes it. This monitor may be moved up and down by a knob in the rear of the analyzer. The slit is also adjusted by a knob in the rear of the instrument. The energy entering the analyzer is kept low by keeping the

slit narrow to prevent damage of any internal optics. Lowering the monitor the beam will pass to a mirror-grating-mirror series creating a total path length of 2.3 meters, and deflecting the beam to a fluorescent UV-illuminated surface which is scaled by wavelength, frequency, and CO_2 laser transition number. A flash is created below the scale where the laser energy strikes the surface of a carbon block. Once the line number is determined the block of wood is placed back in front of the beam and the tuning knob in the rear of the laser is adjusted in the same maner as before (i.e. 1/8 turns) in the direction cooresponding to higher or lower wavelength, which ever is desired.

Several problems with the laser arose during the course of these experiments; the problems and their solutions are briefly discussed here. Mis-firing (no lasing but discharging of the capacitors) may be due to many problems as mentioned in the trouble shooting section of the operation manual. Our most common problem was a dirty spark gap, but this was due mainly to H_2O in the air cylinder (as mentiond previously) and this problem was solved by using N_2 instead of air. If the laser is providing steady repetative pulses and suddenly stops firing with no laser output and no capacior discharge it is quite likely tht the KN-26 high voltage trigger tube needs to be replaced. This tube has a specfied lifetime of about 25,000 shots at 0.5Hz which should provide about 14 hours

of operation. The tubes are available from EG&G Co. at a cost of $200.00 (as of January 1987; up from $130.00 one year earlier). Installation of the tube requires an allen wrench, a soldering iron, some solder, and some patience and the procedure is outlined in the operation manual; however Mr. Al Wyerts is quite familiar with the procedure. Another problem which typically occurs is a continuous drop in the He pressure during the experiment leading to a drop in output energy. To maintain the delivery pressure at 10.0 psig on the He regulator it was necessary to adjust the guage every 30-45 minutes (the pressure generally dropped from 10.0 to 9.5 in this time period). Another (particularly alarming) problem was the generation of extremely loud popping (almost exploding) sounds from within the laser cover when it triggered. With the help of John Linzi the problem was determined to be an oil spill below the capacitor nearest the rear of the laser, which was providing a direct path to ground. So whenever the trigger occured, the capacitor discharged to ground rather than across the electrodes inside the cavity. The oil was cleaned up and the problem was apparently solved. The source of the oil was most probably from the transformer in the rear of the laser, which may have spilled when the laser was moved from the second to the first floor of Willard Hall, as carrying it down the stairs necessitated tilting it slightly.

APPENDIX III MONOCHROMATOR CALIBRATIONS

The calibrations in this appendix were all taken for the 0.3 meter McPherson (Czerny-Turner type) monochromator used for the experiments of this thesis. The first calibration is with the 300 line/mm grating and RCA P28 PMT also used in these experiments. The source used was a D_2 lamp (Optronic Laboratories, Inc., Lamp #268). Table TIII-1 lists the data used to plot figure 2.4. The second calibration is for the same optics and detection system but the source this time was a quartz/I_2 lamp (Optronic Laboratories, Inc., Standard L-205) which permitted more accurate calibration above 300nm as opposed to the D_2 lamp. These calibrations were not used to correct the $XeCl^*$ emission spectra since the response does not vary excessively over the range 230-320 nm where most of the $XeCl^*$ emission occurs. Table TIII-2 lists the data for the second calibration and figure FIII-1 shows the response profile.

The third calibration (Table TIII-3) is for the same monochromator but with a 1200 line/mm grating and RCA R955 cooled PMT. The source was a D_2 lamp (Optronics Laboratories, Inc., Lamp # 425). For the fourth calibration (Table TIII-4) the source was the same quartz/I_2 lamp mentioned above and Table TIII-4 lists the data for the this calibration.

All calibrations were taken with a quartz diffuser in front of the slit to assure dispersion of the source radiation and prevent difraction anomolies. The source lamp was positioned about 1-2 feet in front of the slit. Figure FIII-2 is the combined calibration from Tables TIII-3 and TIII-4.

Each of the following data tables consists of 4 columns. The first two columns are the wavelength and relative spectral irradiance at each wavelength. The spectral irradiance is provided with the calibrated lamp and is made relative by dividing each value by the cooresponding wavelength. The third column is the relative intensity as read from a strip chart recorder. (driven by a photon counting system). The last column is the response curve which is the normalized (to unity) ratio of the relative lamp standard values to the measured intensities.

Table TIII-1
Monochromator Calibration

Source: Deuterium Lamp (#268)
Spectral Range: 180-400nm
Monochromator: 0.3m McPherson
Grating: 300 lines/mm, blazed at 300nm
PM-tube: Hamamatsu R212

wavelength (nm)	spectral irradiance	relative output	response ratio
180	6.210	0.00	0.00
190	5.871	0.13	0.00691
200	5.660	0.75	0.0416
210	5.121	2.60	0.159
220	4.994	5.37	0.338
230	4.899	6.05	0.388
240	4.656	9.25	0.622
250	4.250	9.20	0.678
260	3.796	8.65	0.713
270	3.321	7.95	0.747
280	2.968	7.40	0.778
290	2.694	6.85	0.794
300	2.436	6.30	0.809
310	2.127	5.75	0.844
320	1.939	5.30	0.853
330	1.719	4.80	0.872
340	1.571	4.40	0.875
350	1.414	4.00	0.881
360	1.256	3.65	0.909
370	1.095	3.30	0.941
380	1.022	3.15	0.963
390	0.952	3.05	1.000
400	0.968	2.69	0.841

Table TIII-2
Monochromator Calibration

Source: Quartz/I_2 Lamp (L-205)
Spectral Range: 250-450nm (through 2500nm available)
Monochromator: 0.3m McPherson
Grating: 300 lines/mm, blazed at 300nm
PM-tube: Hamamatsu R212

wavelength (nm)	spectral irradiance	relative output	response ratio
250	0.000923	0.30	0.164
260	0.00169	0.33	0.278
270	0.00305	0.43	0.383
280	0.00515	0.60	0.458
290	0.00827	0.83	0.535
300	0.0132	1.23	0.576
320	0.0281	2.47	0.608
350	0.0735	6.15	0.638
370	0.123	10.17	0.646
400	0.246	18.00	0.730
450	0.599	32.00	1.00

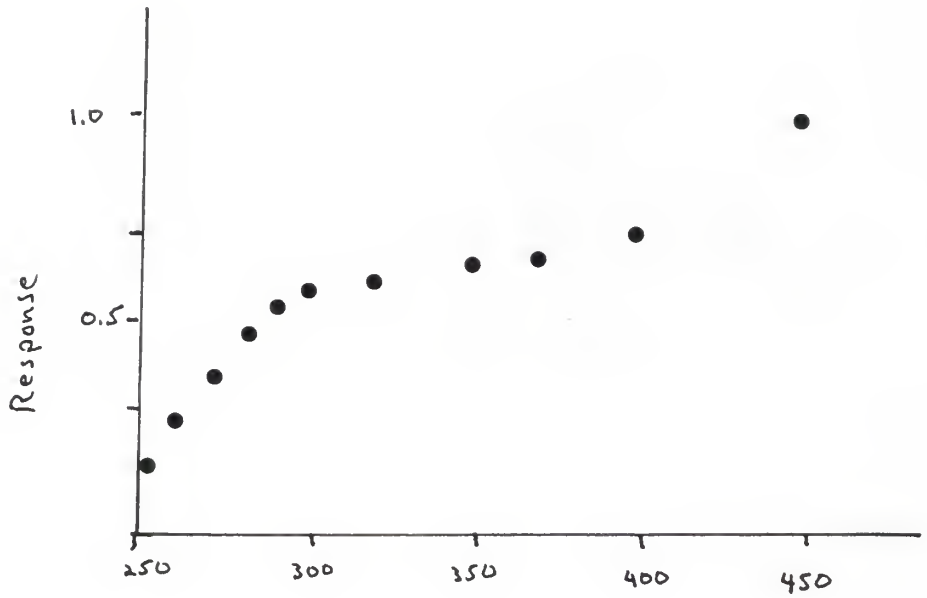

Figure FIII-1 Response curve using Quartz/I_2 lamp. The region of interest for $XeCl^*$ emission studies is relatively flat. This is important for considerations in chapter 4.

Table TIII-3
Monochromator Calibration

Source: Deuterium Lamp (#425)
Spectral Range: 200-400nm
Monochromator: 0.3m McPherson
Grating: 1200 lines/mm, blazed at 150nm
PM-tube: Hamamatsu R955

wavelength (nm)	spectral irradiance	relative output	response ratio
200	3.780	1.65	0.138
210	8.000	4.05	0.370
220	7.282	5.75	0.578
230	6.716	6.95	0.758
240	5.880	7.00	0.835
250	4.875	6.23	0.935
260	4.134	5.50	0.974
270	3.699	5.00	0.990
280	3.332	4.55	1.000
290	3.103	4.08	0.961
300	2.844	3.65	0.939
310	2.616	3.15	0.881
320	2.390	2.80	0.858
330	2.185	2.50	0.838
340	1.989	2.23	0.819
350	1.809	1.95	0.789
360	1.555	1.78	0.836
370	1.406	1.60	0.833
380	1.334	1.45	0.796
390	1.232	1.35	0.802
400	1.228	1.25	0.745

Table TIII-4
Monochromator Calibration

Source: Quartz/I_2 Lamp #L-205
Spectral Range: 350-1000nm
Monochromator: 0.3m McPherson
Grating: 1200 lines/mm, blazed at 150nm
PM-tube: Hamamatsu R955

wavelength (nm)	spectral irradiance	relative output	response ratio
350	0.0735	0.850	1.00
370	0.123	1.400	0.984
400	0.246	2.150	0.755
450	0.599	4.550	0.658
500	1.16	7.000	0.524
550	1.90	7.050	0.321
600	2.81	6.625	0.204
650	3.77	5.750	0.134
700	4.78	5.350	0.097
750	5.74	4.300	0.064
800	6.58	2.900	0.038
900	7.88	0.425	0.0047
1000	8.74	0.550	0.0054

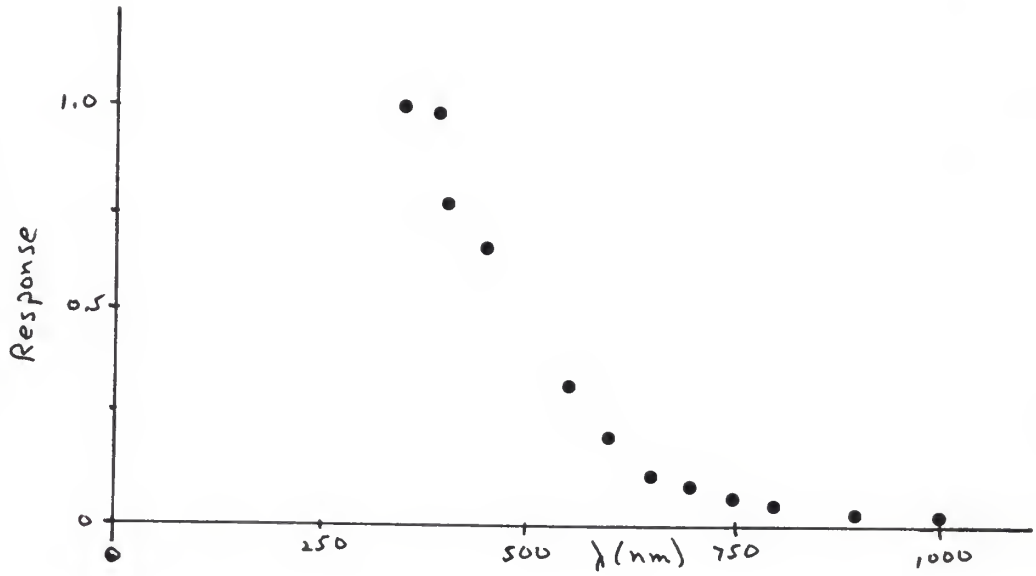

Figure FIII-3 Response curve using Quartz/I_2 lamp. See Appendix III for discussion.

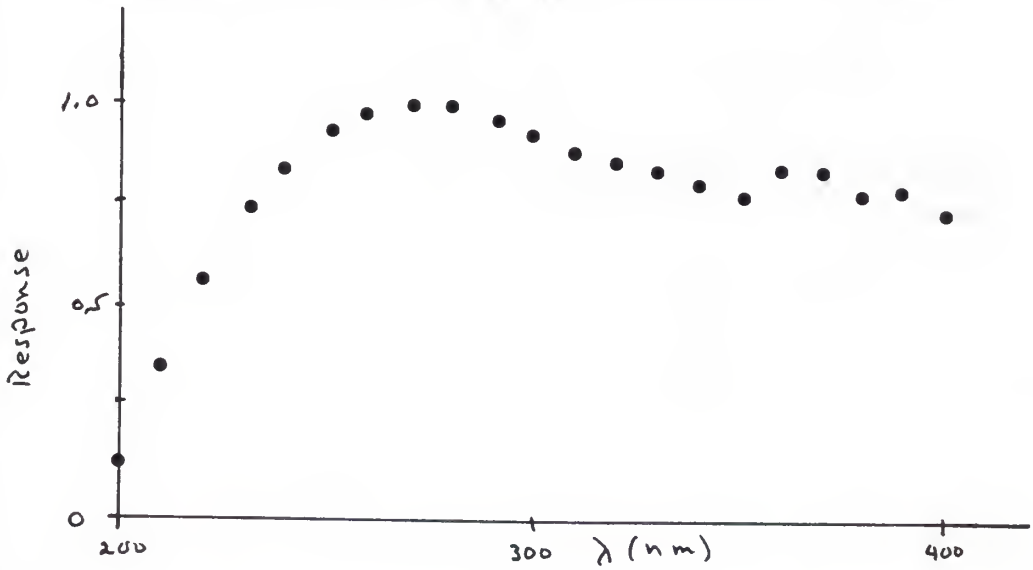

Figure FIII-2 Response curve using D_2 lamp. See Appendix III for discussion.

Acknowledgements

It is, at this point, a pleasure to acknowledge the scientific guidance and advise of Dr. D.W. Setser. He is a prime example of a scientist from whom I have learned much which will be of value to me in my own, further, scientific endeavors. In this regard I am also grateful to Dr. J.C. Ferrero. I would like to especially thank Sanjay Wategaonkar and Tim Nelson for their friendship and for patiently discussing several research problems.

I must also acknowledge the financial support of the chemistry department in the form of teaching and research (NSF) assistantships.

I am very grateful to my wife for her love, support, and patience, particularly during the final stages of this work. Gratitude to my parents and family goes without saying as throughout my life they have provided continuous encouragement and support.

CONTROL OF THE BRANCHING CHANNELS FOR XeCl* FORMATION BY ADDITION OF VIBRATIONAL ENERGY TO CF_2Cl_2, CF_2HCl, AND CF_3Cl

by

ANDREW R. SLAGLE

B.S., Southwestern Oklahoma State University

1984

An abstract of a Master's Thesis

submitted in partial fulfillment of the

requirements for the degree

MASTER OF SCIENCE

Department of Chemistry

Kansas State University
Manhattan, Kansas

1987

Abstract

The XeCl(B,C) formation from the reaction of $Xe(^3P_2)$ with three chlorofluormethanes, CF_3Cl, CF_2HCl, and CF_2Cl_2, has been shown to be enhanced by the addition of vibrational energy to the to the collision pair, Xe^*/RCl. Vibrational energy was provided by the output of a CO_2 laser, which was line tuned to the C-F stretching frequency of the chlorofluoromethanes. The XeCl(B,C) branching fraction, Γ_{XeCl^*}, which is defined as the ratio of the $XeCl^*$ formation rate constant to the total quenching rate constant of the $Xe(^3P_2)$ was also measured. The branching fractions for these compounds are less than 0.03 (3%). The steady-state XeCl(B,C) formation rate constants were measured under first order (in Xe^*) conditions in a flowing afterglow reactor. Spectra of the B-X transition were taken and integrated at a series of RCl concentrations ranging from $3x10^{12}$ to $3x10^{13}$ molecule/cm^3, which was established to be in the pseudo first order domain of the reaction. Similar spectra were taken for the reaction of Xe^* with Cl_2, which is assumed to produce $XeCl^*$ with unit branching. Plots of [RCl] vs the integrated intensities yielded slopes proportional to the $XeCl^*$ formation rate constant. The enhancement of $XeCl^*$ formation following the laser pulse was observed to show a nearly linear dependence

on the CO_2 laser pulse fluence.

In order to estimate of fraction of ground state RCl molecules interacting with the laser field and the amount of energy deposited in the chlorofluormethane molecule by the CO_2 laser pulse, a series of energy absorption experiments were done. Results of these experiments indicate that, under near collisionless conditions, only 10±5% percent of the ground state molecules of interact with the laser pulse. From this and the absorbed energy, the mean energy of the vibrationally excited molecules was assigned as 1-2 eV. The XeCl(B,C) enhancement formation as a result of the vibrational energy is found to occur with nearly unit branching based upon the fractionation value.

The enhancement profiles following the 1.5 us laser pulse show an explainable dependence on experimental parameters. The decay time of the profiles correspond to the time required to remove the vibrationally excited gas sample from the field of observation of the photomultiplier tube. Also, an increase in pressure in the flow tube produces a faster decay time due to collisional deactivation of the vibraionally excited molecules. An increase in RCl concentration also leads to less signal due to self quenching. A delay in the rise time of the profile (the maximum occurs at about 15us) is explained by incomplete mixing of the Xe^*/RCl prior to the laser pulse.